UNCLASSIFIED
SECURITY CLASSIFICATION OF THIS PAGE (When Data Entered)

DTIC FILE COPY ①

AD-A196 403

REPORT DOCUMENTATION PAGE	READ INSTRUCTIONS BEFORE COMPLETING FORM
1. REPORT NUMBER AFIT/CI/NR 88-100 / 2. GOVT ACCESSION NO.	3. RECIPIENT'S CATALOG NUMBER
4. TITLE (and Subtitle) DETERMINATION OF THE UNSTABLE STATES OF THE SOLID STATE PLASMA IN SEMICONDUCTOR DEVICES	5. TYPE OF REPORT & PERIOD COVERED PHD ~~MS~~ THESIS 6. PERFORMING ORG. REPORT NUMBER
7. AUTHOR(s) MARK E. SNYDER	8. CONTRACT OR GRANT NUMBER(s)
9. PERFORMING ORGANIZATION NAME AND ADDRESS AFIT STUDENT AT: TEXAS TECH UNIVERSITY	10. PROGRAM ELEMENT, PROJECT, TASK AREA & WORK UNIT NUMBERS
11. CONTROLLING OFFICE NAME AND ADDRESS	12. REPORT DATE 1988 13. NUMBER OF PAGES 174
14. MONITORING AGENCY NAME & ADDRESS(if different from Controlling Office) AFIT/NR Wright-Patterson AFB OH 45433-6583	15. SECURITY CLASS. (of this report) UNCLASSIFIED 15a. DECLASSIFICATION/DOWNGRADING SCHEDULE

16. DISTRIBUTION STATEMENT (of this Report)

DISTRIBUTED UNLIMITED: APPROVED FOR PUBLIC RELEASE

DTIC
S AUG 0 3 1988 D
H

17. DISTRIBUTION STATEMENT (of the abstract entered in Block 20, if different from Report)

SAME AS REPORT

18. SUPPLEMENTARY NOTES

Approved for Public Release: IAW AFR 190-1
LYNN E. WOLAVER 20 July 88
Dean for Research and Professional Development
Air Force Institute of Technology
Wright-Patterson AFB OH 45433-6583

19. KEY WORDS (Continue on reverse side if necessary and identify by block number)

20. ABSTRACT (Continue on reverse side if necessary and identify by block number)

ATTACHED

DD FORM 1 JAN 73 1473 EDITION OF 1 NOV 65 IS OBSOLETE

UNCLASSIFIED
SECURITY CLASSIFICATION OF THIS PAGE (When Data Entered)

DETERMINATION OF THE UNSTABLE STATES OF THE SOLID STATE PLASMA IN SEMICONDUCTOR DEVICES

by

MARK E. SNYDER, B.S., M.S.

A DISSERTATION

IN

PHYSICS

Submitted to the Graduate Faculty
of Texas Tech University in
Partial Fulfillment of
the Requirements for
the Degree of

DOCTOR OF PHILOSOPHY

Approved

William M Portnoy
Chairperson of the Committee

Charles W. Myles

Osamu Ishihara

R D Peters

Accepted

Clyde Hendrick
Dean of the Graduate School

May, 1988

ACKNOWLEDGEMENTS

It is difficult to pass along the proper regard to everyone who has contributed to my education. Yet, I will attempt to name my mentors, friends and colleagues without whom my time here would have certainly been diminished.

The physics department has given me many opportunities to make the best of my education. I have learned more about teaching and obtained the chance to sharpen my teaching skills. The faculty has provided me with knowledge and experience, which I hope I can continually improve upon.

I wish to thank the members of my dissertation committee: Drs. Myles, Ishihara, Peters and Lichti, who have offered help and feedback that contributed immensely to my dissertation preparation. My committee represents the individuals who have contributed the most to my education.

I wish to especially thank Dr. William Portnoy, who has been a friend and mentor for many years. Dr. Portnoy has provided a perspective on graduate school that has made the means to my educational ends more tolerable.

Finally, I wish to dedicate this dissertation to the memory of my father, who unknowingly, lead me into the wonderful world of science.

TABLE OF CONTENTS

ACKNOWLEDGEMENTS ii

ABSTRACT v

LIST OF TABLES vi

LIST OF FIGURES vii

CHAPTER

I. THE PROBLEM AND ITS HISTORICAL BACKGROUND . . . 1

- The Physics of Device Failure: The Problem . . . 3
  - History of Research Results. 3
  - Preliminary Results of a Formal Redevelopment of Device Failure Phenomena. 18
- Parallels Between Classical Plasmas and Solid State Plasmas 36
- Restatement of the Problem in Light of Current Developments 40

II. GENERAL CHARACTERIZATION OF THE SOLID STATE PLASMA: PLASMA CRITERIA 42

- The Classical Plasma 42
- The Solid State Plasma Criteria. 45

III. ANALYSIS OF SPECIFIC NEGATIVE RESISTANCE IN SOLIDS PROPOSED BY RIDLEY 71

- In-depth Analysis of De Groots's Derivation of the Equations of Motion in Irreversible Processes of Continuous Systems. 72
  - Analysis of Ridley's Derivation 81

Conditions of the Stationary State 84

Application of the Stationary State by Ridley to the Case of CCNR 86

Perturbation Under CCNR 88

IV. QUANTITATIVE ANALYSIS OF THE SOLID STATE PLASMA PINCH 94

The Basic Hydrodynamic Equations 95

The Static Pinch 98

The Hydrodynamic Stability of the Pinch. 109

Solid State Plasma Parameters Necessary to Initiate Pinching 127

V. APPLICATION OF THE PLASMA PARAMETERS TO SEMICONDUCTOR JUNCTIONS 136

Description of Semiconductor Junctions 137

Application of Plasma Pinch to a Transistor 146

Type A Second Breakdown. 151

Type B Second Breakdown. 155

Type C Second Breakdown. 159

VI. GENERAL CONCLUSIONS AND FUTURE WORK. 167

Future Work. 167

Application to Device Failure. 168

LIST OF REFERENCES 170

ABSTRACT

When a semiconductor device fails, a complicated set of actions takes place to move the device from a high voltage, low current state to a low voltage, high current state. Accompanying these changes are the collapse of isotropic current flow to a small column or filament of current which rapidly grows and heats the device to the melting point. These actions are collectively called second breakdown. This work reviews past results to show that second breakdown is the formation of a current controlled negative resistance (CCNR) regime which necessarily forces current flow to form a current filament. The current filament is modeled as a solid state plasma column undergoing a self-induced magnetic pinch as a result of the CCNR. The dispersion relation is derived to first order to show that the pinching leads to an unstable equilibrium that could lead to material failure.

The minimum set of parameters necessary to the formation of second breakdown are determined to be satisfied by the Bennett pinch criterion. Further application is then made to a bipolar power transistor that has been driven into second breakdown to see how the derived criteria applies to a semiconductor device.

DTIC
COPY
INSPECTED
6

☑
☐
☐
By
Distribution/
Availability Codes
Dist | Avail and/or Special
A-1

LIST OF TABLES

1. Type A second breakdown 156

2. Type B second breakdown 160

3. Type C second breakdown 164

LIST OF FIGURES

1. Experimental data points for the IN459 diode . . . 7

2. A composite of data points for eight transistors . 9

3. Failure power versus frequency of occurrence for process 25, topology 13, configuration 1 . . . 12

4. Failure power versus frequency of occurrence for process 5, topology 38, configuration 2 . . . 14

5. Failure power threshold variability versus manufactures for SN4369 transistors. 16

6. Example of the transitions for single carrier space charge limited currents in an insulator. . . 22

7. Forward current-voltage characteristics for alloyed germanium diodes 24

8. Current density versus voltage characteristics for double injection into lightly doped p-type silicon 27

9. Current density versus reverse voltage characteristics for PIN diodes at 300K 29

10. General current density versus voltage for the case of double injection in a semiconductor with recombination centers 32

11. General current density versus voltage for the double injection in a semiconductor with partially filled recombination centers 34

12. Plots of classical plasma parameters 47

13. Relationships for the new plasma parameters . . . 56

14. Plot of the concentration versus quantum degeneracy parameter 58

15. Plot of the concentration versus the plasma parameter for classical coupling 61

16. Plot of the concentration versus the quantum degeneracy parameter for germanium 64

17. Plot of the concentration versus the quantum degeneracy parameter for silicon 66

18. Plot of the concentration versus the quantum degeneracy parameter for gallium arsenide 68

19. Current-voltage characteristic exhibiting current controlled negative resistance 90

20. Geometrical interpretation of equation 96 106

21. Graph of the concentration versus the quantum degeneracy parameter for pinch conditions in germanium 130

22. Graph of the concentration versus the quantum degeneracy parameter for pinch conditions in silicon 132

23. Graph of the concentration versus the quantum degeneracy parameter for pinch conditions in gallium arsenide 134

24. Schematic depiction of a (NPN) transistor 140

25. Schematic depiction of a NPN transistor in cut-off 142

26. Minority carrier density stored in the various regions of a NPN transistor in various conduction states 144

27. Doping profile for the Unitrode power transistor . 148

28. Graph of concentration versus quantum degeneracy parameter for pinch conditions in the Unitrode device 150

29. Typical waveform of current and voltage for type A second breakdown 153

30. Typical waveform of current and voltage for type B second breakdown 158

31. Typical waveform of current and voltage for type C second breakdown 162

CHAPTER I

THE PROBLEM AND ITS HISTORICAL BACKGROUND

At first glance most scientists would expect that determining the conditions necessary to cause a transistor or diode to fail would be related to a few simple factors. These factors would most certainly involve the current and voltage. Failure would then be caused by literally melting the device with a large amount of current or forcing the device to arc over from a high voltage.

Indeed, there is very little proof, considering the material these devices are made of, that the above explanation of device failure is untrue. Common experience shows that when a diode is forced to pass several amperes of current, when it is rated for only a fraction of an ampere, something is going to melt. Similar situations can be constructed for just about any semiconductor device available today.

In the early 1960's the United States Air Force (USAF) and several private firms attempted to determine exactly what conditions of current and voltage caused semiconductor devices to fail. These first researchers took the obvious path already described above and found evidence that devices failed at levels very different than expected. In addition, the devices exhibited phenomena that no one could consistently explain.

This work will attempt to explain and determine the conditions under which a semiconductor device will exhibit signs of impending failure due to an electrical overstress. Device failure will be linked to the onset of negative resistance, which will be shown to force current in the device to collapse. This collapse will be modeled as a solid state plasma that undergoes a self-induced magnetic pinch to an unstable equilibrium under negative resistance conditions. The resultant instability will also be shown to be capable of inducing rapid device heating.

These results will lead to the quantitative development of a minimum pinch criteria that will be compared to a set of measurements on a transistor that is forced into the conditions that are known to precede device failure. The remainder of this chapter will detail the background of device failure research and how experimental evidence led this author to conclude that device failure, and the formation of a negative resistance regime in the device, were one and the same.

The Physics of Device Failure: The Problem

History of Research Results

The first published reports concerning device failure were reported for diodes by Tauc and Abraham [1] in 1957.

Failure of transistors was soon reported by Thornton and Simmons [2] in 1958. These reports demonstrated experimentally that the failure state of a device was characterized by a transition from a high voltage, low current state, to a high current, low voltage state. Soon after this transition the device failed as an open circuit or short. Autopsies of failed devices showed definitive signs of extensive heating leading to melting of the semiconductor material.

For semiconductor devices made of silicon or germanium, this implied that temperatures were approaching the melting point of the materials during failure. Many researchers concluded that such temperatures were a result of ohmic heating of the device in this new regime (of high current, low voltage) that occurred after avalanche breakdown. Thus, many researchers referred to this regime, which occurred after avalanche or first breakdown, as second breakdown.

Continued research soon broke into two approaches in an attempt to determine device failure levels [3]. One group approached failure as a solely thermal event. A second group sought further information concerning why a device went into this new regime of operation called second breakdown. In the early 1960's, a tremendous number of articles were published concerning device failure, of which a partial listing is set forth in reference three.

Two very general conclusions came forth from these reports:

> 1. Attempts to model device failure as a thermal runaway event [4] had very limited success and suffered from extreme problems of repeatability [5].
>
> 2. Devices that entered second breakdown suddenly exhibited the collapse of isotropic current flow to a small current filament or column [6]. This filament soon engulfed the device volume, melting the device as it grew [7].

Such results were quite unexpected and continued to fuel further research along both lines of interest.

Researchers who followed conclusion one above made numerous attempts to model device failure by utilizing extensive thermodynamic approaches coupled with device geometry. These initial ideas became the basis for further research and were developed into models by Wunsch and Bell [8] in 1966 and Tasca [9] in 1970. These models generally utilized a thermal diffusion model incorporating the increasing carrier concentration of a semiconductor with increasing temperature driven by an external current. The feedback mechanism provided by a semiconductor's increasing carrier concentration, with temperature which, in turn, increases the current, became the prime physical explanation of device failure in these models. The two models developed by Wunsch and Tasca could not incorporate all aspects of device design necessary for an accurate model, so a correction factor was added to each model by matching its results empirically to experiment.

Initially, results of applying these models to simple diodes, and transistors treated as diodes, looked very promising (see figures 1 and 2). The only information required to determine a device's failure level consisted of the material parameters and the appropriate device area. Further application of these two models to other diodes and transistors showed very limited results, and more importantly, the correction factor incorporated in the models would have to be changed in an almost random fashion to bring predictions closer to experimental results [10]. Perusal of these studies show that some results were dissimilar due to differences in the definition of what constituted device failure. Variation of what constituted the onset of failure also presented problems in interpreting experimental approaches used by different researchers.

The community of researchers trying to refine thermal models tried to clear up confusion by utilizing the onset of second breakdown as the criterion for device failure. Several researchers then tried to alter the old thermal models to explain second breakdown as an electronic and thermal event. These electrothermal models [11,12] were, by themselves, achievements in modeling device dynamics which occurred on totally different time scales (thermal events occur in microseconds, electrical events occur in

Figure 1. Experimental data points for the IN459 diode. Slope indicates power is inversely proportional to the square root of the time to failure as dictated by the Wunsch-Bell model. The diode is pulsed in reverse bias and failure corresponds to the device assuming a resistor characteristic. Only seven devices were tested. From reference 8.

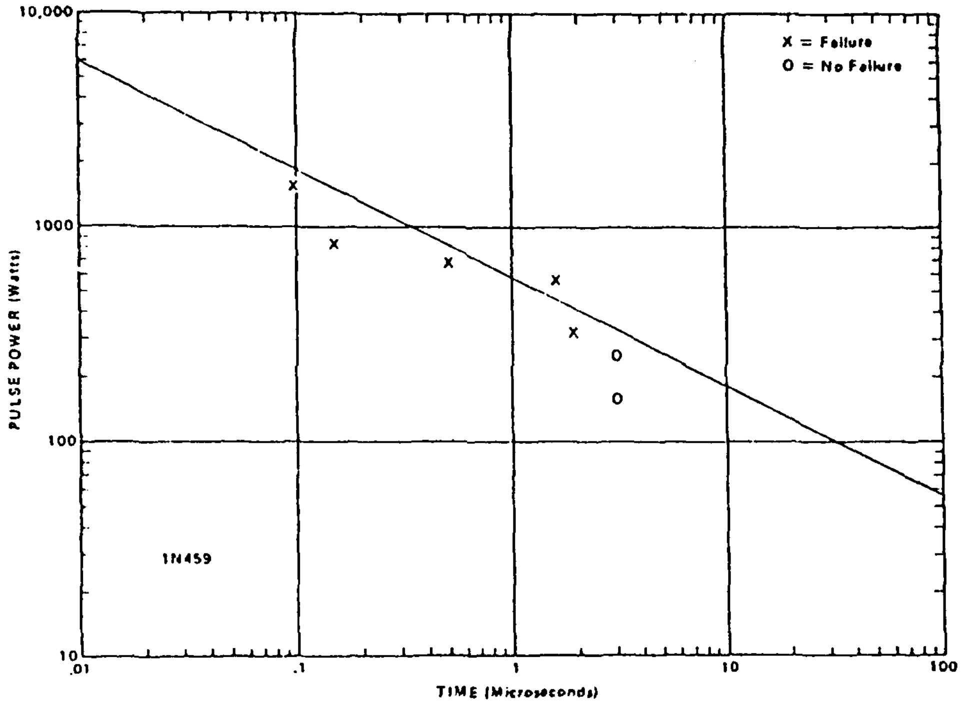
10,000
1000
100
10
PULSE POWER (Watts)
X = Failure
O = No Failure
1N459
.01
.1
1
10
100
TIME (Microseconds)

Figure 2. A composite of data points for eight transistors. All failure was by pulsing the emitter base junction in reverse bias with the collector open. Lines indicate the theoretical failure levels predicted by the Wunsch-Bell model. Failure coresponds to the device assuming a resistor characteristic. From reference 8.

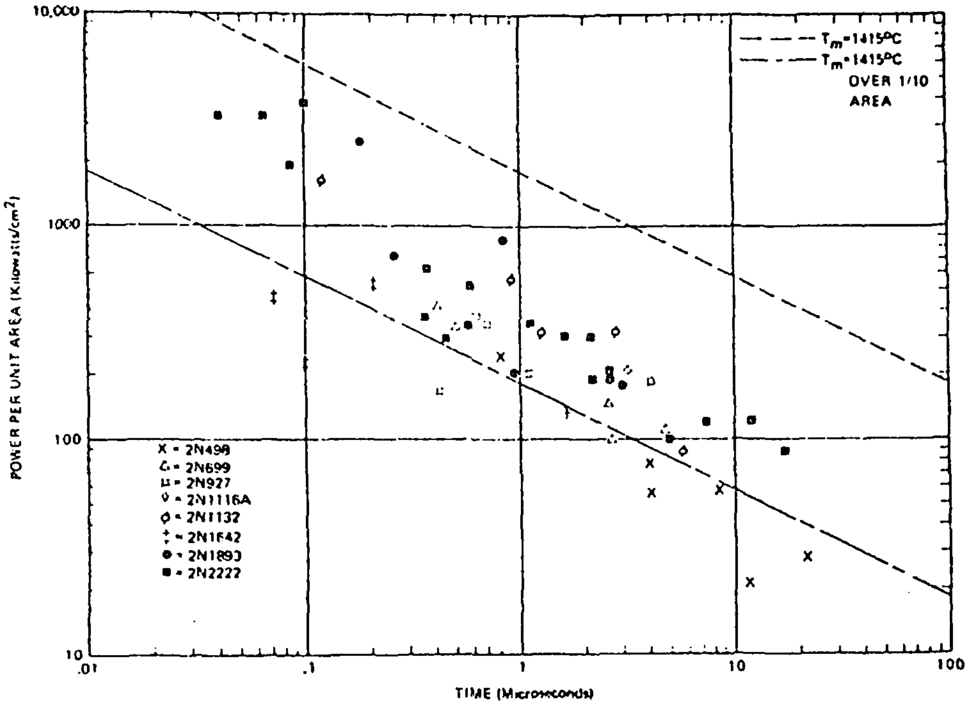
T_m=1415°C
T_m=1415°C OVER 1/10 AREA
X = 2N498
Δ = 2N699
⊔ = 2N927
∇ = 2N1116A
ϕ = 2N1132
‡ = 2N1642
● = 2N1893
■ = 2N2222
10,000
1000
100
10
.01
.1
1
10
100
POWER PER UNIT AREA (Kilowatts/cm²)
TIME (Microseconds)

times on the order of nanoseconds). The general results of these models did show better agreement with experiment, but, they were limited by the extensive information required of a device to determine failure. In simple terms, the model was as accurate as the device information was. Since the electrothermal models required information not readily available for devices, many were hesitant about using electrothermal models for large scale testing of devices.

One study sponsored by the USAF attempted to apply a much reduced version of the electrothermal models to a wide variety of devices where specific design aspects (such as mask architecture, doping levels and mask areas) were systematically varied with another aspect held as a control [13]. Results of this large scale effort did not show any universal trend in the power dissipated versus time to second breakdown for any particular device design aspect. Many individual results showed multiple peaks on graphs of number failed versus power to failure (see figures 3 and 4) and some results did not appear to match the normal distribution assumed for the probability of failure assessment of the devices (many attempts to model device failure sought statistical methods to account for the broad range of power to failure found experimentally).

Although the variation in power to failure had been seen before, it was believed to be due to inter-vendor differences in device design [14] as shown in figure 5.

Figure 3. Failure power versus frequency of occurrence for process 25, topology 13, configuration 1. Fifty devices were tested for this case. A normal distribution is superimposed on the graph. From reference 13.

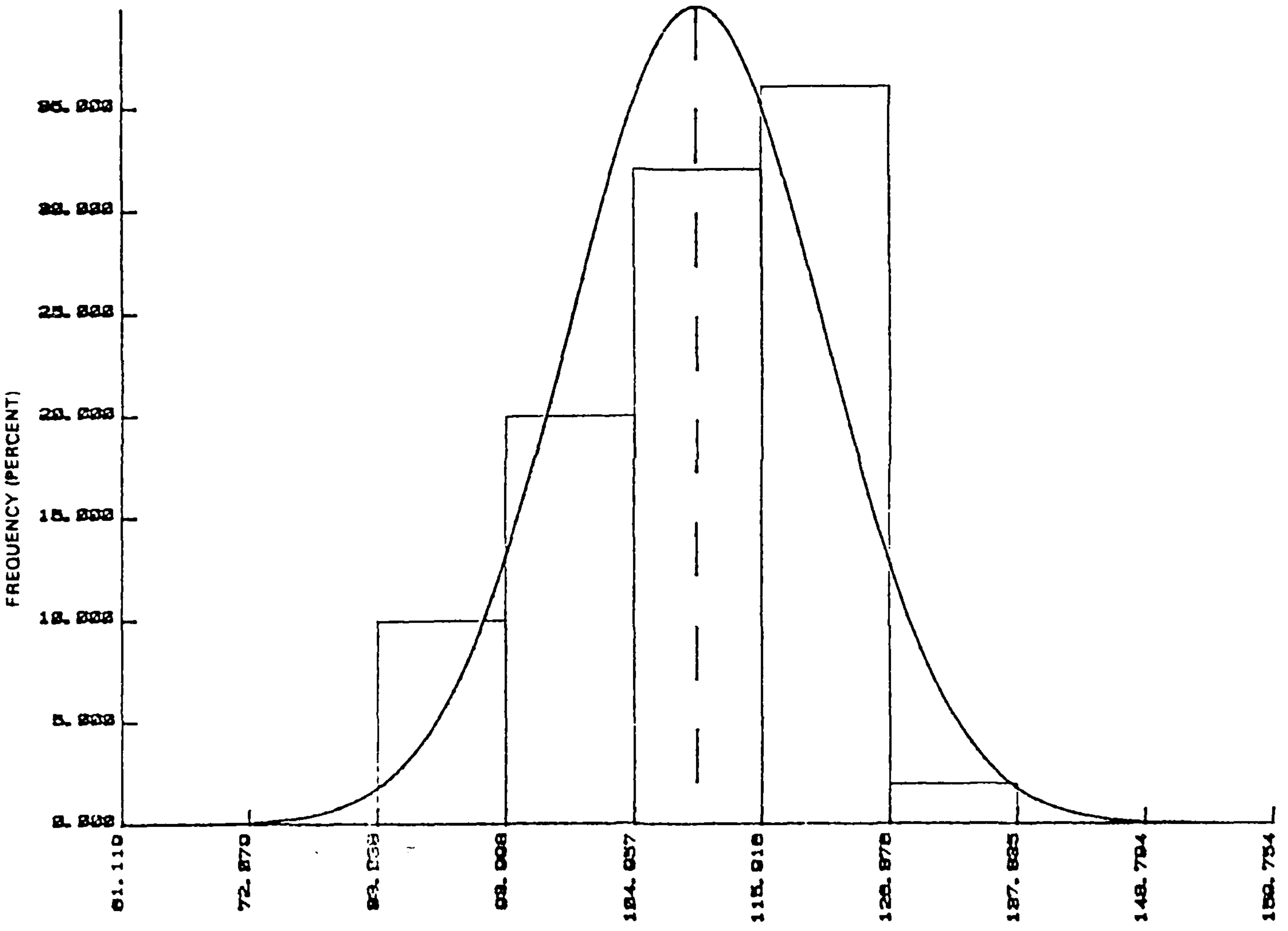
FREQUENCY (PERCENT)
0.000
5.000
10.000
15.000
20.000
25.000
30.000
35.000
61.110
72.070
83.031
93.991
104.952
115.912
126.873
137.833
148.794
159.754
FAILURE POWER (WATTS)

Figure 4. Failure power versus frequency of occurrence for process 5, topology 38, configuration 2. Twenty five devices were tested for this case. A normal distribution is superimposed on the graph. From reference 13.

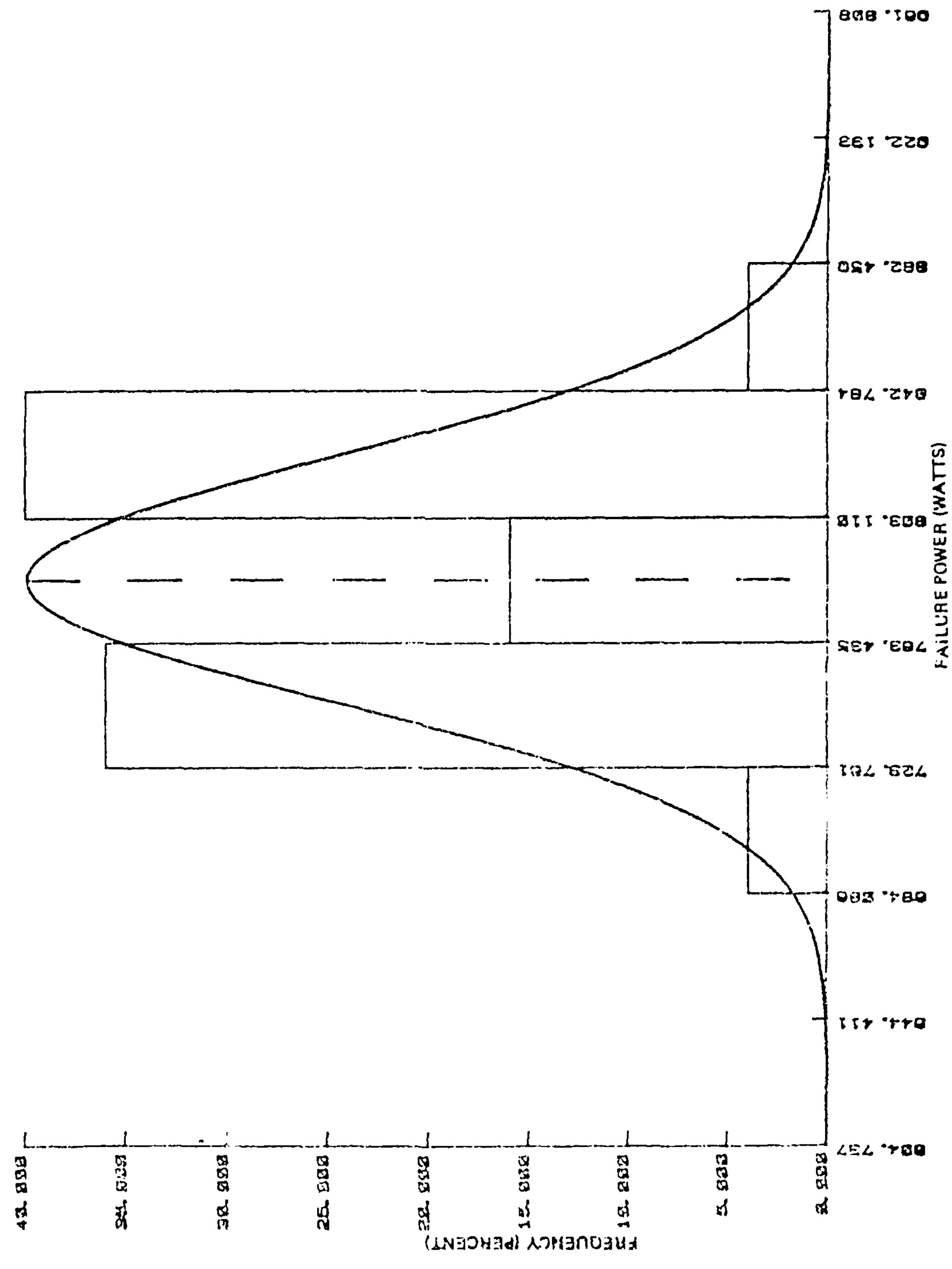
FREQUENCY (PERCENT)
0.000
5.000
10.000
15.000
20.000
25.000
30.000
35.000
40.000
FAILURE POWER (WATTS)
604.757
644.411
684.088
723.761
763.435
803.118
842.784
882.450
922.133
961.808

Figure 5. Failure power threshold variability versus manufacturers for 2N4369 transistors. Circles represent the average value of the failure power. Bars indicate the range of failure found. Devices were tested with the emmiter base in reverse bias and the collector open. From reference 14.

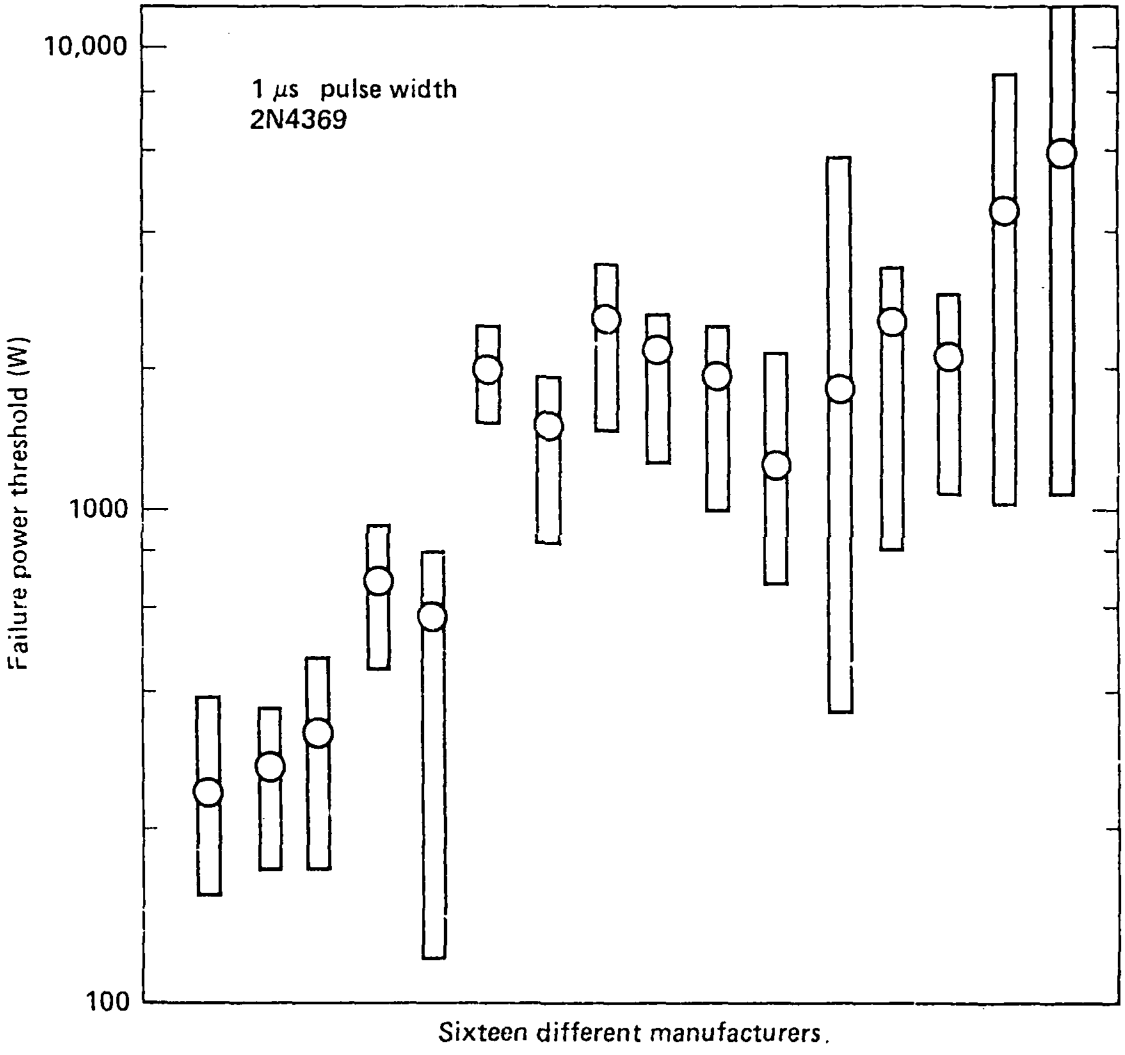
10,000
1000
100
Failure power threshold (W)
1 µs pulse width
2N4369
Sixteen different manufacturers.

Yet, the USAF sponsored work did not show any expected correlation between device design and the distribution of failure.

Critics of this study believed that it suffered the same drawbacks as previous experimentation with thermal models; namely, poor experimental design that did not (or could not) control the primary parameters that effect failure.

These critics, who were investigating conclusion two, also pointed out that second breakdown and device failure by thermal events were not synonymous. In addition, the models used were based on thermal diffusion and were more applicable to device failure due to melting, not the initiation of second breakdown.

These critics had also been able to show experimentally that the fine structure seen upon the initiation of second breakdown was most certainly occurring before melting and was most likely to be due to electronic processes [2,6,7,15].

The most researched cause of second breakdown by this group involved avalanche breakdown in conjunction with heating, defects or surface effects. These conjunctive causes were viewed as necessary to nucleation of the current to a current filament.

Further evidence in favor of this approach was obtained by Sunshine and Lampert [16] that demonstrated that avalanching silicon-on-sapphire diodes repeatably showed multiple filament formation dependent on the degree of electrical stress applied to the device. By the early 1980s it was clear that second breakdown was the precursor of device failure. However, no model was able to explain completely both the characteristic low voltage, high current state and the formation or collapse of current to a small filament(s). In fact, some researchers believed that avalanche breakdown and device heating would not allow filament formation due to thermalization of the carrier distribution. If this was found to be true, no simple solution appeared to be able to explain the complex phenomena accompanying second breakdown.

Preliminary Results of a Formal Redevelopment of Device Failure Phenomena

After a perusal of past research, the author of this work set out to re-examine the problem of explaining device behavior preceding failure by finding a physical explanation for the current filamentation seen under second breakdown.

The starting point for this effort was basic carrier transport under low and high voltages in insulators and semiconductors. These states of electrical conductivity in materials were chosen because an active semiconductor device is dominated by the electrical activity in the depletion region, which can exhibit insulator or semiconductor characteristics dependent on an external bias. Also, second breakdown in devices appeared exclusively in depletion regions as determined from experiments [17] and postmortem examinations [18].

Explaining current transport in a device in this manner will allow us to determine when, and if, a negative resistance regime has been achieved in a sample or device.

To begin this analysis, we will describe the basic transport mechanisms for space charge limited single carrier injection in an insulator. This will be followed by a short description of two carrier currents in insulators and semiconductors. Each case comes closer to describing current flow in the depletion region of a device or a sample of material. These treatments follow from the work of Mark and Lampert [19] and were extensively used by the author in a previous effort [20]. Since these derivations appear elsewhere their results will simply be stated here.

The first case of interest deals with single carrier injection in insulator-like materials. To approximate the effect more closely to a semiconductor device's depletion region, the insulator we discuss has connections that are ohmic to electrons only. Under these conditions, the insulator is found to transition through four different types of space charge limited current flow with increasing applied (direct current) voltage. At low voltages, current follows Ohm's law. As the voltage increases, more electrons are injected and begin to fill any traps in the material near the cathode. Yet, an insufficient number of electrons exist, after trapping, to transit the material. Hence, a buildup of space charge begins near the cathode. Increasing the applied voltage further will fill more traps and some electrons make it through the material to the anode. Eventually, the voltage is raised enough so that all traps in the material are filled and the current follows a trap-free square law characteristic (see figure 6). Electrons are now able to recombine primarily at the anode and little trapping takes place in the bulk.

These results are quite similar to current flow in a forward biased diode [21] where current flow is dominated primarily by recombination of minority carriers at the depletion layer edge (see figure 7). Whether or not a diode follows a trap-free square law is unclear at present.

If we remove the constraint of ohmic contacts for electrons only, space charge build-up in the previously modeled insulator, is eliminated. The insulator is now modeled with a cathode that injects electrons and an anode that injects holes. The only limiting mechanism to current flow in this situation is recombination. This recombination occurs via two primary mechanisms which are dependent on the applied potential. Some recombination takes place at traps in the material during low and moderate voltages. When the applied voltage is large enough, carrier transit times becomes equal to the lifetime, through recombination, and carriers recombine primarily at the injecting contacts.

The experimental results found for the above case of ohmic contacts for electrons and holes [20] is somewhat

Figure 6. Example of the transitions for single carrier space charge limited currents in an insulator. Calculated values are from reference 19.

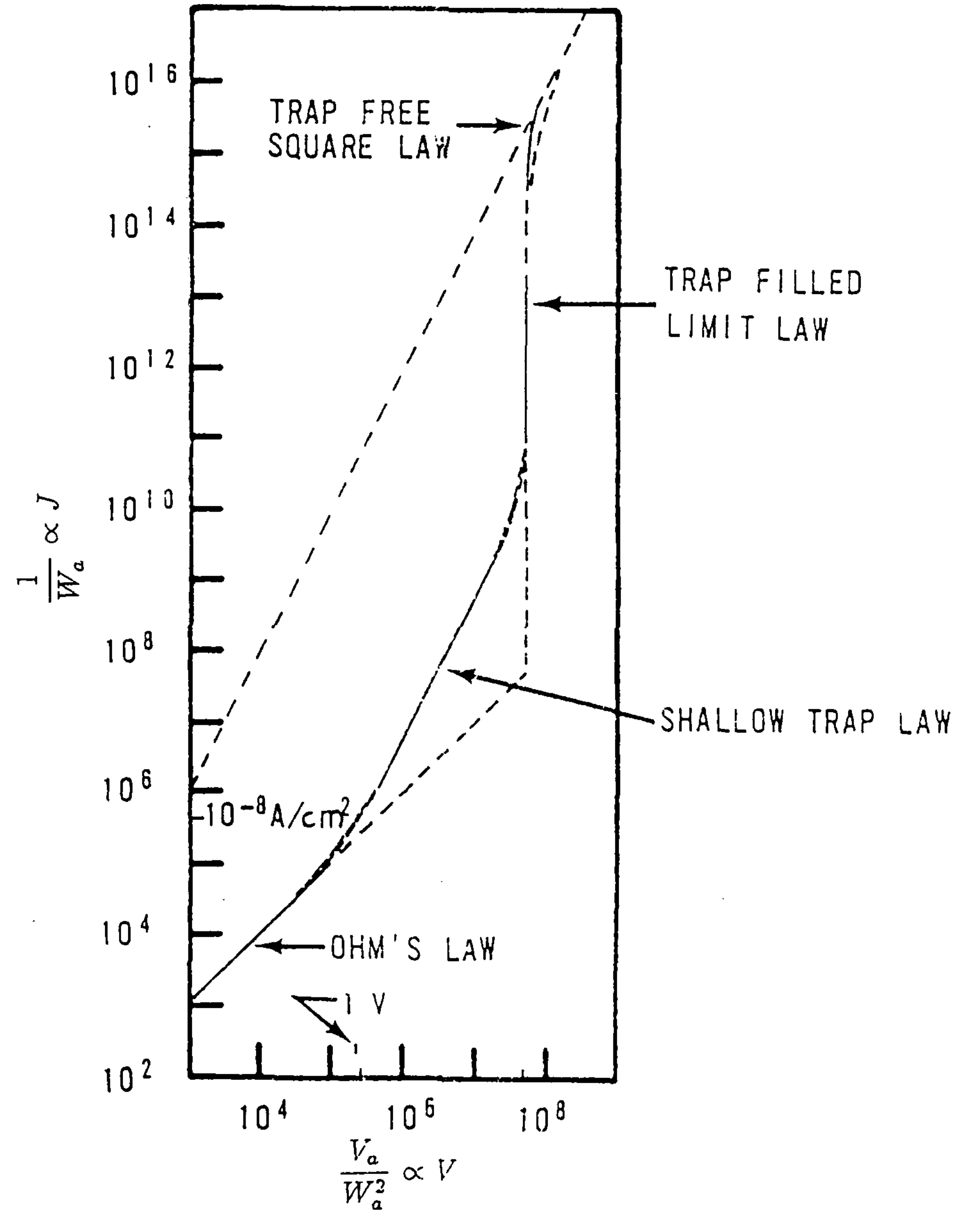

10^{16}
10^{14}
10^{12}
10^{10}
10^{8}
10^{6}
10^{4}
10^{2}
$\frac{1}{W_a} \propto J$
TRAP FREE SQUARE LAW
TRAP FILLED LIMIT LAW
SHALLOW TRAP LAW
10^{-8}A/cm^2
OHM'S LAW
1 V
10^4
10^6
10^8
$\frac{V_a}{W_a^2} \propto V$

Figure 7. Forward current--voltage characteristics for alloyed germanium diodes. Current is proportional to the voltage squared. This indicates, from the previous discussion, that current is dominated by single carrier injection and recombination at the contacts. From reference 21.

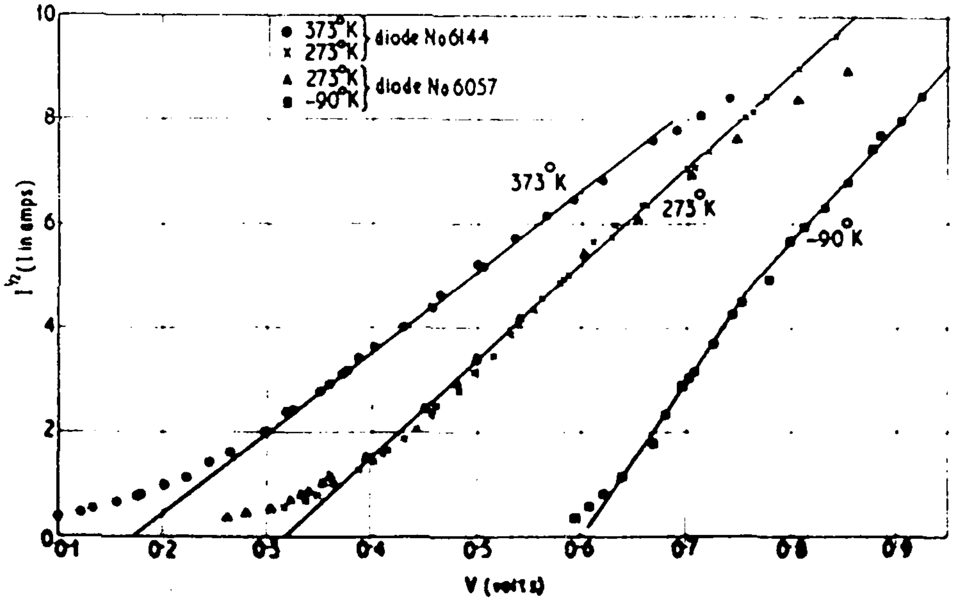
● 373°K
x 273°K
diode No 6144
▲ 273°K
■ -90°K
diode No 6057
373°K
273°K
-90°K
10
8
6
4
2
0
$I^{1/2}$ (I in amps)
0·1
0·2
0·3
0·4
0·5
0·6
0·7
0·8
0·9
V (volts)

similar to single carrier injection results. At low voltages the current follows a square law very similar to the trap-free square law relation. In essence, we have a single carrier current until a balance is reached with the traps, which preferentially block the motion of one carrier, until all traps are filled. As the voltage increases, the current becomes dominated by both carriers (the traps are now filled) to produce a double injection cube law for current flow.

We next bring attention to a semiconductor material where, unlike an insulator, a number of thermally generated free carriers are present. We model this case with an electron injecting cathode and a hole injecting anode in a semiconductor that is slightly dominated by electrons or holes. Results of calculation show the current follows a square law which matches experimental results quite well for a low number of carriers [22] (see figure 8). When a large number of carriers are present (from injection or thermal production) the current follows a cubed law [23] (see figure 9). An examination of the carrier concentration in both cases of injection indicates a build-up of carriers at one of the material contacts (dependent on the dominant carrier sign) is occurring. This effect creates an effective anode or cathode which makes the semiconductor seem electrically shorter. In a sense, a portion of the sample experiences a space charge limited current flow, and the rest of the sample experiences a trap free current characteristic.

Figure 8. Current density versus voltage characteristics for double injection into lightly doped p-type silicon. Note the square law regime. From reference 22.

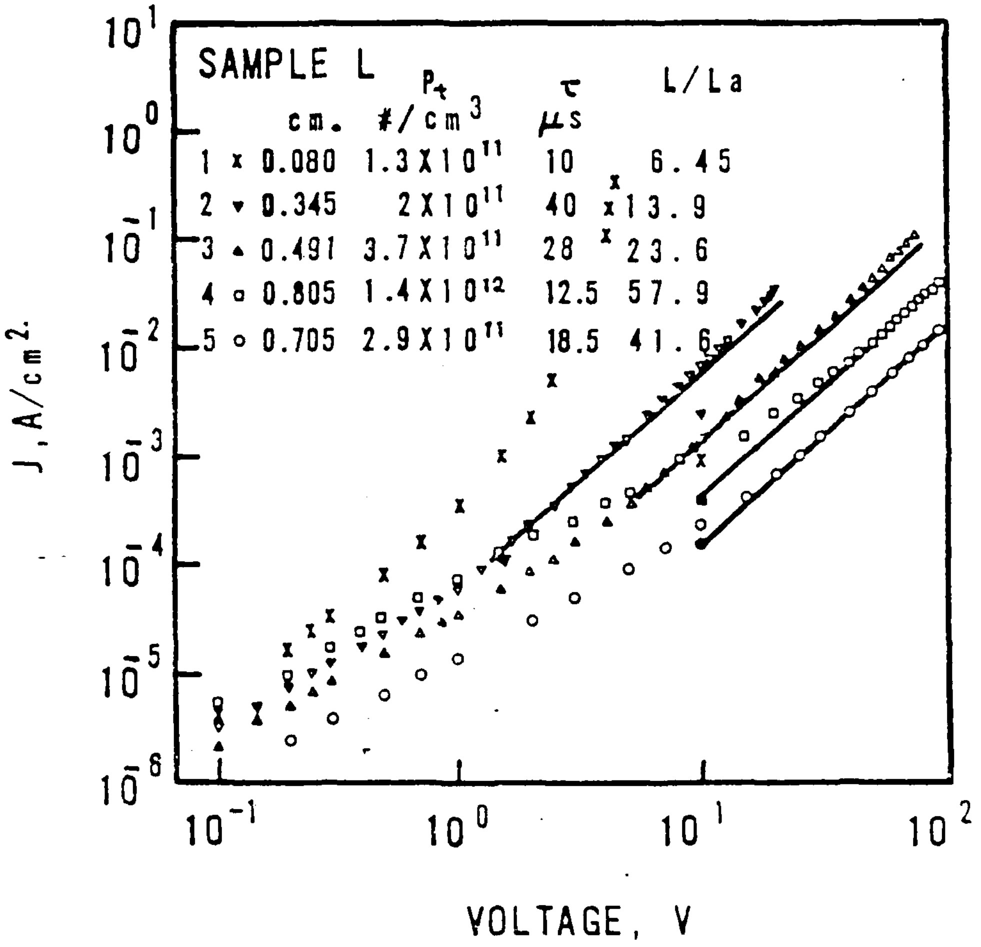
SAMPLE L
cm.
P_t #/cm^3
τ μs
L/La
1 x 0.080 1.3X10^{11} 10 6.45
2 ▼ 0.345 2X10^{11} 40 13.9
3 ▲ 0.491 3.7X10^{11} 28 23.6
4 □ 0.805 1.4X10^{12} 12.5 57.9
5 ○ 0.705 2.9X10^{11} 18.5 41.6
J, A/cm^2
10^1
10^0
10^{-1}
10^{-2}
10^{-3}
10^{-4}
10^{-5}
10^{-6}
10^{-1}
10^0
10^1
10^2
VOLTAGE, V

Figure 9. Current density versus reverse voltage characteristics for PIN diodes at 300K. Note the expected cube law regime holds for a device also. From reference 23.

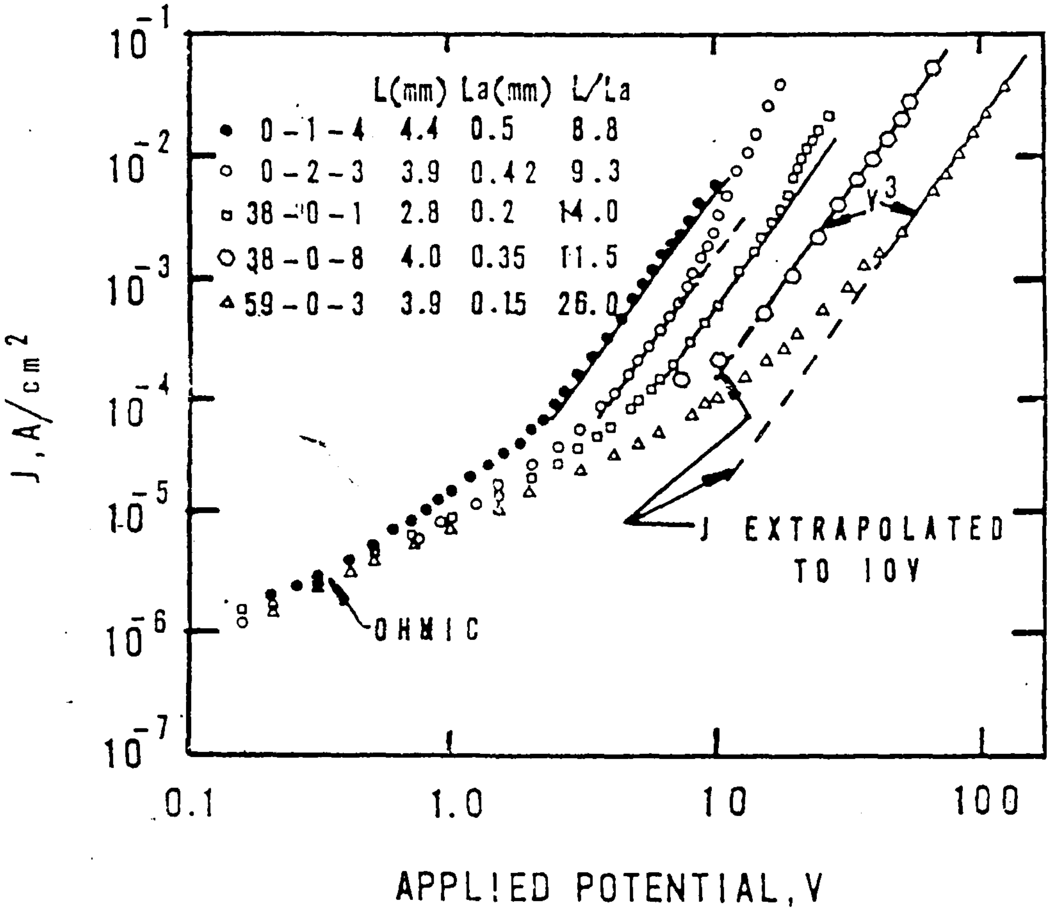
L(mm) La(mm) L/La
● 0-1-4 4.4 0.5 8.8
○ 0-2-3 3.9 0.42 9.3
▫ 38-0-1 2.8 0.2 14.0
○ 38-0-8 4.0 0.35 11.5
△ 59-0-3 3.9 0.15 26.0
10^{-1}
10^{-2}
10^{-3}
10^{-4}
10^{-5}
10^{-6}
10^{-7}
J, A/cm²
0.1
1.0
10
100
APPLIED POTENTIAL, V
OHMIC
V3
J EXTRAPOLATED TO 10V

We now deal with a semiconductor with contacts as discussed before, but, we add a set of recombination centers deep in the forbidden zone. This is usually accomplished by placing additional dopants in the material during the crystallization process to provide an additional set of traps for recombination. These traps are usually formed in the forbidden zone a fraction of an electron volt from the energy bands. At room temperature, these levels are empty. Analysis shows the presence of these shallow recombination centers, presents an additional potential that the minority carriers must overcome with the aid of an external voltage. Until the externally applied voltage is greater than this recombination potential current follows a trap-free space charge limited square law. Once the recombination barrier is surpassed by the applied voltage, the sample potential drops precipitously and follows a square law as arrived at earlier for a semiconductor [24] (see figure 10).

When the recombination centers, added to the sample as doping during crystallization process, form traps near the center of the forbidden zone they exist in a partially filled state at room temperature. Analysis shows that both carriers now see a potential barrier that must be overcome by the external voltage before current can flow [25] (see figure 11).

These last two situations with semiconductors show current and voltage characteristics which exhibit signs of

Figure 10. General current density versus voltage for the case of double injection in a semiconductor with recombination centers. Ratios of the carrier capture cross-sections are listed for electrons and holes. Calculated by Lampert and Mark using general parameters. From reference 19.

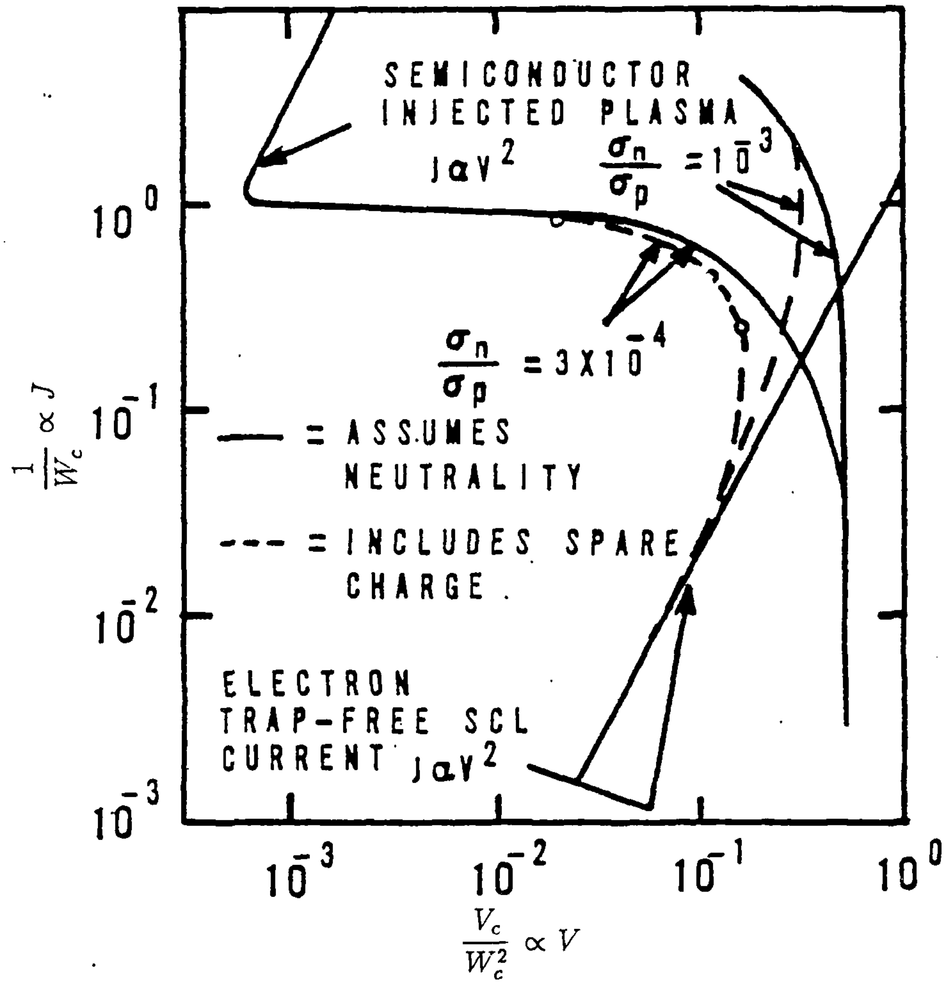
SEMICONDUCTOR INJECTED PLASMA
$J \alpha V^2$
$\frac{\sigma_n}{\sigma_p} = 10^{-3}$
$\frac{\sigma_n}{\sigma_p} = 3 \times 10^{-4}$
—— = ASSUMES NEUTRALITY
--- = INCLUDES SPARE CHARGE.
ELECTRON TRAP-FREE SCL CURRENT $J \alpha V^2$
10^0
10^{-1}
10^{-2}
10^{-3}
10^{-3}
10^{-2}
10^{-1}
10^0
$\frac{1}{W_c} \propto J$
$\frac{V_c}{W_c^2} \propto V$

Figure 11. General current density versus voltage for double injection in a semiconductor with partially filled recombination centers. The transition to negative resistance occurs at a lower current density than seen in figure 10. Calculated by Lampert and Mark in reference 19.

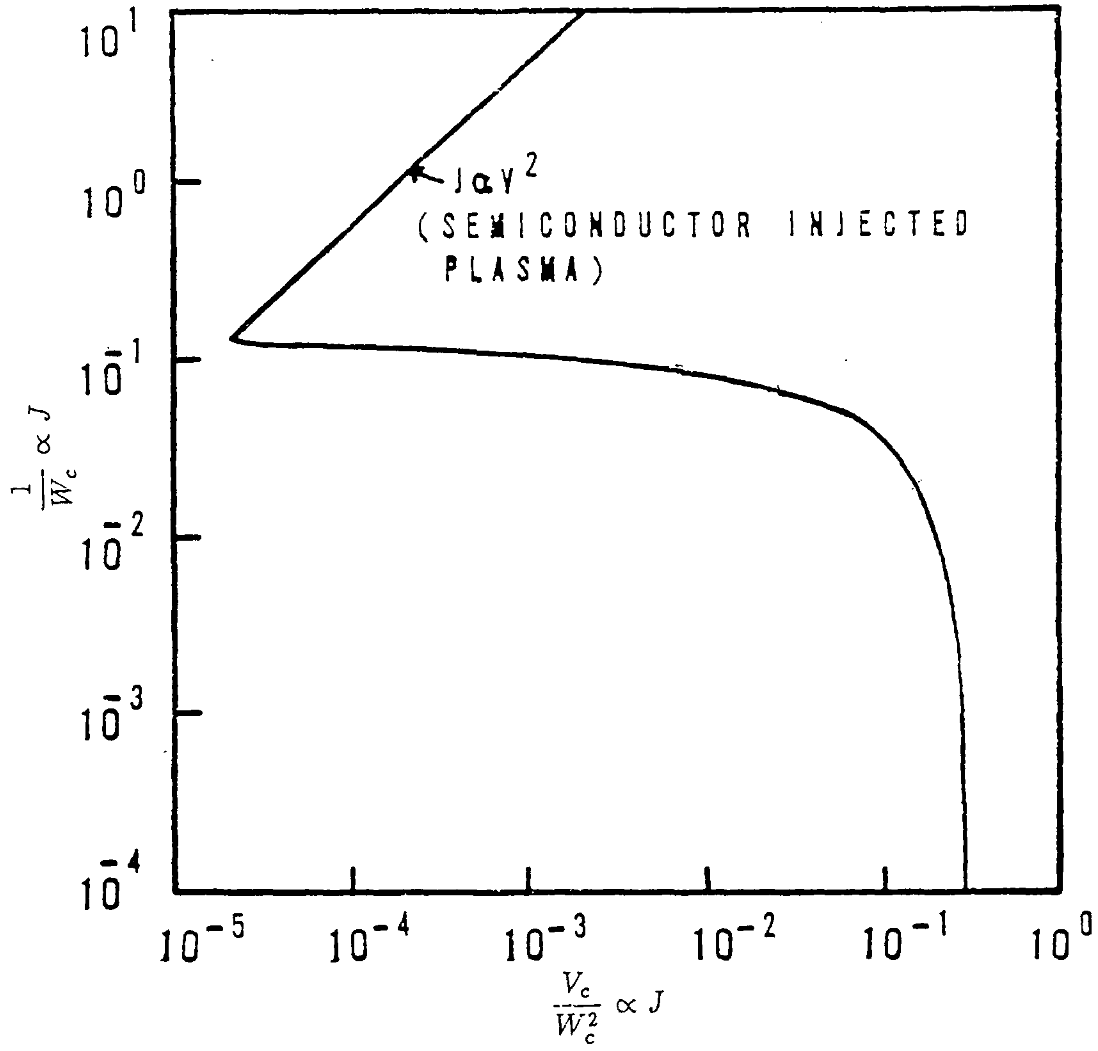
10^1
10^0
10^{-1}
10^{-2}
10^{-3}
10^{-4}
10^{-5}
10^{-4}
10^{-3}
10^{-2}
10^{-1}
10^0
$J \alpha V^2$
(SEMICONDUCTOR INJECTED PLASMA)
$\frac{1}{W_c} \propto J$
$\frac{V_c}{W_c^2} \propto J$

what is called negative resistance. Negative resistance, in the above cases, exhibits a transition from a high voltage, low current, to a low voltage, high current state quite like the characteristics seen during second breakdown. Since the previous analysis for single and double carrier currents is applicable to the depletion region of devices, it can be inferred that second breakdown in devices is the transition from single carrier to double carrier injection, creating a negative resistance characteristic.

Ridley [26] demonstrated that current controlled negative resistance (CCNR) creates a regime where current flow is unstable against the formation of a current filament. This type of negative resistance is called CCNR after the multi-valued current that can be exhibited for a single voltage. In a similar fashion, Ridley [26] demonstrated that a under a voltage controlled negative resistance (VCNR), current is unstable against formation of current domains. VCNR is named after the multi-valued voltages that occur for a particular current level. Both aspects of negative resistance have been verified experimentally to lead to filament formation under CCNR [27,28] and domain formation under VCNR [29,30].

If second breakdown is the initiation of CCNR, then second breakdown could be analyzed through the device's material parameters. Yet, Ridley's proof of filament formation is macroscopic, from a thermodynamic point of view, and a further explanation would be required in order to characterize the filament in terms of a model.

Only one physical mechanism appeared capable of producing the filamentary current channel seen in experiments: self-induced magnetic pinch of the current column. Initially, this premise was considered quite controversial. Yet, research in plasma physics applied to semiconductors has shown modeling current flow as a solid state plasma is quite realistic.

Parallels Between Classical Plasmas and Solid State Plasmas

To demonstrate the utility of modeling current flow in a semiconductor as a solid state plasma, a short history of the development of plasma physics and its analogous counterparts in the development of solid state plasma physics will be examined.

The results of this section will lay the foundation for the approach in later chapters to model the solid state plasma in terms of well known classical plasma parameters.

The term plasma was first applied by Langmuir [31], in 1928, to the ionized gas in an electrical discharge. A plasma was dominated by coulomb forces between individual parts of the plasma that gave it a cohesiveness that has been termed, collective behavior. Following these discoveries Bennett [32], in 1934, predicted the self-induced compression of an electron beam could be produced by its self-magnetic field. Tonks [33] called this behavior the pinch effect.

Later in 1935, Eckersley [34] determined the dispersion relationship for electromagnetic waves that propagate through the ionosphere along the Earth's magnetic field lines. The group velocity of these waves increases with frequency such that an observer detecting such waves finds a tone that falls with time. Barkhausen [35] had detected these waves as early as World War I and coined the term by which they are presently called: whistlers.

In 1942 Alfvėn [36] predicted a new type of electromagnetic wave propagating through a highly conductive plasma in a strong magnetic field. Alfvėn determined this from a study of the phenomena that occur near sunspots. Their subsequent discovery in the laboratory has lead to the appropriate name: Alfvėn waves.

Plasmas in solids were first postulated by the studies of Rutheman [37] and Lang [38] in 1948. In their experiments, the passage of an electron beam through a metal foil exhibited energy losses that were discrete in nature. Later, in 1952, this effect was explained by Bohm and Pines [39] as the excitation of electron plasma oscillations in the metal in the form of plasmons (a quantized oscillation of the electron plasma).

In the late 1950's and early 1960's, a number of results were reported concerning anomalous electrical behavior in germanium, indium antimonide, gallium arsenide and bismuth. Oscillations were reported in indium antimonide and gallium arsenide under conditions of impact ionization and in the presence of a longitudinal magnetic field that was comparable in magnitude to the intrinsic magnetic field at the samples' surface [40,41]. Studies of germanium at low temperatures and strong magnetic fields showed low frequency current oscillations [42]. Absorption of electromagnetic waves in the centimeter range in bismuth, under strong magnetic fields, exhibited a linear dependence of the absorption coefficient with magnetic field strength [43].

Researchers found that these phenomena could not be explained in terms of simple current transport variables and a new approach certainly seemed warranted.

The results found for germanium under high magnetic fields were soon explained by Glicksman [44] on the basis of treating current flow as a solid state plasma using the theory of the helicon instability (similar to whistlers in the ionosphere). The results in bismuth were determined to be due to propagation of an Alfvėn wave whose phase velocity is proportional to the magnetic field strength which governs the absorption coefficient [45].

Finally, the results in indium antimonide and gallium arsenide were explained by Glicksman and Steele [45,46] with the use of the pinch effect. In their work, an electron-hole plasma is strongly compressed by the sample's current interaction with its self-magnetic field. As the density rises in the column, the resistance increases as enhanced electron-hole scattering and bulk recombination occur. The study also demonstrated that the criterion for compression developed by Bennett [35] was well satisfied experimentally [47]. Later, Glicksman and Ando [48] demonstrated that under a strong enough longitudinal magnetic field, the pinch transformed into a helicon instability. In 1963, Gunn [49] determined that microwave radiation was generated by gallium arsenide and indium phosphide under strong electric fields. The effect, which was named after Gunn, was found to be due to VCNR and was predicted earlier by Ridley [26]. The Gunn effect had no counterpart in gaseous plasma physics experiments. Yet, a rigorous derivation of the Gunn effect was carried out using the formalism of collisionless shock waves developed by Sagdeev [50]. Later, an effect analogous to the Gunn effect was found in gaseous plasmas in the study of ion acoustic shock waves [51]. Here was a case where developments in solid state plasmas were a precursor to discovery of the same effects in gaseous plasma experiments.

At this point, it should be quite clear to the reader that although there are differences between a solid state plasma and a gaseous plasma, the approach to problems and much of the phenomena they share (such as instabilities) are grounds of commonality. Modeling current flow in a semiconductor as a solid state plasma is well qualified.

Restatement of the Problem in Light of Current Developments

If the reader accepts the previous argument by analogy of the correspondence between gaseous plasmas and solid state plasmas, then second breakdown in semiconductor devices could be explained by modeling current flow as a solid state plasma under CCNR conditions. Filamentation could then be explained as a result of the plasma pinch.

The balance of this work will be devoted to determining if pinching of the solid state plasma does occur under CCNR conditions, whether or not the pinch is stable, and what additional effects could ensue if the pinch forms.

Chapter II will start with a detailed examination of plasmas to determine a set of parameters to characterize a solid state plasma in a way that is analogous to known parameters for a classical plasma.

Chapter III will examine the conditions, and limitations, CCNR places on the environment that contains the solid state plasma.

Chapter IV will model a solid state plasma under CCNR conditions and determine if pinching occurs, and whether or not it is stable. This analysis will develop a set of criteria to determine the initiating conditions for the pinch.

Chapter V will look at experimental measurements of a transistor that was driven electrically to the initiation of second breakdown, then recovered safely. Analysis of the device physics will be performed to determine if pinching conditions were achieved at the initiation of second breakdown.

CHAPTER II

GENERAL CHARACTERIZATION OF THE SOLID STATE PLASMA: PLASMA CRITERIA

It was proposed in chapter I that the electron-hole cloud in a semiconductor could be treated as a solid state plasma. Parallels were drawn between developments in classical plasma physics and experimental work that demonstrated similar plasma characteristics in solids.

This chapter will elaborate on the connection between classical plasmas and solid state plasmas by utilizing a set of parameters to characterize all plasmas.

The well known classical plasma parameters (e.g., Debye length and Debye sphere) will be found to represent a subset of the most general parameters a plasma can possess.

Application of these new parameters to a solid will show the solid state plasma, although quantum mechanical in origin, can be treated as a weakly-coupled classical plasma at room temperature, in intrinsic germanium, silicon and gallium arsenide.

The Classical Plasma

A plasma is generally defined as an ionized gas of electronically quasi-neutral particles that exhibit a collective behavior in reaction to the surrounding environment [52]. The term quasi-neutral refers to a neutrality that occurs due to the kinetic action of the particles forming an electrostatic shield between unlike charges. As a result of this shielding, the potential field from a test charge placed in the plasma falls off faster than in a vacuum. This action is also a direct consequence of the kinetic energy of the particles being greater than the potential energy between particles. By solving Poisson's equation for a plasma, or looking at the ratio of kinetic and potential energies of the particles, a simple relationship evolves specifying a distance (similar to a skin depth) over which external potentials vanish. This action is known as Debye shielding and forms a critical concept necessary to the definition of a plasma. The term collective behavior describes how a plasma reacts as a single system to the surrounding environment in order to maintain its shielding characteristics.

In order to differentiate between a plasma and a collection of free particles, a set of criterion have been derived, based on classical grounds, to determine the degree of collective behavior in the presence of electromagnetic fields.

The simplest criterion deals with the Debye length. If the entire system of charges is larger than the Debye length then Debye screening of external electromagnetic fields is meaningful. In CGS units the Debye length takes the form

$$\lambda_D \equiv \left(\frac{K_B T \epsilon}{4\pi n e^2}\right)^{\frac{1}{2}} \ll \text{ the systems's dimensions },\qquad (1)$$

where

K_B = Boltzmann's constant.

T = The carrier temperature.

n = The carrier density.

e = The electronic charge.

ϵ = The material's dielectric constant.

A second criterion determines if there are enough charge carriers within a sphere of radius equal to the Debye length to accomplish shielding of external fields. This criterion can be derived from the carrier density and the definition of a sphere to arrive at

$$N_D = \frac{4}{3} n \pi \lambda_D^3 \gg \quad 1 \text{ electron }.\qquad (2)$$

The final criterion deals with a plasma's ability to possess collective behavior that is not swamped out by its own random collisions. To fulfill this criterion, the product of the frequency of oscillation in the plasma (ω) and the mean time between collisions (τ) must be greater than unity. This relationship can be written as

$$\omega\tau > 1. \tag{3}$$

These criteria (λ_D , N_D and $\omega\tau$), also detail general characteristics of a plasma that are useful in dealing with the scale and types of flux and forces at work in a plasma. It is easy to graph these relations to see the general scope that plasmas cover using these classical criteria. Figure 12 clearly shows known plasmas exist for a broad range of temperatures and carrier densities. It is also clear that the dominant forces driving any particular plasma will differ depending on the plasma's characteristics. For example, at low temperatures coulomb forces are important while at high temperatures thermal forces dominate. At high densities quantum mechanical forces cannot be ignored, while at low densities carriers act as a free classical gas.

Since the plasma criteria discussed above are for a classical plasma (i.e., a gas that follows Maxwell-Boltzmann statistics) we cannot apply them directly to plasmas where quantum mechanical effects become dominant, as they would in a solid state plasma. Thus, we will have to derive new criteria for the solid state plasma.

The Solid State Plasma Criteria

The primary distinction between a classical gas and a quantum mechanical gas is the distribution of carriers with

Figure 12. Plots of classical plasma parameters. Part a is a plot of the Debye length in meters versus the concentration. Part b is a plot of the concentration within the Debye sphere versus concentration.

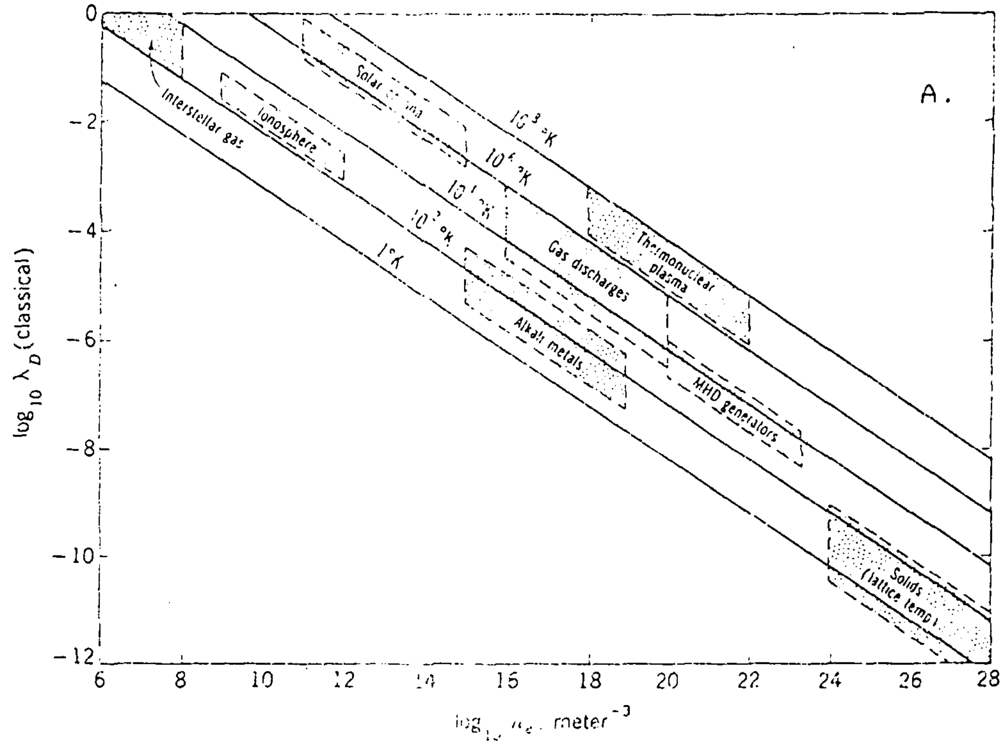
A.
log₁₀ λ_D (classical)
log₁₀ n_e, meter⁻³
0
-2
-4
-6
-8
-10
-12
6
8
10
12
14
16
18
20
22
24
26
28
Interstellar gas
Ionosphere
Solar corona
10⁸ °K
10⁶ °K
10⁴ °K
10² °K
1°K
Thermonuclear plasma
Gas discharges
Alkali metals
MHD generators
Solids (lattice temp)

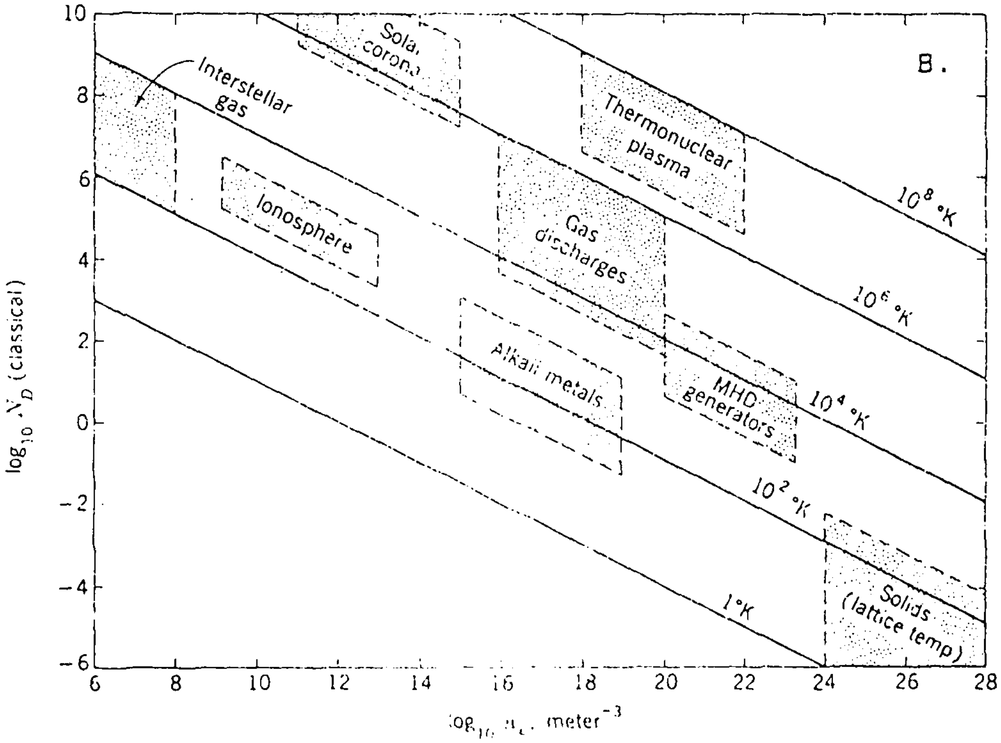
B.
log₁₀ N_D (classical)
log₁₀ n_e, meter⁻³
10
8
6
4
2
0
-2
-4
-6
6
8
10
12
14
16
18
20
22
24
26
28
Interstellar gas
Solar corona
Ionosphere
Thermonuclear plasma
Gas discharges
Alkali metals
MHD generators
Solids (lattice temp)
10⁸ °K
10⁶ °K
10⁴ °K
10² °K
1°K

the system's possible energy states. A classical gas reflects a Maxwell-Boltzmann distribution while a quantum mechanical gas reflects a Fermi-Dirac distribution (since we are dealing with electrons as the prime carriers within a solid).

This distinction is important, since the classical gas was the basis for the previously reviewed plasma criteria. Simple re-application of those criteria is meaningful, if the carriers present in a material can be treated using Maxwell-Boltzmann statistics. If conditions do not exist to favor a Maxwell-Boltzmann distribution the gas may be affected by quantum mechanical effects, and a quantum mechanical distribution would be required.

To accommodate this possibility it is necessary to be able to distinguish between plasmas utilizing a classical or a quantum mechanical approach [53,54]. The simplest dividing post is a comparison of the chemical potential or Fermi energy and the thermal energy. Classically, we have the kinetic energy

$$E = \frac{p^2}{2m}. \tag{4}$$

The De Brogile relation $p = \hbar k$ allows us to rewrite equation 4 to arrive at

$$E_F = \frac{\hbar^2 k^2}{2m}. \tag{5}$$

Where E_F is the Fermi energy. The Fermi energy generally represents the energy of carriers from a quantum mechanical perspective. Comparison of the Fermi energy and a classical kinetic energy would determine which perspective dominates carrier activity. A simple calculation shows that the Fermi energy for copper is around 6.9 eV compared to the thermal energy at room temperature of about 0.021 eV. Quantum mechanical effects certainly cannot be ignored since the energy from a quantum mechanical perspective is over 300 times greater than the classical kinetic energy. If we express the Fermi energy, via the De Brogile relationship, as a temperature, we arrive at the familiar equation for the De Brogile wavelength

$$\lambda_{DB}^2 = \frac{\hbar^2}{2\pi m^* K_B T}. \tag{6}$$

Where

m^* = The effective mass.

T = The carrier temperature.

The effective mass reflects the quantum mechanical effect of the carrier moving through the lattice potentials, which alter the carrier's response to an external electromagnetic field.

If the average distance between carriers is on the order of, or smaller than λ_{DB} , the gas is quantum mechanical in behavior. In explicit terms we can define this as

$$\Lambda \equiv \lambda_{DB} n^{1/3}. \tag{7}$$

If Λ is greater than or equal to unity, the gas is quantum mechanical and if Λ is much smaller than unity, it behaves like a classical gas. Use of the De Brogile wavelength gives a well known rule of thumb measure of the quantum mechanical effects that could occur in various situations. Application of the relationship shows quantum mechanical effects dominate at high densities and low temperatures. At low densities and high temperatures, quantum mechanical effects are minimized. This criterion allows a distinction to be made between a classical plasma and a quantum mechanical plasma.

Our Debye sphere (equation 2) requirement could be rewritten as

$$N_D = \frac{4}{3}\pi n \lambda_{DB}^3 = \Gamma^{-1}, \tag{8}$$

where Γ must be less than unity to satisfy the criterion for a classical plasma. Inherent in this derivation is the understanding that the potential energy between two carriers is small compared to their kinetic energy. This can be seen by taking the ratio of the two energies as follows (in CGS units)

$$\frac{\text{potential energy}}{\text{kinetic energy}} = \frac{2e^2 n^{\frac{1}{3}}}{3\epsilon K_B T}, \tag{9}$$

or

$$\Gamma^{\frac{2}{3}} \approx C \ \frac{\text{potential energy}}{\text{kinetic energy}}. \tag{10}$$

Where C is some constant and ϵ is the material's dielectric constant.

The new plasma parameter Γ reflects the fact that the potential energy between particles should be much smaller than the kinetic energy of a particle to satisfy our previous criteria for classical plasma behavior ($\Gamma << 1$ implies $N_D \gg 1$). A plasma with a Γ much smaller than unity is called a weakly-coupled plasma [55].

The case of Γ greater than or equal to unity corresponds to what is called a strongly-coupled plasma. This case does not have a classical analog since this type of plasma is controlled by the coulombic potential between individual particles. Inspection of equations 7 and 8 for a strongly-coupled plasma indicates a very high carrier density must be present [56] and quantum mechanical forces will dominate.

Very high carrier densities in a solid would see quantum mechanical affects from the lattice potentials and a spread in carrier momentums due to the Heisenburg Uncertainty Principle. We can quantify these affects on the kinetic energy as

$$E = \frac{(\triangle p)^2}{2m} \approx \frac{\hbar^2}{2m^*}\frac{1}{\triangle x^2} \approx \frac{\hbar^2}{2m^*}n^{2/3}. \quad (11)$$

Equation 11 can be restated in terms of the Fermi energy as

$$E_F = \frac{\hbar^2}{2m^*}\left(3\pi^2 n\right)^{2/3}. \quad (12)$$

To satisfy our definition of a plasma the potential energy between particles must be less than the kinetic energy. Taking the ratio of potential to kinetic energies yields

$$\frac{V}{E_F} = \frac{\frac{e^2 n^{1/3}}{\epsilon}}{\frac{\hbar^2}{2m^*}\left(3\pi^2 n^{2/3}\right)} = C_p, \quad (13)$$

$$C_p = \frac{2m^*\varepsilon^2}{\hbar^2\epsilon(3\pi^2)^{2/3}n^{1/3}}. \quad (14)$$

The ratio C_p is equivalent to the inverse of the Debye sphere in a classical plasma, but, since the plasma is quantum mechanical in origin, it is called a degenerate plasma. If C_p is less than or equal to unity, the plasma is a weakly-coupled degenerate plasma (analogous to $N_D \gg 1$ in a classical plasma). If C_p is greater than unity then the plasma is a strongly-coupled degenerate plasma (which has no classical counterpart). C_p can also be arrived at by comparing the radius of the effective Bohr orbit (for n = 1) to the interparticle spacing as,

$$n^{1/3} = \frac{4}{3}\pi r_o^3, \tag{15}$$

$$a_o = \frac{\epsilon \hbar^2}{m^* e^2}, \tag{16}$$

and

$$\frac{r_o}{a_o} = \left(\frac{3}{4\pi}\right)^{\frac{1}{3}} \frac{m^* e^2}{\epsilon \hbar^2 n^{1/3}} = r_s. \tag{17}$$

Here, r_s is related to C_p by

$$r_s = \frac{3\pi}{2^{5/3}} C_p. \tag{18}$$

Liboff [57] calls r_s the quantum compression parameter. Values of r_s less than or equal to unity correspond to a weakly-coupled degenerate plasma and r_s values greater than unity corresponds to a strongly-coupled degenerate plasma. When r_s is greater than unity the plasma approaches a quantized state (plasmons are formed). Similar statements can be made for C_p .

We can now examine classical and degenerate plasmas in terms of the new plasma parameters.

As shown in figure 13, classical plasmas correspond to Λ and Γ much smaller than unity, that is, they are weakly-coupled classical plasmas. Degenerate, or quantum mechanical plasmas, are characterized by Λ equal to, or greater than unity. Application of r_s (or C_p) indicates the degree of quantization the degenerate plasma possesses. A value of r_s greater than unity indicates the plasma is highly quantized (plasmons form, equivalent to a strongly-coupled plasma), and values of r_s less than unity indicate the plasma is approaching the classical characteristics of a weakly-coupled plasma.

Redrawing the plots of figure 12 in terms of the quantum degeneracy parameter, Λ ,the plasma coupling parameter, Γ , and the quantum compression parameter, r_s indicates how the carrier distributions for a system of particles dictates the type of plasma behavior obtained.

Figure 14 shows a plot of concentration versus the quantum degeneracy parameter. This plot shows how specific

Figure 13. Relationships for the new plasma parameters. These relationships are more general than those utilized for a classical plasma alone.

	QUANTUM DEGENERACY PARAMETER	CLASSICAL PLASMA (coupling) PARAMETER
CLASSICAL PLASMA	$\Lambda \ll 1$	weakly coupled $\Gamma \ll 1$
		strongly coupled $\Gamma \geq 1$
DEGENERATE PLASMA	$\Lambda \geq 1$	weakly coupled r_s or $C_p \leq 1$
		strongly coupled r_s or $C_p \gg 1$
	QUANTUM DEGENERACY PARAMETER	QUANTUM COMPRESSION PARAMETER

Figure 14. Plot of the concentration versus quantum degeneracy parameter. Areas where known plasmas may exist are indicated. The key is as follows: a = solar corona, b = gaseous discharge, c = interstellar gas, d = semiconductors, e = thermonuclear plasma, f = metals, g = Jovian interior, h = red giant star interior.

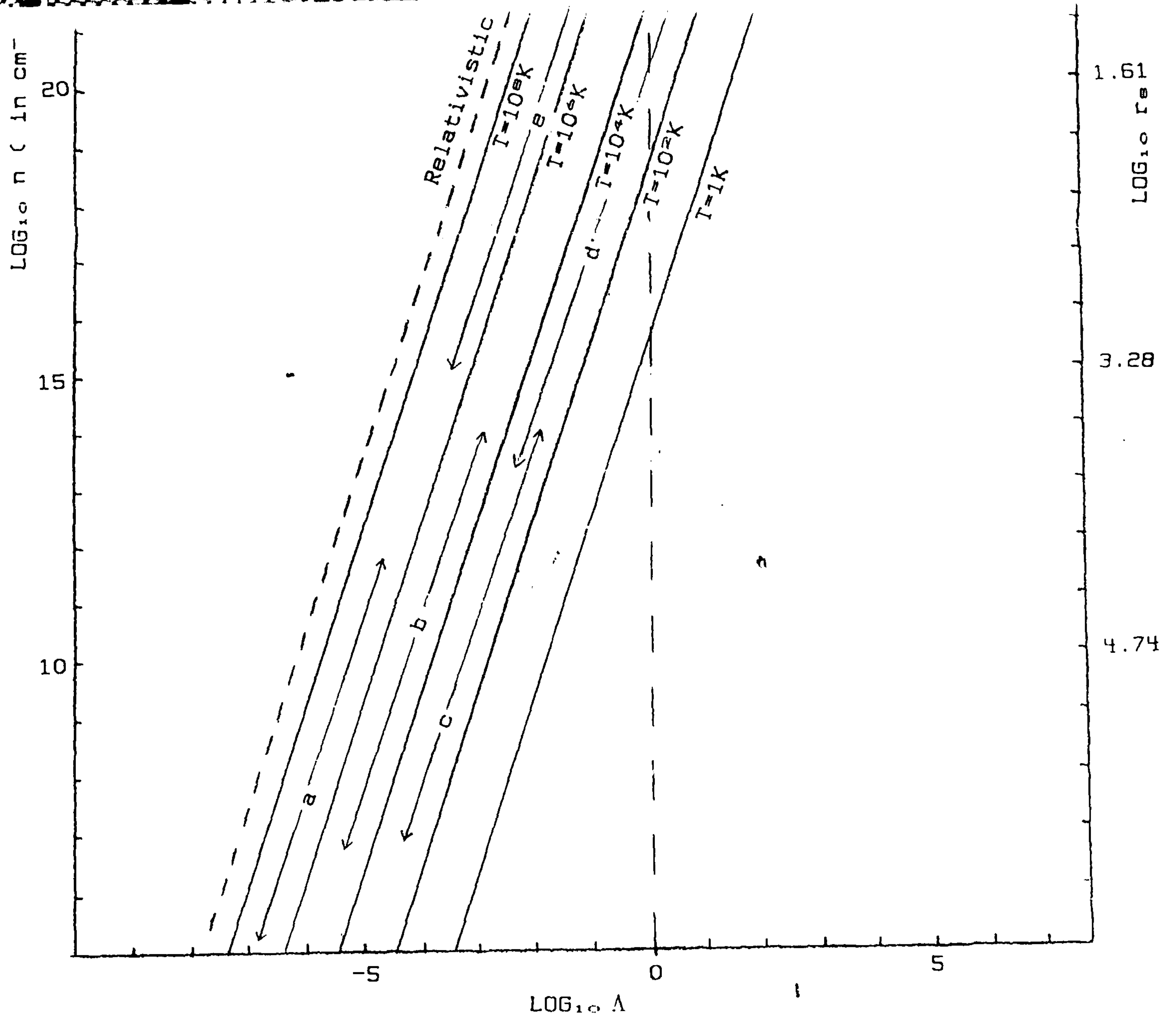
LOG₁₀ n (in cm⁻
20
15
10
-5
0
5
LOG₁₀ Λ
LOG₁₀ rₛ
1.61
3.28
4.74
Relativistic
T=10⁸K
e
T=10⁶K
d
T=10⁴K
T=10²K
T=1K
a
b
c

A

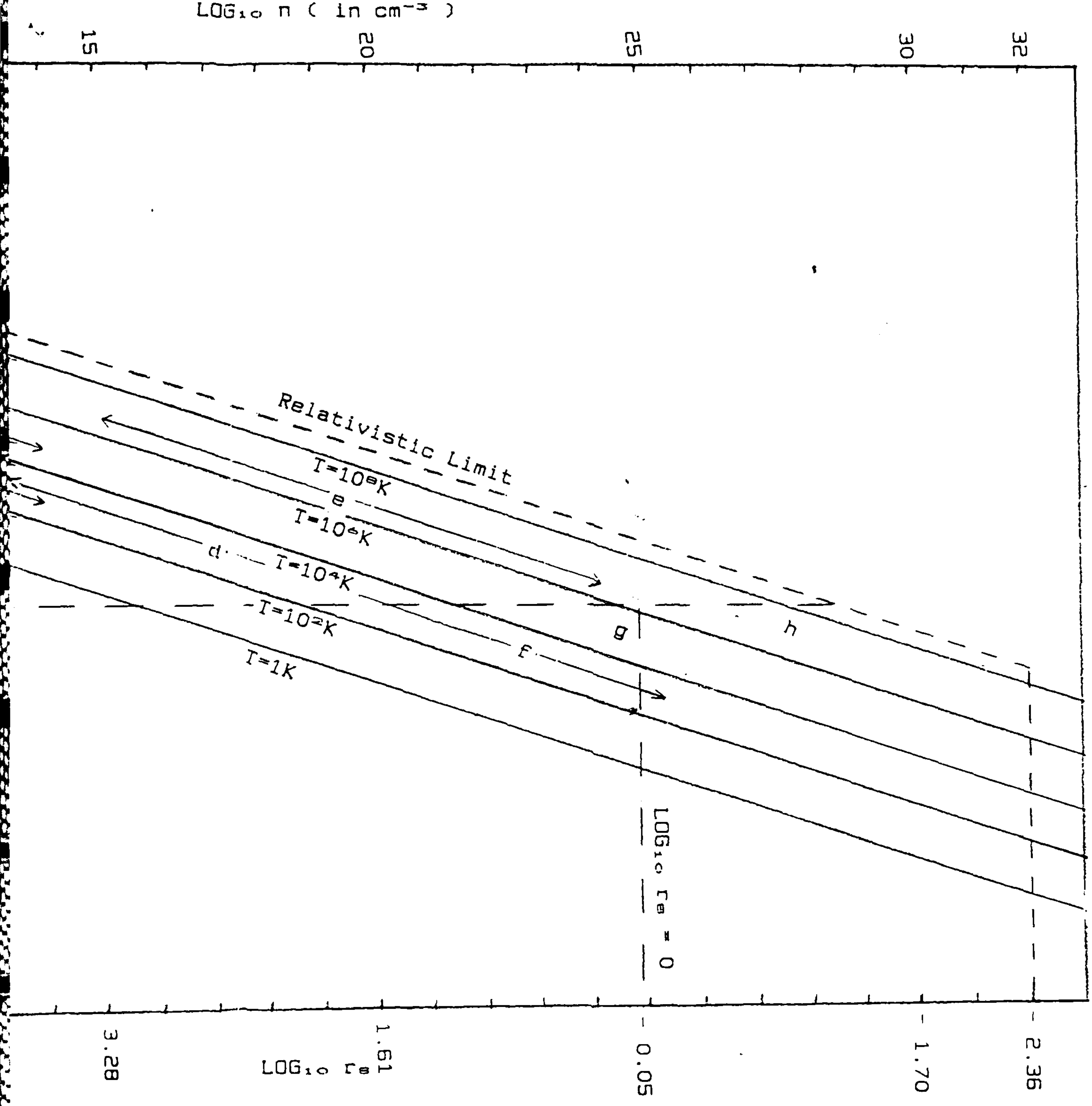

LOG₁₀ n (in cm⁻³)
15
20
25
30
32
Relativistic Limit
T=10⁸K
e
T=10⁶K
d
T=10⁴K
T=10²K
T=1K
g
h
f
LOG₁₀ rs = 0
3.28
1.61
-0.05
-1.70
-2.36
LOG₁₀ rs

B

details, such as the concentration and temperature, result in either a classical or degenerate plasma. The quantum compression parameter shows how solid state plasmas vary from a highly quantized plasma in a metal, to a classical plasma in some semiconductors.

Figure 15 shows a plot of the carrier concentration versus the plasma coupling parameter. This plot indicates the close analogy between r_s and Γ as they are applied to a degenerate or classical plasma. For a solid state plasma with low carrier concentrations we can utilize classical results, since this area corresponds to a weakly-coupled plasma.

These graphs indicate that in order to call a collection of particles a plasma they must exhibit collective behavior in some surrounding environment. For example, an interstellar gas, such as the solar wind, may have a concentration of 5 electrons per cubic centimeter. With an electron temperature around 50 eV and an ion temperature near 10 eV the Debye length for the solar wind is around 24 meters and the Debye sphere criteria is satisfied. Yet, the solar wind does not qualify as a classical plasma until we talk of scales much larger than 24 meters. At these scales, the kinetic energy of the particles are much larger than the potential energy of interaction, which satisfies our definition of a plasma.

Similar reasoning applies to a solid state plasma. Calculations of the Debye length for electrons in a

Figure 15. Plot of the concentration versus the plasma parameter for classical coupling. Some areas where known plasmas may exist are indicated. The key is as follows: a = solar corona, b = gaseous discharge, c = interstellar gas, d = semiconductors, e = thermonuclear plasma, f = metals, g = Jovian interior, h = red giant star interior.

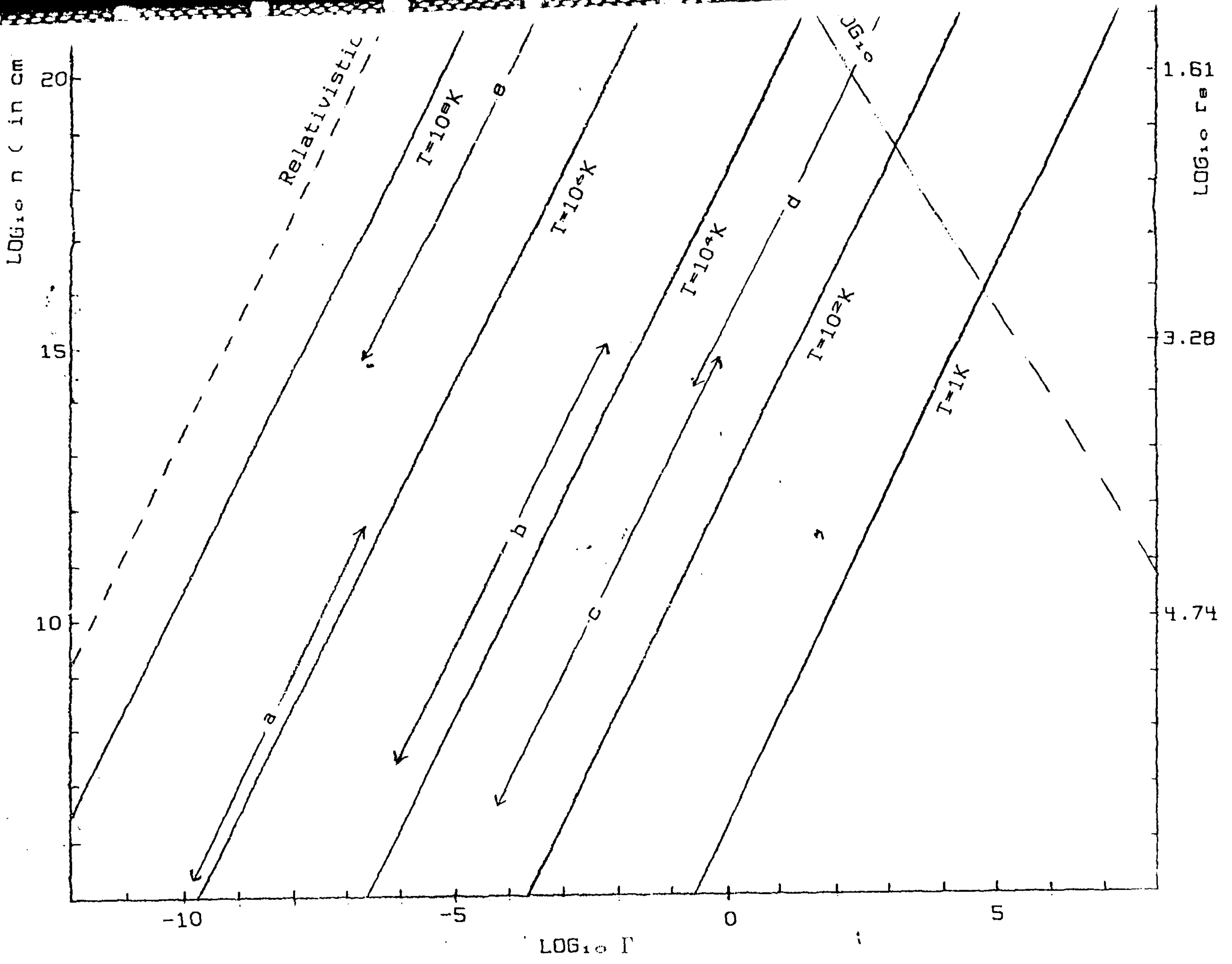
LOG₁₀ n (in cm
20
15
10
Relativistic
T=10⁸K
e
T=10⁶K
T=10⁴K
d
T=10²K
T=1K
LOG₁₀
a
b
c
-10
-5
0
5
LOG₁₀ Γ
1.61
3.28
4.74
LOG₁₀ rₑ

A

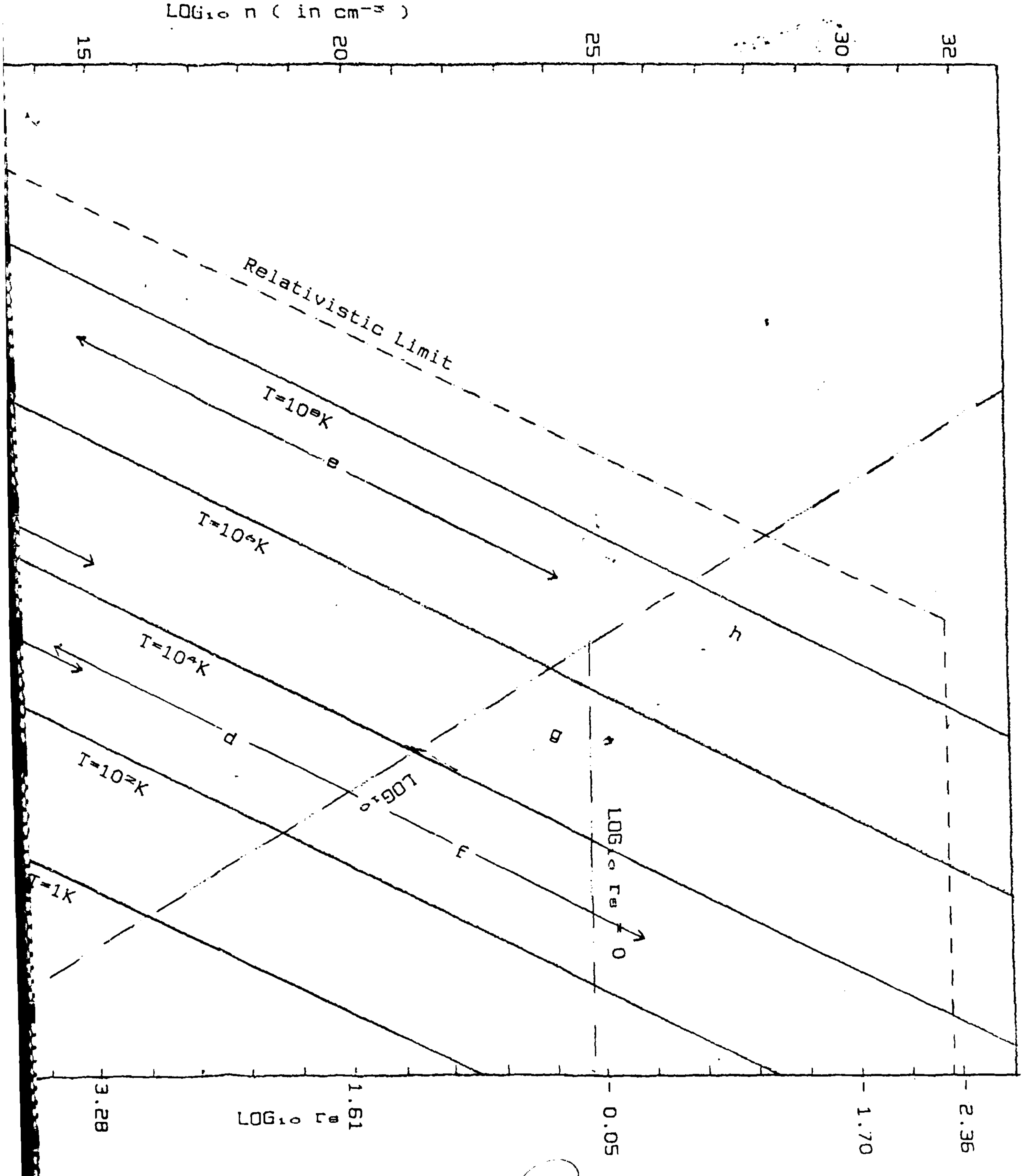
LOG₁₀ n (in cm⁻³)
15
20
25
30
32
Relativistic Limit
T=10⁸K
T=10⁶K
T=10⁴K
T=10²K
T=1K
e
d
f
g
h
LOG₁₀ r
LOG₁₀ rₛ = 0
LOG₁₀ rₛ
3.28
1.61
-0.05
-1.70
-2.36

B

semiconductor yield values that are small compared to a laboratory sample scale. But, such samples barely satisfy the Debye sphere criterion. Large carrier concentrations force us to account for the quantum mechanical source of the plasma. That source is the lattice. At values of the quantum compression parameter near unity the effect of the ion potentials of the lattice are nil on the plasma, and we have a weakly-coupled plasma. At larger values of the compression parameter, the plasma is strongly-coupled, or, the presence of the lattice determines the plasma's character. In other words, the solid state plasma is a plasma because of the lattice. Remove the lattice, or speak of scales very large compared to the solid state plasma, and plasma behavior disappears.

With these ideas in mind, similar graphs can be produced for the semiconductors of interest in this study. Those semiconductors are: germanium, silicon and gallium arsenide. Results are shown on figures 16, 17 and 18 respectively. These semiconductors are used often in semiconductor devices and graphs of the quantum degeneracy parameter versus concentration shows what plasma characteristics we could expect.

These graphs demonstrate that most of the plasma regime for these semiconductors is classical in nature. This result is quite consistent with the Fermi-Dirac distribution these semiconductors follow.

Figure 16. Plot of the concentration versus the quantum degeneracy parameter for germanium.

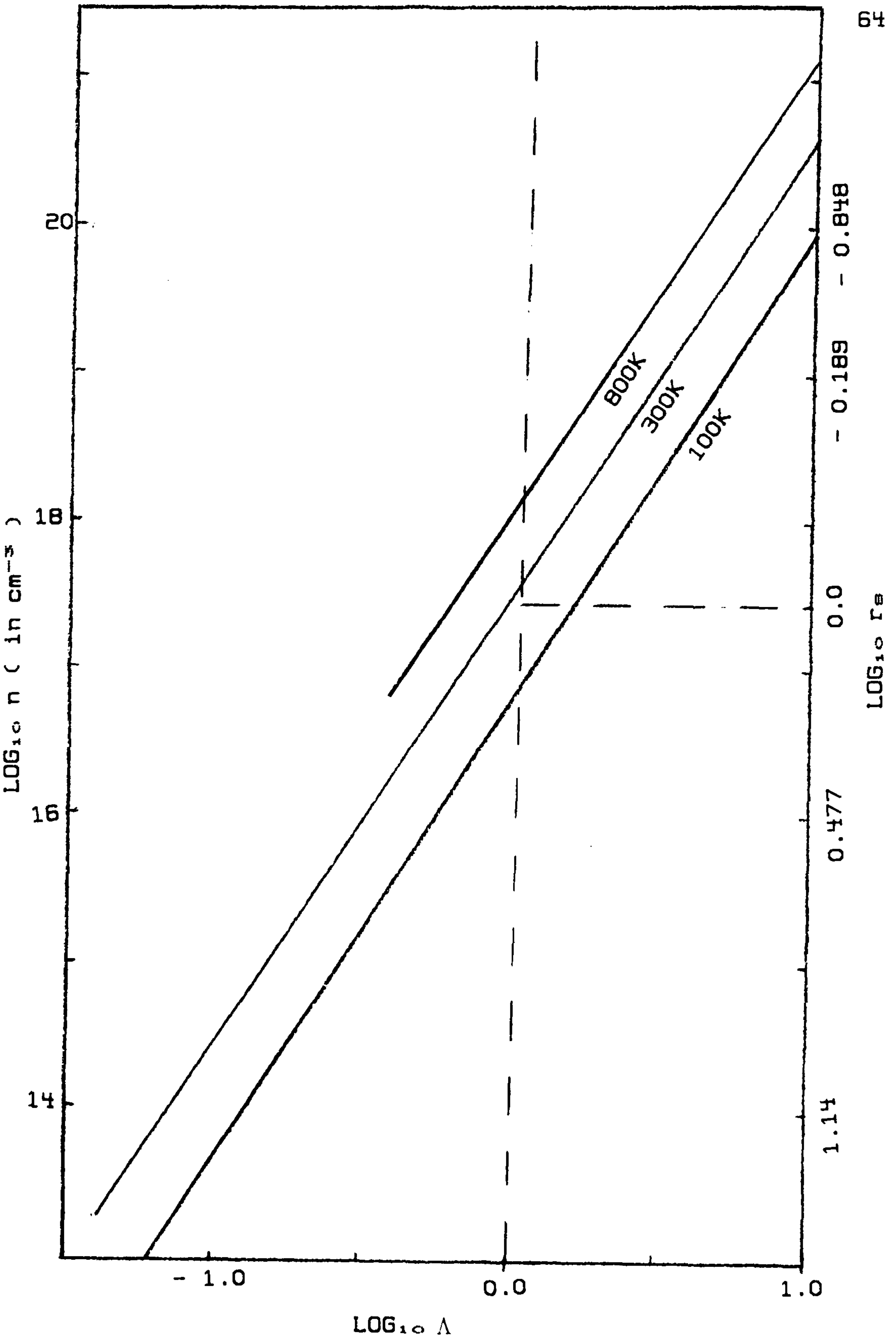
LOG₁₀ n (in cm⁻³)
20
18
16
14
800K
300K
100K
- 1.0
0.0
1.0
LOG₁₀ Λ
- 0.848
- 0.189
0.0
0.477
1.14
LOG₁₀ r_s

Figure 17. Plot of the concentration versus the quantum degeneracy parameter for silicon.

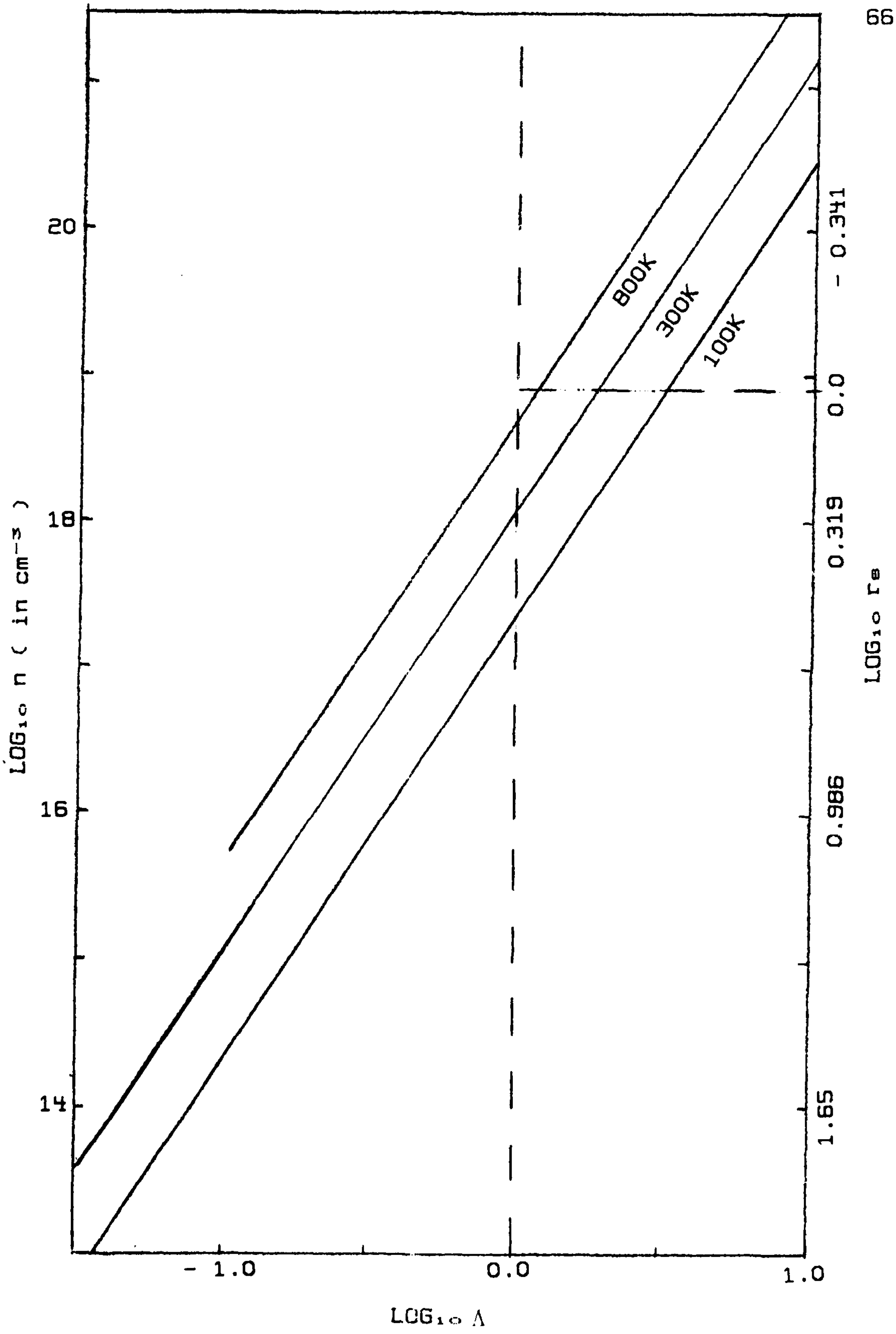
20
18
16
14
LOG₁₀ n (in cm⁻³)
- 1.0
0.0
1.0
LOG₁₀ Λ
800K
300K
100K
- 0.341
0.0
0.319
0.986
1.65
LOG₁₀ rs

Figure 18. Plot of the concentration versus the quantum degeneracy parameter for gallium arsenide.

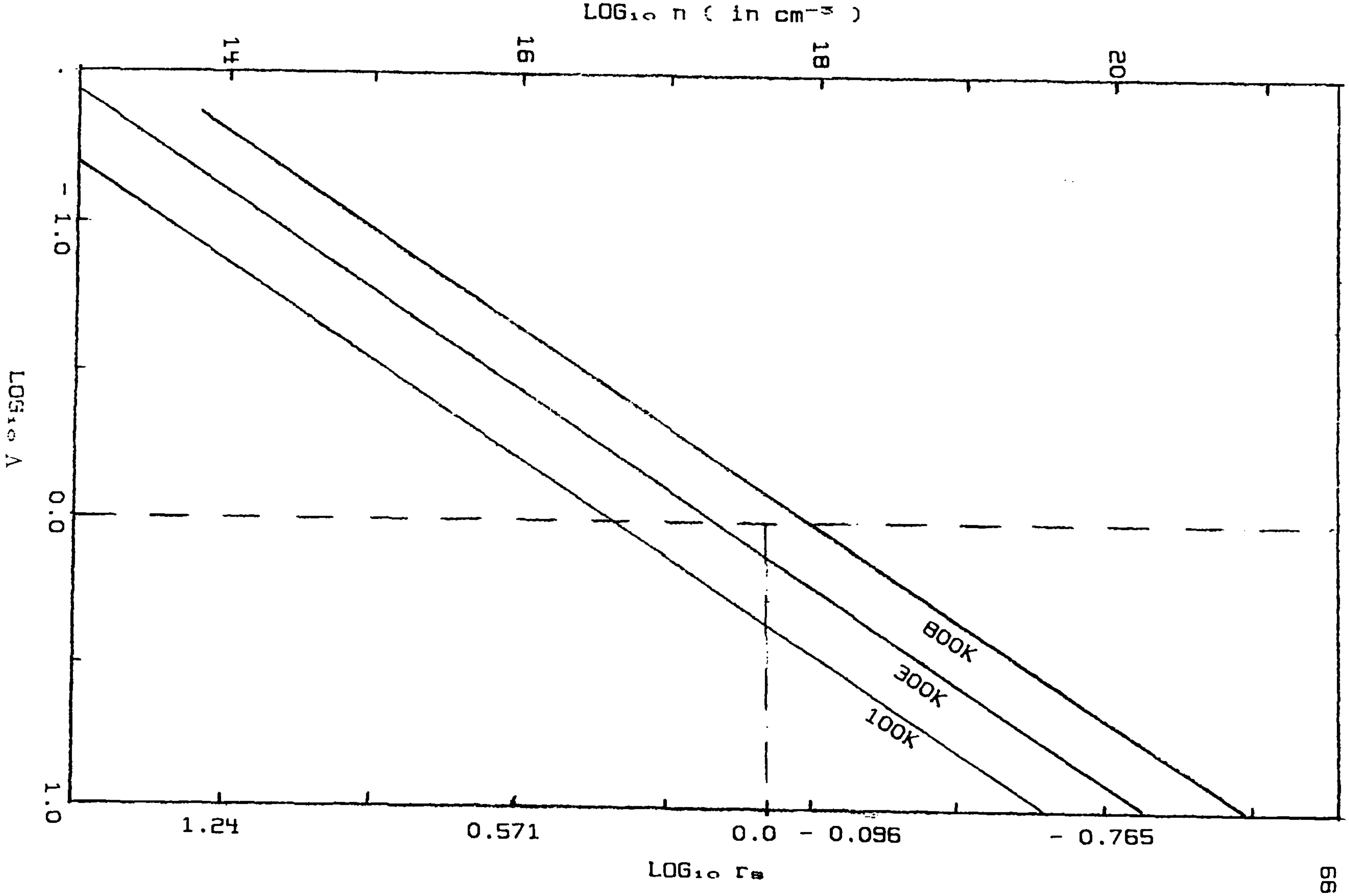
LOG₁₀ n (in cm⁻³)
14
16
18
20
LOG₁₀ Λ
-1.0
0.0
1.0
800K
300K
100K
1.24
0.571
0.0
-0.096
-0.765
LOG₁₀ rₛ

Due to the structure of this distribution, only carriers in the tail of the distribution contribute to the semiconductor's electrical properties for temperatures greater than zero. Yet, the tail of the Fermi-Dirac distribution falls off approximately like a Maxwell-Boltzmann distribution. Therefore, the conclusions, showing classical plasma behavior, drawn are is not in error.

It is also interesting to observe the effect, in figures 16, 17 and 18, of the effective mass and the dielectric constant on solid state plasma behavior. In most semiconductors the effective mass is usually less than unity and the dielectric constant is greater than unity. The combined effect of these variables has a general tendency to move the solid state plasma in semiconductors toward greater degeneracy (or metallic behavior) at low temperatures or large concentrations.

By analogy with a classical plasma, we would also expect a classically treated solid state plasma to be most sensitive to large scale perturbations (on the scale of the plasma in the sample). Highly degenerate solid state plasmas would be more sensitive to variations in the distribution of carriers.

Instabilities at the sample size could be modeled using macroscopic approaches, like magnetohydrodynamics. Instabilities at the carrier distribution level would require modeling using kinetic theory via the Boltzmann equation.

This analogy between classical and solid state plasmas will allow us to model solid state plasmas in close correspondence to weakly coupled gaseous plasmas. This will certainly be true for hydrodynamic instabilities. Kinetic modeling may be similar, but, care would have to be exercised since the recombination-generation mechanisms present, in either case, are not analogous.

CHAPTER III

ANALYSIS OF SPECIFIC NEGATIVE RESISTANCE IN SOLIDS PROPOSED BY RIDLEY

B. K. Ridley's paper [26] on specific negative resistance is central to understanding the conditions surrounding CCNR. Ridley utilized an approach based on arguments from irreversible thermodynamics, applied to a situation where a general CCNR characteristic occurs. Knowledge of the general tendencies that occur in CCNR could then be applied to second breakdown.

This chapter will examine the basic equations of motion in irreversible processes to allow a quantification of the CCNR state in terms of specific variables such as the current, electric and magnetic fields, and thermal forces. This information is necessary in order to obtain boundary conditions to model current flow as a solid state plasma.

Ridley's arguments will also be examined in the light of criticisms put forth by Volkov and Kogan [59], and a later paper by Takeyama and Kitahara [60], which casts doubts on the validity of Ridley's approach compared to the previous work of De Groot and Prigogine.

De Groot's derivation will be shown first and compared to Ridley's derivation.

In-depth Analysis of De Groot's Derivation of the Equations of Motion in Irreversible Processes of Continuous Systems

The state variables of a continuous system can depend on time and space. For a semiconductor, this is certainly true if temperatures (of the lattice and carriers) are allowed to vary due to external driving forces, such as, the electric field and current. These various driving forces and fluxes are fundamental variables relating conservation of mass, energy, balance of forces and Gibb's equation. The usual forms for these relationships are

$$\frac{\partial \rho}{\partial t} + \nabla \cdot (\rho \vec{v}) = 0, \tag{19}$$

$$\frac{D}{Dt}(\frac{1}{2}\rho v^2 + \rho U) = \vec{F} \cdot \vec{v} - \nabla \cdot (P\vec{v} + \vec{J}_q) \tag{20}$$

$$\rho \frac{d\vec{v}}{dt} = -\nabla \vec{P} + \vec{F}, \tag{21}$$

$$T\frac{dS}{dt} = \frac{dU}{dt} + P\frac{dV}{dt} - \sum_k \mu_k \frac{D\rho_k}{Dt}. \tag{22}$$

where the variables are identified as

ρ = mass density,

$\vec{v}$ = velocity,

$\frac{D}{Dt}$ = convective derivative,

$\vec{J}_q$ = heat flow,

$\vec{F}$ = external forces,

U = internal energy (per unit volume),

V = volume,

T = temperature,

S = entropy(per unit volume),

P = pressure,

μ_k = chemical potential for species k.

The general procedure relating the various driving forces and their resultant fluxes has been derived by De Groot[67] and is repeated here. De Groot's goal is to arrive at a continuity equation for the entropy flows. If a stationary state (a non--equilibrium state of an open system) exists, the principle of least entropy production can be applied to the entropy flows to determine the general direction the state variables will take.

The law of conservation of mass is written as

$$\frac{\partial \rho_k}{\partial t} + \nabla \cdot (\rho_k \vec{v}_k) = \nu_c J_c = \frac{1}{V}\frac{dM_k}{dt}. \tag{23}$$

where

J_c = chemical reaction rate in mass per unit volume and time.

ρ_k = mass density of the kth component,

$\vec{v_k}$ = velocity of the kth component,

M_k = mass of the kth component,

$\sum_c \nu_c$ = stoichiometric number of components.

Summing equation 23 over k yields

$$\frac{\partial \rho}{\partial t} = -\nabla \cdot \rho \vec{v}, \qquad (24)$$

where we have used the center of mass velocity $\vec{v}$ defined as

$$\vec{v} = \frac{\sum_k \rho_k \vec{v_k}}{\rho}. \qquad (25)$$

De Groot also introduces a component flow with respect to the center of mass movement

$$\vec{J_k} = \rho_k(\vec{v_k} - \vec{v}). \qquad (26)$$

Equation 26, with the definition of the convective derivative, allows the equation of conservation of mass to be rewritten as

$$\frac{d\rho_k}{dt} = \nu_k J_c - \rho_k \nabla \cdot \vec{v} - \nabla \cdot \vec{J}_k, \tag{27}$$

or, from equation 24,

$$\frac{d\rho_k}{dt} = \nu_k J_c - \nabla \cdot \vec{J}_k, \tag{28}$$

where we have used

$$c_k \equiv \frac{\rho_k}{\rho} \equiv \quad \text{concentration.} \tag{29}$$

Conservation of momentum can be written as a balance of forces in the form

$$\rho \frac{d\vec{v}}{dt} = -\nabla P + \sum_k \vec{F}_k \rho_k. \tag{30}$$

Here $\vec{F}_k$ is the external force per unit mass. We could write this $\vec{F}_k$ as

$$\sum_k \vec{F}_k \rho_k = \sum_k \vec{F}_k \quad \text{(per unit volume)}, \tag{31}$$

but, De Groot is writing the equation for a chemical reaction where mass is a more important variable.

Conservation of energy is written as

$$\rho\frac{d}{dt}\left(\frac{1}{2}\vec{v}\cdot\vec{v}+U\right)=-\nabla\cdot\left(P\,\vec{v}+\vec{J}_q\right)+\sum_k\vec{F}_k\cdot\vec{v}_k\rho_k, \qquad (32)$$

for $\vec{J}_q$ representing a heat flow (usually electrical in origin) and P is the pressure reduced to a scaler quantity from its tensor quality.

Gibb's equation is the final piece of the puzzle necessary to connect all of the important state variables.

$$T\frac{dS}{dt}=\frac{dU}{dt}+P\frac{dV}{dt}-\sum_k\mu_k\frac{dc_k}{dt}. \qquad (33)$$

Again, we have the state variables S, U and P are per unit mass.

We can take the force balance equation (equation 30), multiply by the center of mass velocity $\vec{v}$, and subtract the equation for conservation of energy to obtain

$$\rho\frac{dU}{dt}=-P\rho\nabla\cdot\vec{v}-\nabla\cdot\vec{J}_q+\sum_k\vec{F}_k\cdot\vec{J}_k. \qquad (34)$$

This equation, plus the equation of conservation of mass-(using c_k), can be substituted into Gibb's equation to yield

$$\rho T\frac{dS}{dt}=-\nabla\cdot\vec{J}_q+\sum_k\vec{F}_k\cdot\vec{J}_k+\sum_k\mu_k\nabla\cdot\vec{J}_k-J_c\sum_k\mu_k\nu_k. \qquad (35)$$

De Groot rearranges this equation to explicitly show the thermodynamic driving forces with their conjugate fluxes

$$\begin{aligned}\rho\frac{dS}{dt} &= -\nabla\left(\frac{\vec{J}_q - \sum_k \mu_k J_k}{T}\right) + \frac{\vec{J}_q \cdot \vec{X}_u + \sum_k \vec{J}_k \cdot \vec{X}_k + AJ_c}{T} . \\ &= -\nabla \cdot \vec{J}_s + \Xi\end{aligned} \tag{36}$$

where

$\vec{X}_u = -\frac{1}{T}\nabla T$, the thermal driving force,

$\vec{X}_k = \vec{F}_k - T\nabla\left(\frac{\mu_k}{T}\right)$, the diffusion force,

$A = -\sum_k \mu_k \nu_k$, the chemical affinity,

$\vec{J}_s$ = the entropy flow,

Ξ = entropy production.

We can now arrive at the simpler form

$$\rho\frac{dS}{dt} = \frac{\partial S_v}{\partial t} + \nabla \cdot S_v\vec{v}, \tag{37}$$

where S_v is the entropy per unit volume.

Equation 36 can be reformed as

$$\frac{\partial S_v}{\partial t} = -\nabla \cdot \left(\vec{J}_s + S_v\vec{v}\right) + \Xi. \tag{38}$$

Now, the total entropy flow contains a convective term also.

Equation 38 is in the form of a continuity equation for entropy flow. The entropy production term, Ξ ,comes from the irreversible processes that occur as heat conduction, diffusion or chemical reactions. Since the velocity $\vec{v}$ is not in Ξ , the bulk motion of the system is considered a reversible phenomenon.

We now apply equations 36 and 38 to a system where electrical conduction occurs to determine if the continuity equation for entropy changes form. Since no chemical reaction occurs we can drop the chemical affinity from the equations. The external forces due to an applied potential or electric field in a solid are

$$\vec{F_k} = q_k \vec{E} = -e_k \nabla \phi. \tag{39}$$

Here, the electric potential is ϕ and e_k is the charge (charge per unit mass) on the kth component of concern. In a solid the applied potential also alters the chemical potential or Fermi level. Thus, the chemical potential takes the form

$$\tilde{\mu_k} = \mu_k + e_k \phi. \tag{40}$$

The internal energy must also include the added electrical energy of the carriers as

$$\bar{U} = U + e_k c_k \phi. \qquad (41)$$

The thermodynamic flux, or energy flow $\bar{J}_q$, must now include a contribution from the current where

$$\sum_k e_k \vec{J}_k \phi = \vec{I} \phi, \qquad (42)$$

and $\vec{I}$ is the total current density. Following De Groot's procedure, just outlined to arrive at the entropy rate equation, we start with balance of forces

$$\rho \frac{d\vec{v}}{dt} = \sum_k \bar{F}_k \rho_k - \rho \sum_k e_k c_k \nabla\phi - \nabla \cdot \overleftrightarrow{P} . \qquad (43)$$

The $\bar{F}_k$ term contains the external non-electrical forces.

The energy equation becomes

$$\rho \frac{d}{dt}\left(\frac{1}{2}\vec{v}\cdot\vec{v} + \bar{U}\right) = -\nabla\cdot\left(\overleftrightarrow{P}\,\vec{v} + \bar{J}_q\right)$$

$$(44)$$

$$+ \sum_k \bar{F}_k \cdot \vec{v}_k \rho_k + \rho \sum_k e_k c_k \frac{\partial\phi}{\partial t}.$$

Gibb's equation, with electrical contributions, becomes

$$T\frac{dS}{dt} = \frac{d\tilde{U}}{dt} + P\frac{dV}{dt}$$

$$- \sum_k \tilde{\mu}_k \frac{dc_k}{dt} - \sum_k e_k c_k \frac{d\phi}{dt}. \tag{45}$$

Following De Groot's procedure we arrive at

$$\rho\frac{d\tilde{U}}{dt} = -P\nabla \cdot \vec{v} - \nabla \cdot \vec{J}_q$$

$$+ \sum_k \vec{F}_k \cdot \vec{J}_k + \sum_k e_k c_k \frac{d\phi}{dt}. \tag{46}$$

Substituting equation 46 and the convective derivative for the concentration into Gibb's equation results in the following form

$$\rho\frac{dS}{dt} = -\nabla \cdot \left(\frac{\vec{J}_q - \sum_k \tilde{\mu}_k \vec{J}_k}{T} + \frac{\vec{J}_q \cdot \vec{X}_u + \sum_k \vec{J}_k \cdot \vec{X}_k}{T}\right)$$

$$= -\nabla \cdot \vec{J}_s + \bar{\Xi}. \tag{47}$$

and

$$\bar{X}_k = \bar{F}_k - T\nabla\left(\frac{\bar{\mu}_k}{T}\right) = \vec{X}_k - e_k\phi\vec{X}_u \quad .$$

$$\bar{X}_k = \bar{F}_k - e_k\nabla\phi \qquad (48)$$

This is expanded further, using equation 48, as

$$\rho\frac{dS}{dt} = -\nabla\cdot\left(\frac{\vec{J}_q - \sum_k \mu_k\vec{J}_k}{T}\right)$$

$$+\frac{\vec{J}_q\cdot\vec{X}_u + \vec{J}_k\cdot\vec{X}_k}{T}. \qquad (49)$$

which is the form arrived at previously. The forces and fluxes derived for electrical conduction are invariant under a linear transformation of $\mu_k + e_k\phi$.

Analysis of Ridley's Derivation

We examine Ridley's derivation to insure that his procedure did not yield a result different then De Groot's results. Ridley's derivation starts with Gibb's equation where the variables have been expressed as per unit volume.

$$T\frac{dS}{dt} = \frac{dU}{dt} - \sum_k \mu_k \frac{d\rho_k}{dt}. \tag{50}$$

For a solid, the volume does not change under current conduction, which allows us to drop the work due to pressure and volume. The use of ρ_k comes from multiplying De Groot's previous form of Gibb's equation by ρ to change the variables to per unit volume.

Ridley introduces the additional electrical contributions of the chemical potential and internal energy as

$$\begin{aligned} \tilde{U} &= U + \sum_k e_k \rho_k \phi \\ &= \tilde{\mu_k} + e_k \phi \end{aligned} \tag{51}$$

Which is the same as De Groot's formulation. The energy balance equation can be written as

$$\begin{aligned} &\frac{dU}{dt} + \frac{d}{dt}\left(\sum_k e_k \rho_k \phi\right) \\ &= -\nabla \cdot \left(\vec{J}_q + \sum_k e_k \vec{J}_k \phi\right) + \sum_k e_k \rho_k \frac{d\phi}{dt}. \end{aligned} \tag{52}$$

This form matches De Groots formulation for the change in internal energy.

Ridley substitutes equations 51 and 52 into Gibb's equation to obtain a form similar to De Groot's formulation

$$\frac{dS}{dt} = -\nabla \cdot \left(\frac{\vec{J}_q - \sum_k \mu_k \vec{J}_k}{T} \right) + \frac{1}{T} \Big(\vec{J}_q \cdot X_q - \sum_k \mu_k \vec{J}_k \cdot \vec{X}_q \tag{53}$$

$$+ \vec{F} \cdot \vec{J} + \sum_k \vec{X}_k \cdot \vec{J}_k - \sum_k \mu_k \frac{\partial \rho_k}{\partial t} \Big).$$

where

$\vec{F} = -\nabla \phi$,

$\vec{J} = \sum_k e_k \vec{J}_k$,

$\vec{X}_q = -\vec{X}_u$,

$\vec{X}_k = -\nabla \mu_k$.

Ridley has broken the ohmic term $\vec{F} \cdot \vec{J}$ out explicitly in equation 53, and has allowed for local fluctuation of the mass density, an aspect De Groot did not allow. The formulation still demonstrates that the change in entropy is a sum of the negative divergence of flow and a positive production rate.

Conditions of the Stationary State

We can now apply the conditions of the stationary state to our entropy rate equations to determine the action of the state variables in the solid.

Prigogine [62] describes a stationary state as a condition where the state variables do not depend on time. Yet, the net mass flow is zero, and entropy production does not vanish. This is considered a non-equilibrium state of an open system as opposed to an equilibrium state of an isolated system where there is no entropy production (because all forces vanish).

In a sense, the non-equilibrium stationary state is similar to a steady state of the system with the condition that the entropy production rate is not zero.

Prigogine [63] characterizes the stationary state as a situation where we allow the transfer of matter and energy between two phases of a system at different temperatures such that the entropy production rate is positive, or

$$\frac{dS}{dt} = J_{th}X_{th} + J_m X_m > 0. \tag{54}$$

Onsager's equations allow us to view the fluxes and forces in terms of linear relations such that

$$J_{th} = L_{11}X_{th} + L_{12}X_m, \tag{55}$$

and

$$J_m = L_{21} X_{th} + L_{22} X_m . \tag{55}$$

For the stationary state, the mass flow is zero

$$J_m = L_{21} X_{th} + L_{22} X_m = 0. \tag{56}$$

Onsager's reciprocal relations require $L_{12} = L_{21}$ so that

$$\frac{dS}{dt} = L_{11} X_{th}^2 + 2L_{21} X_{th} X_m + L_{12} X_m^2 > 0. \tag{57}$$

If we take the derivative with respect to X_m at constant X_{th} we arrive at

$$\frac{\partial}{\partial X_m}\left(\frac{dS}{dt}\right) = 2\Big(L_{21} X_{th} + L_{22} X_m\Big) = 2J_m = 0. \tag{58}$$

Therefore, the two conditions

$$J_m = 0 \quad or \quad \frac{\partial}{\partial X_m}\left(\frac{dS}{dt}\right) = 0 \tag{59}$$

are equivalent as long as Onsager's equations are of linear form for the system.

The procedure followed above, where the stationary states are characterized by the conjugate flows being zero, is similar to the analogous mechanical situation where the conjugate momentums, of the forces, vanish. The stationary state defines a minimum for the entropy production rate and is referred to as the state of minimum entropy production. If a stationary state exists, then the entropy is independent of time and the entropy production rate must be balanced by the outward flow of entropy.

Application of the Stationary State by Ridley to the Case of CCNR

In this section we look at how Ridley applied the concept of the stationary state to his entropy rate equation. Ridley applies the idea of the stationary state to the situation of CCNR and VCNR by using the following argument[70].

> In the steady state $\frac{dS}{dt}$ [the total entropy change] is zero, as are the overall rates which appear in equations like
>
> $$\frac{d\tilde{U}}{dt} = -\nabla \cdot \vec{J}_u + \sum_k e_k \rho_k \frac{d\phi}{dt}$$
>
> and
>
> $$\frac{d\rho_k}{dt} = -\nabla \cdot \vec{J}_k + \frac{\partial \rho_k}{\partial t}$$
>
> and in each case the production is balanced by the divergence of the flow. At equilibrium both the production and flow are zero. Since it is to be expected that the steady state will be as near the

> equilibrium state as the various constants will allow, we expect the entropy production rate will be as small as possible. This plausible argument is at the basis of the principle of least entropy production.

The equilibrium Ridley talks about is a thermostatic equilibrium; all the driving forces vanish. This is not the case for the situation he wishes to portray. Why he has stated this is not clear and it may have contributed to later criticisms of the paper.

Following Prigogine's arguments, Ridley assumes we have a stationary state; no mass flow and a balance of entropy flow. Ignoring heat flows, the remaining term for the total change of entropy contains an entropy production rate which should be at a minimum value for a stationary state.

From equation 53, the remaining term for the entropy production rate is

$$\Xi = -\sum_k \frac{\mu_k \vec{J}_k \cdot \vec{X}_q}{T_k} + \frac{\vec{F} \cdot \vec{J}}{T_k}$$

$$+\sum_k \frac{\vec{X}_k \cdot \vec{J}_k}{T_k} - \sum_k \frac{\mu_k}{T_k}\frac{\partial \rho_k}{\partial t}. \qquad (60)$$

The T_k term allows different carrier species to have different temperatures. In a stationary state no mass flow occurs so $\vec{J}_k$ is zero. But, since the charge flow is in filaments(for CCNR) and layers(for VCNR) the mass flow is not

not zero for these structures. Furthermore, Ridley assumes that there is no temperature or chemical potential gradients in these structures. This implies that the driving forces $\vec{X_q}$ and $\vec{X_u}$ are zero. Since Ridley assumes these structures are stationary states, the rate of change of the structures at their interfaces must be equal, but opposite.

These arguments leave the joule heating term as the sole source of entropy production in the structures or

$$T\Xi = \vec{F} \cdot \vec{J} = \vec{F} \cdot \sum_k e_k \vec{J_k}. \tag{61}$$

Perturbation Under CCNR

For the case of CCNR Ridley explains the curve in figure 19 as a single filamentary structure with cross-section, a , which is a percentage of the total cross-section.

$$T\Xi = E_1 J_1(1 - a) + E_2 J_2 a, \tag{62}$$

where

$$J_1(1 - a) + J_2 a = J_0, \tag{63}$$

Figure 19. Current-voltage characteristic exhibiting current controlled negative resistance. *The figure is not drawn to scale.*

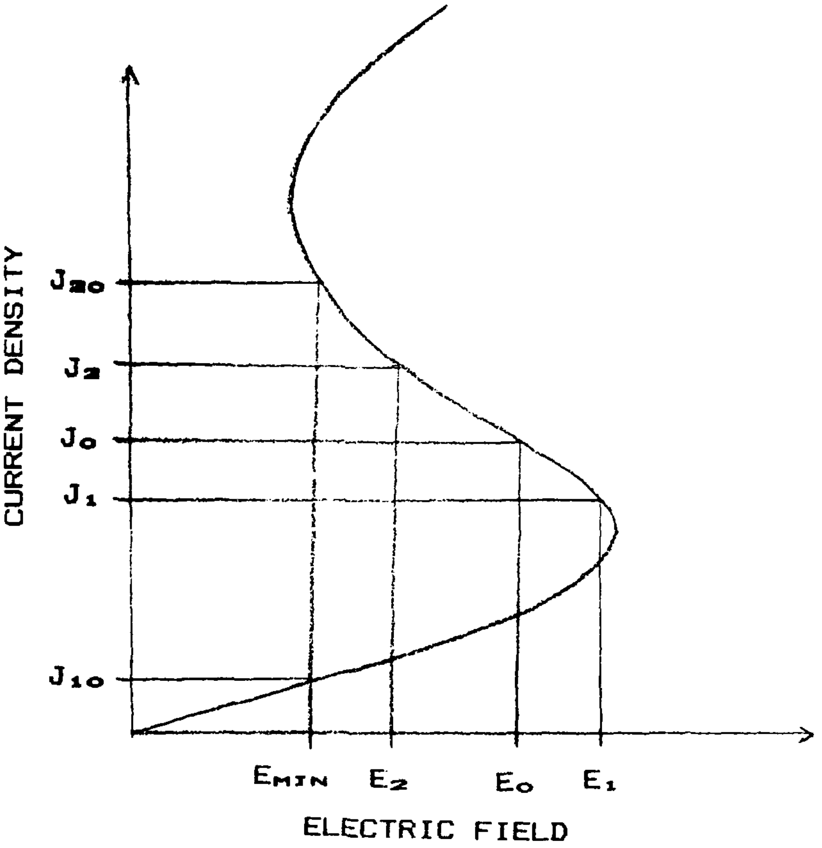
CURRENT DENSITY
J20
J2
J0
J1
J10
EMIN
E2
E0
E1
ELECTRIC FIELD

and

$$\delta J_1(1-a)+\delta J_2 a=0. \tag{64}$$

We now apply a perturbation through the field variables as required by Prigogine's results for equation set 59.

$$E_1=E_0+\delta E_1, \qquad E_2=E_0+\delta E_2. \tag{65}$$

$$J_1=J_0+\frac{dJ}{dE}\delta E_1, \qquad J_2=J_0+\frac{dJ}{dE}\delta E_2. \tag{66}$$

to arrive at

$$T\delta\Xi=\frac{(1-a)}{a}\frac{dJ}{dE}\delta E_1^2. \tag{67}$$

When $\frac{dJ}{dE}$ is negative, as seen in experiment, the production rate decreases and filamentary structures are favored. This is in accord with Prigogine's statement that the contribution of the rate of change of forces to the total entropy production is negative or zero in a stationary state. But, Prigogine [64] states that this is true only under the following conditions.

1. Linear phenomenological laws apply.

2. Onsager's reciprocal relations are valid.

3. Phenomenological coefficients can be treated as constants.

Violation of these conditions are the basis for criticism of Ridley's paper by Volkov and Kogan [59], and Takeyama and Kitahara [60]. Let us examine Ridley's arguments to see if he has violated Prigogine's conditions.

An examination of condition one, in light of the current-voltage characteristic of figure 19 certainly seems to be a flaw in Ridley's reasoning based on the fact that CCNR and VCNR are inherently non-linear in their entirety. But, examination of Ridley's work shows that his analysis applies to the negative differential region only. Experimental evidence at that time, and later do not dispute that this region is linear in a number of cases. Thus, Ridley's paper does not fall into dispute due to the first condition.

If the negative differential region is linear, and no extensive heat build-up is allowed, then, quantities dependent on heating are not changing. If we proceed further into the positive resistance region, heat build-up is quite likely, from Ridley's development, and linearity is lost. Thus, Ridley's derivation satisfies the second and third conditions required by Prigogine's arguments.

It is interesting to observe that the two papers cited also try to utilize Prigogine's methods by linearizing the particular phenomena they believe is causing negative resistance in a material. Both papers show that CCNR occurs, but only if the generation and recombination mechanisms present are linear (a fact that is not clear from experimental evidence). Ridley's arguments are far more general. In his view, what ever the mechanism, it must be linear in the negative resistance regime or the negative resistance regime cannot occur (it would violate the total entropy production rate for a stationary state). Any proposed mechanism would have to be demonstrated to be linear in order to apply it to the stationary state conditions.

As shown earlier in chapter II, and other studies [65], negative resistance can be caused by a transition from a single carrier current regime to a double carrier current regime. As double carrier current begins to dominate current flow, the negative resistance region disappears.

Therefore, as the current transitions via CCNR, we can treat the negative resistance regime as a stationary state. This allows us to utilize the general results of Ridley's work as we model current flow under CCNR as a solid state plasma.

CHAPTER IV

QUANTITATIVE ANALYSIS OF THE SOLID STATE PLASMA PINCH

In chapter III, we determined that the conditions surrounding CCNR place limits of action on certain macroscopic variables dealing with driving forces that influence carrier transport.

If we model the solid state plasma under these limitations, it should be possible to determine a set of parameters that describe the plasma's motion under CCNR. Application of a perturbation to the plasma's motion under CCNR will allow us to determine the plasma's stability.

The motion of a plasma, under the influence of electromagnetic fields, are best handled using the equations of motion for a fluid and Maxwell's equations. Utilizing this information, attention in this chapter will first be given to the similarity between diffusive fluid flow and diffusion of magnetic fields in preparation to solve for the equilibrium condition between the thermal and magnetic forces that occur in and around the solid state plasma under CCNR conditions.

This same problem will then be solved using a perturbation to determine if the magnetohydrodynamic equations are stable under CCNR.

The Basic Hydrodynamic Equations

The basic moment equations for conservation of mass, momentum and energy are

$$\frac{\partial \rho}{\partial t} + \nabla \cdot (\rho \vec{U}) = 0,$$

$$\rho \frac{D\vec{U}}{Dt} = -\nabla \overleftrightarrow{P} + \frac{1}{c}(\vec{J} \times \vec{B}), \tag{68}$$

$$\frac{D}{Dt}(P\rho^{-5/3}) = \frac{2}{3}\frac{\rho^{5/3}}{\sigma}J^2 \quad \text{or} \quad \frac{D}{Dt}(P\rho^{-\gamma}) = \frac{(\gamma-1)^2 J^2}{\sigma\rho\gamma}.$$

where

ρ = the mass density,

$\vec{U}$ = the velocity,

$\overleftrightarrow{P}$ = the pressure,

$\vec{J}$ = the current density,

$\vec{B}$ = the magnetic field strength,

σ = the conductivity,

γ = the ratio of specific heats.

Maxwell's equations can be written as

$$\vec{J_k} = \sigma(\vec{E} + \frac{\vec{U} \times \vec{B}}{c}),$$

$$\nabla \times \vec{E} = -\frac{1}{c}\frac{\partial \vec{B}}{\partial t}, \tag{69}$$

$$\nabla \times \vec{B} = \frac{4\pi}{c}\vec{J} = \frac{4\pi\sigma}{c}\Big(\vec{E} + \frac{\vec{U} \times \vec{B}}{c}\Big).$$

Taking the curl of the last equation yields

$$\nabla \times \nabla \times \vec{B} = \frac{4\pi\sigma}{c}\Big(\frac{1}{c}\nabla \times (\vec{U} \times \vec{B}) - \frac{1}{c}\frac{\partial \vec{B}}{\partial t}\Big). \tag{70}$$

and using $\nabla \cdot \vec{B} = 0$ we obtain

$$\frac{4\pi\sigma}{c^2}\frac{\partial \vec{B}}{\partial t} = \nabla^2 \vec{B} + \frac{4\pi\sigma}{c^2}\nabla \times (\vec{U} \times \vec{B}). \tag{71}$$

By defining the magnetic viscosity as

$$\eta = \frac{c^2}{4\pi\sigma}, \tag{72}$$

we can rearrange equation 71 to obtain

$$\frac{\partial \vec{B}}{\partial t} = \eta\nabla^2 \vec{B} + \nabla \times (\vec{U} \times \vec{B}), \tag{73}$$

The first term on the right hand side is a diffusion term and the second term is a convection term. This equation is similar in form to the hydrodynamic equation of flow past an object.

If the fluid is at rest, the convective term vanishes and we arrive at a solution similar to Stoke's equation [66]

$$\frac{\partial \vec{B}}{\partial t} = \eta \nabla^2 \vec{B}, \tag{74}$$

Equation 74. like Stoke's equation, relates the diffusion of physical quantities. From a fluid context, the diffusion equation states that the rate of fluid density changes by the transfer of molecules from one region to another (i.e., the process of diffusion). For the hydromagnetic case, the rate of change of the magnetic field changes by diffusing through the electrically conducting fluid.

Continuing the similarities between fluid and hydromagnetic diffusion, we can observe that the magnetic viscosity can be related to how fast the field diffuses in some time τ (similar to a lifetime) into the fluid or

$$\tau = \frac{L^2}{\eta} = \frac{4\pi\sigma L^2}{c^2}, \tag{75}$$

where L is a characteristic length (or penetration depth). Convection can dominate diffusion in the same manner as inertial forces in a fluid can dominate viscous forces. A measure of the dominance of convection to diffusion is found in the ratio of these values that yields the Reynolds number [67]

$$R_m = \frac{LU}{\eta}. \tag{76}$$

The conditions of the stationary state (from chapter III) cause diffusive forces to vanish. This implies the solid state plasma is highly conductive compared to the semiconductor surrounding it, or, the Reynold's number of the solid state plasma is much smaller than unity under CCNR conditions. We can utilize this information to solve for the balance of forces in the plasma.

The Static Pinch

The similarities between fluid and hydromagnetic descriptions allow us to look at the effect of a magnetic field on the motion of a highly conductive fluid. In particular, we can examine the effect of the pinching term,

under the conditions where the fluid is at rest with the magnetic field lines. This does not mean the fluid is not flowing in the material, merely that the magnetic field is frozen into the fluid and moves along with it (as a consequence of the fluid's high conductivity).

The procedure will start with the hydrodynamic equation for conservation of energy in inviscid flow. Equations relating the velocity of waves parallel and perpendicular to the field lines in the fluid will be used to arrive at a simple relation between the outward thermal pressure and the inward magnetic pressure. This relation will be found to be the Bennett pinch criterion.

Under the assumption of a small Reynold's number we have what is called steady, creeping flow. Under these conditions the velocity, U , is inviscid(independent of time). From reference 74 the hydrodynamic equation for conservation of energy under inviscid flow is

$$\nabla(P + \frac{1}{2}\rho U^2) + \rho(\vec{\omega} \times \vec{U}) = 0, \qquad (77)$$

where the vorticity is defined as $\vec{\omega} = \nabla \times \vec{U}$. Expanding the gradient of $\frac{U^2}{2}$ we get

$$\nabla\left(\frac{U^2}{2}\right) = \vec{U} \times (\nabla \times \vec{U} + (\vec{U} \cdot \nabla)\vec{U}). \qquad (78)$$

Simplifying equation 77 yields

$$\nabla P + \rho(\vec{U} \cdot \nabla)\vec{U} = 0. \qquad (79)$$

Using conservation of momentum with the rate of change of velocity being zero yields

$$\rho(\vec{U} \cdot \nabla)\vec{U} = -\nabla P + \frac{1}{c}\vec{J} \times \vec{B} = -\nabla P + \frac{(\nabla \times \vec{B}) \times \vec{B}}{4\pi}$$

$$\nabla(P + \frac{B^2}{4\pi}) + \rho(\vec{U} \cdot \nabla)\vec{U} - \frac{(\vec{B} \cdot \nabla)\vec{B}}{4\pi} = 0 \tag{80}$$

This is simplified further by using the following quantities

$$V = \frac{1}{\sqrt{2}}(\vec{U} + \vec{V_o}),$$

$$W = \frac{1}{\sqrt{2}}(\bar{U} - \vec{V_o}), \tag{81}$$

$$v_a = \frac{B}{(4\pi\rho)^{1/2}} \quad .$$

Here, $\vec{U}$ is the fluid velocity (which will vanish under inviscid conditions) and velocities V and W are resultant vector velocities found from adding the fluid velocity U and some phase velocity of waves parallel to the magnetic field lines.

The last quantity, v_a , in equation set 81, is known as the Alfvèn velocity. This quantity is similar to the wave velocity along a stretched wire. For our case, the Alfvèn velocity is the phase velocity of a wave along a magnetic line of force. Substituting equation set 81 into 80 yields

$$\nabla\left(P + \frac{B^2}{8\pi}\right) + \rho[(V \cdot \nabla)W + (W \cdot \nabla)V] = 0, \tag{82}$$

and for equal zero (inviscid flow)

$$\nabla(P + \frac{B^2}{8\pi}) - \rho(v_a \cdot \nabla)v_a = 0. \tag{83}$$

Equation 82 is the magnetohydrodynamic equation for inviscid flow and has the same form as the hydrodynamic equation for steady fluid flow

$$\nabla P + \rho(\vec{U} \cdot \nabla)\vec{U} = 0. \tag{84}$$

Clearly, the pressure in equation 82 has been augmented by the magnetic pressure, and the Alfvèn velocity is the characteristic velocity for waves along the magnetic field lines when static conditions prevail.

For the stationary state, the current is not changing rapidly. This implies a magnetostatic situation may exist for times short compared to the time CCNR occurs. For a magnetostatic situation, where the magnetic force is balanced by the pressure gradient, and the fluid velocity is zero, conservation of momentum, equation 68, allows us to write

$$\rho(\vec{U} \cdot \nabla)\vec{U} = -\nabla P + \frac{(\nabla \times \vec{B}) \times \vec{B}}{4\pi}. \tag{85}$$

Where the left hand side of equation 85 vanishes as a consequence of the stationary state. From our Stoke's like equation 74 we have

$$\frac{\partial \vec{B}}{\partial t} - \eta \nabla^2 B = 0. \tag{86}$$

We can rewrite the second term on the right hand side of equation 85 for the static case as

$$\frac{(\nabla \times \vec{B}) \times \vec{B}}{4\pi} = \frac{1}{4\pi}(\vec{B} \cdot \nabla)\vec{B} - \frac{1}{8\pi}\nabla \vec{B}^2 = \nabla \cdot \left(\frac{\vec{B}\vec{B}}{4\pi}\right) - \nabla \frac{B^2}{8\pi}. \tag{87}$$

And in tensor notation

$$\left(\frac{(\nabla \times \vec{B}) \times \vec{B}}{4\pi}\right)_i = \frac{\partial}{\partial r_k}\left(\frac{B_i B_k}{4\pi}\right) - \frac{\partial}{\partial r_k}\left(\frac{B^2}{8\pi}\delta_{ik}\right). \tag{88}$$

The Maxwell stress tensor is defined in Jackson [68] as

$$T_{ik} = \frac{1}{4\pi}[E_i E_k + B_i B_k - \frac{\delta_{ik}}{2}(E^2 + B^2)]. \tag{89}$$

Dropping the electric field stress term we arrive at a form equivalent to that obtained for equation 88 (we are not discounting the electric field at this point).

$$T_{ik} = \frac{B_i B_k}{4\pi} - \frac{B^2}{8\pi}\delta_{ik}, \tag{90}$$

or

$$\frac{\partial}{\partial r_k}T_{ik} = \frac{\partial}{\partial r_k}\left(\frac{B_i B_k}{4\pi}\right) - \frac{\partial}{\partial r_k}\left(\frac{B^2}{8\pi}\delta_{ik}\right) = \left(\frac{(\nabla \times \vec{B}) \times \vec{B}}{4\pi}\right)_i. \tag{91}$$

Our static equation 85 now reads as

$$\frac{\partial}{\partial r_k}[P\delta_{ik} - T_{ik}] = 0 \quad \text{or} \quad \frac{\partial}{\partial r_k}F_{ik} = 0. \tag{92}$$

where F_{ik} is defined as the total stress tensor equal to

$$\left(P + \frac{B^2}{8\pi}\right)\delta_{ik} - \frac{B_i B_k}{4\pi}. \tag{93}$$

This can be reduced to diagonal form via transformation to the principal axes

$$|F_{ik} - \delta_{ik}\lambda| = 0. \tag{94}$$

This reduces, after some algebra to

$$\lambda_1 = P + \frac{B^2}{8\pi},$$

$$\lambda_2 = P + \frac{B^2}{8\pi}, \tag{95}$$

$$\lambda_3 = P - \frac{B^2}{8\pi}.$$

or

$$F_{ik} = \begin{pmatrix} P + \frac{B^2}{8\pi} & 0 & 0 \\ 0 & P + \frac{B^2}{8\pi} & 0 \\ 0 & 0 & P - \frac{B^2}{8\pi} \end{pmatrix}. \tag{96}$$

A geometric interpretation of this matrix shows that λ_3 is parallel to the field and λ_1, λ_2 are perpendicular to the field as shown in figure 20.

Under static conditions, the self magnetic force takes on the form

$$\nabla P = \frac{\vec{J} \times \vec{B}}{c}, \tag{97}$$

Figure 20. Geometrical interpretation of equation 96. A tube of force in a magnetic field is like a string under tension. Increasing the field strength stretches the tube of force, and the wave velocity increases.

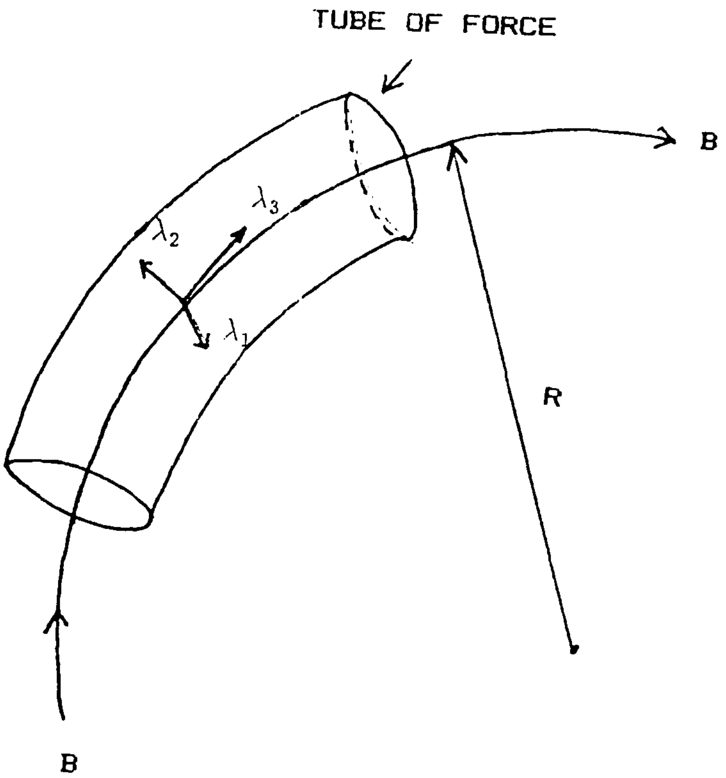
TUBE OF FORCE
B
λ_3
λ_2
λ_1
R
B

or

$$\vec{B} \cdot \nabla \vec{P} = \vec{J} \cdot \nabla \vec{P} = 0. \qquad (98)$$

This demonstrates further that the magnetic field lines and the current lie on lines of symmetry as drawn in figure 20. For a straight column these equations give the appearance of a shell(or shells) of current and their accompanying field lines nested around the center of the pinch column.

We can solve for the self magnetic force of the plasma column in cylindrical coordinates to obtain

$$\frac{dP}{dr} = -\frac{B}{4\pi r}\frac{d}{dr}(rB). \qquad (99)$$

Multiplying by r^2 and integrating out to the radius of the pinch (initially at r_o) yields

$$\int_0^{r_o} r^2 \frac{dP}{dr} dr = -\frac{1}{4\pi} \int_0^{r_o} (rB)d(rB),$$

(100)

$$r^2 P \Big|_0^{r_o} - 2\int_0^{r_o} rP dr = \frac{1}{8\pi}(rB^2)_{r=r_o}.$$

If the thermal pressure vanishes at the surface, and the energy of holes and electrons are the same, then

$$2K_BT\int_0^{r_o} n2rdr = \frac{1}{8\pi}(rB)^2_{r=r_o},$$

$$N = 2\int_0^{r_o} \pi rndr = \text{ carriers/ unit length,} \qquad (101)$$

$$2NK_BT = \left(\frac{1}{8}\right)(rB)^2_{r=r_o}.$$

Solving for the current related to the field

$$\frac{1}{r}\frac{d}{dr}(rB) = \frac{4\pi}{c}J, \qquad (102)$$

or

$$(rB)_{r=r_o} = \frac{2}{c}\int_0^{r_o} J2\pi rdr. \qquad (103)$$

Solving equation 103 we arrive at the Bennett pinch criterion

$$2NK_BT = \frac{I^2}{2c^2} \quad \text{or} \quad I^2 = 4NK_BTc^2. \qquad (104)$$

This result shows how the macroscopic variables, such as, the current, temperature and carrier density are related to achieve a balance between thermal forces and magnetic forces under stationary state conditions in the solid state plasma.

This result is also utilized in classical gaseous plasma discharges for determining the minimum conditions necessary to pinch the column.

At this point, objections may be raised concerning the previous derivations which lead to the Bennett pinch criterion. In chapters I and II, it was stated that semiconductors undergoing second breakdown have very intense electric fields and heating present. Also, it is unclear that the situation in the device can be approximated by a magnetostatic case during second breakdown.

These criticisms are valid if one considers the entire second breakdown current characteristic. Yet, Chapter III demonstrated that a stationary state is linear in character during the CCNR regime. Thus, over times that are short compared to the total time when CCNR occurs, the field does approximate a steady state, and under CCNR the plasma column will reach a static pinch.

The Hydromagnetic Stability of the Pinch

Under CCNR a solid state plasma column appears to obtain an equilibrium condition described before as a static pinch.

We now relax the conditions on the solid state plasma by allowing all of our pertinent variables to vary slightly from the equilibrium situation. If the static pinch is in a state of stable equilibrium, a perturbation of the pinch will return to its equilibrium condition. If the pinch is not stable upon perturbation, the pinch represents an unstable equilibrium. This can be determined by solving for the dispersion relationship for the pinch column.

To determine if an instability occurs we will resolve the magnetohydrodynamic equations (equation set 68) under a small perturbation. Variables with an o subscript are first order quantities and all perturbations are noted with primes.

$$\rho = \rho_o + \rho',$$

$$\vec{U} = \vec{U}_o + \vec{U}' = \vec{U}',$$

$$P = P_o + P', \tag{105}$$

$$\vec{J} = \vec{J}_o + \vec{J}',$$

$$\vec{B} = \vec{B}_o + \vec{B}'.$$

We will also maintain our result from chapter III that the plasma column has a conductivity much higher than the surrounding semiconductor. Ignoring products of perturbations we find that the zeroth order quantities for equation set 68 are related as

$$\nabla P_o = \frac{1}{c}(\vec{J_o} \times \vec{B}),$$

$$P_o \rho_o^{-\gamma} = \text{constant}, \tag{106}$$

$$\nabla \times \vec{B_o} = \frac{4\pi}{c}\vec{J_o}.$$

The first order results are

$$\frac{\partial \rho'}{\partial t} + \nabla \cdot (\rho_o \vec{U}') = 0,$$

$$\rho_o \frac{\partial \vec{U}'}{\partial t} = -\nabla P' + \frac{1}{c}(\vec{J}' \times \vec{B_o} + \vec{J_o} \times B'), \tag{107}$$

$$P' \rho_o = \gamma \rho' P_o,$$

$$\begin{gathered} \frac{\partial \vec{B}}{\partial t} = \nabla \times (\vec{U}' \times \vec{B_o}), \\ \nabla \times \vec{B}' = \frac{4\pi}{c}\vec{J}'. \end{gathered} \tag{108}$$

Using equation sets 107 and 108, we want to arrive at a force equation involving some small displacement of the plasma column in terms of zeroth order quantities after eliminating the first order results. Eliminating ρ' and $\vec{J}'$ from the first order equations yields

$$\frac{\rho_o}{P_o}\frac{\partial \rho'}{\partial t} + \gamma \nabla \cdot (\rho_o \vec{U}') = 0, \tag{109}$$

for the first order continuity equation. The displacement of the plasma can be defined as

$$\begin{gathered} \vec{\xi}(\vec{r}_o, t) = \vec{r} - \vec{r}_o, \\ \vec{U}' = \frac{D\vec{\xi}}{Dt} = \frac{Dr}{Dt}. \end{gathered} \tag{110}$$

Integrating the continuity equation in equation set 107 yields

$$P' = -\gamma \frac{P_o}{\rho_o} \nabla \cdot (\rho_o \vec{\xi}) = -\gamma P_o \nabla \cdot \vec{\xi}$$

(111)

$$-\gamma \frac{P_o}{\rho_o} \vec{\xi} \cdot \nabla P_o = -\gamma P_o \nabla \cdot \vec{\xi} - \vec{\xi} \cdot \nabla P_o .$$

Where $\nabla P_o \rho_o^{-\gamma}$ vanishes because $P_o \rho_o^{-\gamma}$ is a constant. Integrating the first order rate of change of the magnetic field in equation set 108 results in

$$\vec{B}' = \nabla \times (\vec{\xi} \times \vec{B}_o). \qquad (112)$$

Placing $\nabla \times \vec{B}_o = \frac{4\pi}{c} \vec{J}_o$, $\nabla \times \vec{B}' = \frac{4\pi}{c} \vec{J}'$ and equation 112 into the force balance equation of equation set 107 yields

$$\rho_o \frac{\partial^2 \vec{\xi}}{\partial t^2} = \nabla(\vec{J} \cdot \nabla P_o + \gamma P_o \nabla \cdot \vec{\xi}) + \frac{1}{4\pi} (\nabla \times \nabla \times (\vec{\xi} \times \vec{B}_o)) \times \vec{B}_o$$

(113)

$$+(\nabla \times \vec{B}_o) \times (\nabla \times (\vec{\xi} \times \vec{B}_o)).$$

which we define as the quantity $Q(\vec{\xi}(\vec{r},t))$.

Solving equation 113 with the appropriate boundary conditions will determine $\vec{\xi}$, which is a function of displacement and time. The normal method of tackling this equation is expanding $\vec{\xi}$ as a Fourier series of the form

$$\vec{\xi} = \sum \vec{\xi} exp(i\omega_n t). \tag{114}$$

Equation 113 now appears as follows with equation 114 substituted on the left hand side to yield a set of normalized equations

$$-\rho_o \omega_n^2 \vec{\xi} = Q(\vec{\xi}), \tag{115}$$

where ω_n are the normal frequencies. For $\omega_n^2 > 0$ all modes should be periodic or oscillating around some initially stable point. If $\omega_n^2 < 0$ the perturbation grows exponentially and the resulting configuration is unstable.

For our boundary conditions, we can use the external fields (outside the plasma) and the fields from the perturbed quantities to arrive at

$$\vec{E}_{ext} = \vec{E}_{oext} + \vec{E'_{ext}} = \vec{E'_{ext}} = -\frac{1}{c}\frac{\partial \vec{A'}}{\partial t},$$

(116)

$$\vec{B}_{ext} = \vec{B}_{oext} + \vec{B}'_{ext} = \vec{B}_{oext} + \nabla \times \vec{A'},$$

where primed quantities are the results of perturbations such that $\nabla \times \nabla \times \vec{A}'$ vanishes.

The tangential field can be found from the image force of the plasma at the plasma's surface as

$$\vec{n} \times (\vec{E}'_i + \frac{1}{c}(\vec{U}' + \vec{B}_{o,i}))$$

$$= \vec{n} \times (\vec{E}'_{ext} + \frac{1}{c}(\vec{U}' \times \vec{B}_{oext})). \tag{117}$$

where quantities with an i subscript are at or near the plasma column surface (as a consequence of the plasma column's conductivity being much higher than the surrounding semiconductor). We can then conclude that

$$\vec{E}'_i + \frac{1}{c}(\vec{U}' \times \vec{B}_{o,i}) = 0. \tag{118}$$

This allows us to write equation 117 with equation 116 as

$$\vec{n} \times \frac{\partial \vec{A}'}{\partial t} = \vec{n} \times \left(\frac{\partial \vec{\xi}}{\partial t} \times \vec{B}_{oext}\right). \tag{119}$$

Integrating equation 119

$$\vec{n} \times \vec{A}' = \vec{n} \times (\vec{\xi} \times \vec{B}_{oext}) = -(\vec{n} \cdot \vec{\xi})\vec{B}_{oext}. \tag{120}$$

which is arrived at by having the plasma column parallel to the outer surface of the semiconductor. This is also a consequence of the static pinch results. The plasma column initially filled the semiconductor sample, and as a result of balance of forces, retreated a constant distance from the sample surface. No isotropies in position are allowed initially under stationary state conditions.

Hydrodynamic considerations for conservation of energy require the total pressure to be continuous,

$$(P_o + \vec{\xi} \cdot \nabla P_o) + P' + \frac{1}{8\pi}[(\vec{B}_{o,i} + (\vec{\xi} \cdot \nabla)\vec{B}_{o,i} + \vec{B}'_i)]^2 \tag{121}$$

$$= \frac{1}{8\pi}[(\vec{B}_{oext} + (\vec{\xi} \cdot \nabla)\vec{B}_{oext}) + \vec{B}'_{ext}]^2. \tag{122}$$

Using our equilibrium condition

$$P_o = \frac{B_{o,i}^2}{8\pi} = \frac{B_{oext}^2}{8\pi}, \tag{123}$$

equation 122 becomes upon linearization (using our perturbed quantities)

$$-\gamma P_o \nabla \cdot \vec{\xi} + \frac{\vec{B_{o,i}}}{4\pi}\left(\vec{B}_i' + (\vec{\xi} \cdot \nabla)\vec{B_{o,i}}\right)$$

$$= \frac{\vec{B}_{oext}}{4\pi}\left(\vec{B}'_{ext} + (\vec{\xi} \cdot \nabla)\vec{B}_{oext}\right) \tag{124}$$

after using $P' = -\gamma P_o \nabla \cdot \vec{\xi} - \vec{\xi} \cdot \nabla P_o$. We now require further information on the magnetic field to proceed further.

Initially there is an azimuthal magnetic field external to the plasma. Under the conditions of the static pinch, the magnetic field will not penetrate the plasma to any depth of consequence. Further perusal of the procedure used to solve a similar situation in classical gaseous plasma columns demonstrates that an axial magnetic field is necessary for stability of the pinch. Since some experimental results show that an axial magnetic field is important to stable some solid state plasma instabilities (see chapter II), we will add an axial magnetic field to our derivation also. Later, this condition can be removed. Our magnetic field conditions external and internal to the plasma column are now

$$\vec{B}_{oext} = (0, \vec{B}_\theta(r), 0) \tag{125}$$

and

$$\vec{B}_{o,i} = (0, 0, B_{oz} = \text{constant}). \qquad (126)$$

To further simplify the derivation, we will assume that no pressure gradient exists radially in the plasma column, as required from the stationary state. This may appear to be an oversimplification, when it seems quite probable that a concentration gradient may exist under a perturbation. Yet, there is no experimental evidence describing what type of concentration gradients exist, if any. Also, the stationary state does not allow any initial concentration gradients (concentration gradients would cause diffusive forces, which vanish under the stationary state).

Placing these conditions into equation 124 results in

$$-\rho_o \omega^2 \vec{\xi} = \gamma P_o \nabla(\nabla \cdot \vec{\xi}) + \frac{1}{4\pi}[\nabla \times \nabla \times (\vec{\xi} \times \vec{B}_{o,i})] \times \vec{B}_{o,i}. \qquad (127)$$

For cylindrical perturbations we have

$$\vec{\xi}(\vec{r}) = \vec{\xi}(\vec{r}) exp(im\theta + ikz)$$

$$(128)$$

$$= (\xi_r(r), \xi_\theta(r), \xi_z(r)) exp(im\theta + ikz).$$

and since we are using very low orders of approximation for our static pinch, we will only utilize m equal zero. Results for the classical plasma pinch indicate m equal zero corresponds to inducing a sausage instability and m equal one a kink instability [69]. Research documented by Snyder [70] suggests that semiconductor devices could exhibit plasma instabilities resembling a sausage or kink instabilities depending on the actual geometry of current flow. Expanding 129 with m = 0 in equation 128 yields

$$-\rho\omega^2\xi_r = \gamma P_o \exp^{ikz}\frac{\partial}{\partial r}(\nabla\cdot\vec{\xi})$$

$$+\frac{\vec{B_{oz}}}{4\pi}\left[\frac{\partial}{\partial r}\left(\frac{\vec{B_{oz}}}{r}\frac{\partial}{\partial r}(r\xi_r)\right) - k^2\vec{B_{oz}}\xi_r\right]. \tag{129}$$

and

$$-\rho\omega^2\xi_\theta = -\frac{k^2\vec{B_{oz}}^2}{4\pi}\xi_\theta,$$

$$-\rho\omega^2\xi_z = ik\gamma P_o\exp^{-ikz}(\nabla\cdot\vec{\xi}). \tag{130}$$

Using the definitions $c_s = \left(\frac{\gamma P_o}{\rho}\right)^{1/2}$ for the speed of sound, and

$v_a = \left(\frac{B_{0z}^2}{4\pi\rho}\right)^{1/2}$ for the Alfvén velocity, we can simplify these equations to

$$(k^2 v_a^2 - \omega^2) = (c_s^2 + v_a^2)\frac{d}{dr}\left[\frac{1}{r}\frac{d}{dr}(r\xi_r)\right] + ikc_s^2\frac{d\xi_z}{dr},$$

$$(k^2 v_a^2 - \omega^2)\xi_\theta = 0, \qquad (131)$$

$$(k^2 c_s^2 - \omega^2) = c_s^2\left[\frac{ik}{r}\frac{d}{dr}(r\xi_r)\right].$$

These equations relate the displacement of the pinch to the perturbation initially started with equation set 105. Eliminating ξ_r from the above equations to arrive at the displacement in terms of the z component yields, after some algebra,

$$\frac{d^2\xi_z}{dr^2} + \frac{1}{r}\frac{d\xi_z}{dr} + \frac{(k^2 c_s^2 - \omega^2)(k^2 v_a^2 - \omega^2)}{k^2 c_s^2 v_a^2 - \omega^2(c_s^2 + v_a^2)}\xi_z = 0. \qquad (132)$$

This equation is in the form of a Bessel equation, and the solutions are modified Bessel functions, $\xi_z = I_o(kr)$. The I_n are not solutions at r equals zero. Our argument for the Bessel function is rather complicated and takes the extended form

$$H^2 = \frac{(k^2c_s^2 - \omega^2)(k^2v_a^2 - \omega^2)}{k^2c_s^2v_a^2 - \omega^2(c_s^2 + v_a^2)}$$

$$= k^2\left[1 + \frac{(\frac{w}{k})^4}{c_s^2v_a^2 - \left(\frac{w}{k}\right)^2(c_s^2 + v_a^2)}\right], \tag{133}$$

and solving for the z component of the displacement

$$\xi_r = \frac{H}{ik}\left[\frac{c_s^2(k^2v_a^2 - \omega^2) - \omega^2v_a^2}{c_s^2(k^2v_a^2 - \omega^2)}\right]{I_o}'. \tag{134}$$

If we use $\vec{B}' = \nabla \times (\vec{\xi} \times \vec{B}_o)$ for $\vec{B}_i'$. the z component is

$${B_{iz}}' = -\frac{B_{oz}}{r}\frac{d}{dr}(r\xi_r). \tag{135}$$

Placing the z components into our perturbation result, equation 124, we get

$$-\gamma P_o \exp^{i(\cdot\, kz}\nabla\cdot\vec{\xi} - \frac{{B_{oz}}^2}{4\pi r}\frac{d}{dr}(r\xi_r) = \frac{\vec{B_{oe}}}{4\pi}\cdot\left[\nabla\times\vec{A'} + \xi_r\frac{d\vec{B_{oe}}}{dr}\right]. \tag{136}$$

From $\vec{n} \times \vec{A'} = \vec{n} \times (\vec{\xi} \times \vec{B_{oe}}) = -(\vec{n} \cdot \vec{\xi})\vec{B_{oe}}$ we see that

$$\vec{A'} = \xi_r B_\theta \vec{z} + \alpha \vec{r}, \tag{137}$$

where α is some arbitrary function so that

$$\nabla \times \vec{A'} = \vec{\theta}\Big[\frac{\partial \alpha}{\partial z} - \frac{\partial}{\partial r}(\xi_r B_\theta)\Big], \tag{138}$$

and

$$\nabla \times \nabla \times \vec{A'} = \vec{r}\Big[\frac{-\partial^2 \alpha}{\partial z^2}\Big] + \vec{z}\Big[\frac{\partial^2 \alpha}{\partial r \partial z} - \frac{\partial^2}{\partial r^2}(\xi_r B_\theta)\Big] = 0. \tag{139}$$

These last two equations imply that

$$\frac{\partial \alpha}{\partial z} = f(r) \quad \text{and} \quad \frac{\partial \alpha}{\partial z} - \frac{\partial}{\partial r}(\xi_r B_\theta) = g(z). \tag{140}$$

But, since $\xi_r B_\theta$ is a function of r only $g(z)$ must be a constant and

$$\nabla \times \vec{A'} = g(z)\vec{\theta} = 0, \tag{141}$$

since $\vec{E'}$ is zero initially. We can now rewrite equation 136 to get closer to the dispersion relation

$$\frac{\gamma\omega^2\rho\xi_z}{\imath k c_s^2} + \frac{B_{oz}^2(k^2c_s^2-\omega^2)\xi_z}{4\pi\imath k c_s^2} = \frac{B_\theta^2\xi_r}{4\pi r}. \tag{142}$$

Substituting in for ξ_z and ξ_r

$$(c_s^2\omega^2 - v_a^2(k^2c_s^2-\omega^2))I_o(Hr)$$

$$= -\frac{B_\theta^2}{B_{oz}^2}v_a^2\frac{H}{r}I_o'(Hr)\left[\frac{c_s^2(k^2v_a^2-\omega^2)-\omega^2v_a^2}{k^2v_a^2-\omega^2}\right]. \tag{143}$$

Simplifying further we arrive at

$$\omega^2 = k^2v_a^2 - \frac{B_\theta^2}{B_{oz}^2}v_a^2\frac{H}{r}\frac{I_o'(Hr)}{I_o'(Hr)}, \tag{144}$$

$$\omega^2 = \frac{k^2B_{oz}^2}{4\pi\rho} - \frac{B_\theta^2}{4\pi\rho r^2}\left[\frac{HrI_o'(Hr)}{I_o(Hr)}\right]. \tag{145}$$

If we drop the axial magnetic field, which was initially put in for stability in analogy to the classical case, we find an unstable result ensues,

$$\omega^2 = -\frac{B_\theta^2H}{4\pi\rho r}\frac{I_o'(Hr)}{I_o(Hr)}. \tag{146}$$

This situation is stable if an axial magnetic field is present such that

$$B_{oz}{}^2 \geq \left(\frac{B_\theta}{kr}\right)^2 \left[\frac{HrI_o'(Hr)}{I_o(Hr)}\right]. \tag{147}$$

We can expand the dispersion relation further by approximating the Bessel functions. Standard expansions of these functions are

$$I_o(x) = 1 + \frac{x^2}{4} + \frac{x^4}{64} + \cdots,$$

$$I_o{}'(x) = I_1(x) = \frac{x^2}{2} + \frac{x^3}{16} + \frac{x^5}{384} + \cdots. \tag{148}$$

If we expand them to first order only, our dispersion relation (equation 144) simplifies to

$$\omega^2 = k^2 v_a^2 - \frac{B_\theta^2}{4\pi\rho}\left[\frac{(k^2 c_s^2 - \omega^2)(k^2 v_a^2 - \omega^2)}{k^2 c_s^2 v_a^2 - \omega^2(c_s^2 + v_a^2)}\right]. \tag{149}$$

Utilizing the definition for the speed of sound in a material as

$$c_s^2 = \left(\frac{\omega_p}{k_D}\right)^2. \tag{150}$$

where

k_D = Debye wavenumber,

ω_p = plasma frequency,

and eliminating the axial magnetic field leaves our first order dispersion equation as

$$\begin{aligned} \omega^2 &= -\frac{B_\theta^2}{4\pi\rho}\left[\frac{k^2 c_s^2 - \omega^2}{c_s^2}\right], \\ &= -\frac{B_\theta^2}{4\pi\rho}\left[k^2 - k_D^2\left(\frac{w}{\omega_p}\right)^2\right]. \end{aligned} \tag{151}$$

or

$$\omega^2 = \frac{\frac{-B_\theta^2}{4\pi\rho}k^2}{1-\frac{B_\theta^2}{4\pi\rho c_s^2}} = \frac{-\frac{B_\theta^2}{4\pi\rho}k^2}{1-\frac{B_\theta^2 k_D^2}{4\pi\rho\omega_p^2}}. \tag{152}$$

For this solution to be stable would require

$$\frac{B_\theta^2}{4\pi\rho c_s^2} > 1, \tag{153}$$

which is not a physically admissable solution in the material.

These results show a static plasma pinch is unstable under the conditions of CCNR. The growing oscillations of the pinch would certainly result in anistropies in carrier concentration in the column, resulting in a movement away from the stationary state.

This action allows thermal and electrical driving forces to reappear and the rate of entropy production would rapidly increase, and possibly surpass the flow of entropy from the sample. This suggests rapid ohmic heating from an decrease in the conductivity of the plasma column. Growing oscillations at the column surface would certainly be limited by phonon dispersion which would transfer the kinetic energy of plasma oscillations to the lattice, aiding heating of the device. An exact determination of this type of activity is beyond the scope of this work, but, is consistent with results that show devices exhibit signs of thermal shock after the initiation of second breakdown.

Solid State Plasma Parameters Necessary to Initiate Pinching

The results of the last section indicate attempts to determine when a device will fail after second breakdown occurs is an attempt to model an inherently non-linear event.

Therefore, it seems more amenable to determine when a CCNR regime occurs under device operation. The Bennett pinch criterion could be utilized to determine a minimum condition, beyond which, self-induced magnetic forces overcome thermal forces and produce unstable pinching. This can be related to the quantum degeneracy parameter to yield a set of conditions that are inherently unstable under CCNR conditions.

Our starting point is the Bennett pinch criterion, as applied to a situation where equilibrium is initiated. In this case, the thermal forces just balance the magnetic forces. Further increases in the magnetic force initiates unstable pinching. This can be quantified as

$$NK_BT < \frac{I^2}{2\pi c^2 r^2}, \tag{154}$$

where the current is in statamps and r is the column radius.

$$NT < \frac{I^2}{2\pi c^2 r^2 K_B}. \tag{156}$$

This value can be substituted into our relations for the quantum degeneracy parameter, or the plasma coupling parameter, to determine a set of maximum current curves for a material.

Results are shown for the materials of interest on figures 21, 22 and 23 using material parameters from [64]. Values of N are graphed as concentrations per cubic centimeter and all results are for a plasma column of radius 10^{-2} centimeters.

For the lowest current shown on the figures, the equivalent current density is greater than 3 A/cm^2 .

To determine the current required to support an unstable plasma pinch, the concentration of carriers in the pinch is followed horizontally across the graph until it intersects the appropriate isotherm. These values are placed into equation 155 to determine the maximum current that can flow before magnetic forces destabalize the plasma. For example, on figure 21, a concentration of around $6.3 \times 10^{12} cm^{-3}$ at 300K, requires about 10^{-2} amperes to become unstable with a column radius of $10^{-2}\,cm$. Additionally, the quantum degeneracy parameter at this point indicates the plasma is classical in nature, which reaffirms our results which indicated pinch results similar to those found in classical gaseous plasmas.

These results also indicate that for a given concentration, temperature and current, more than one filament could form. The smaller filaments would each have to posses values

Figure 21. Graph of the concentration versus the quantum degeneracy parameter for pinch conditions in germanium. Pinch radius is 10^{-2} centimeters.

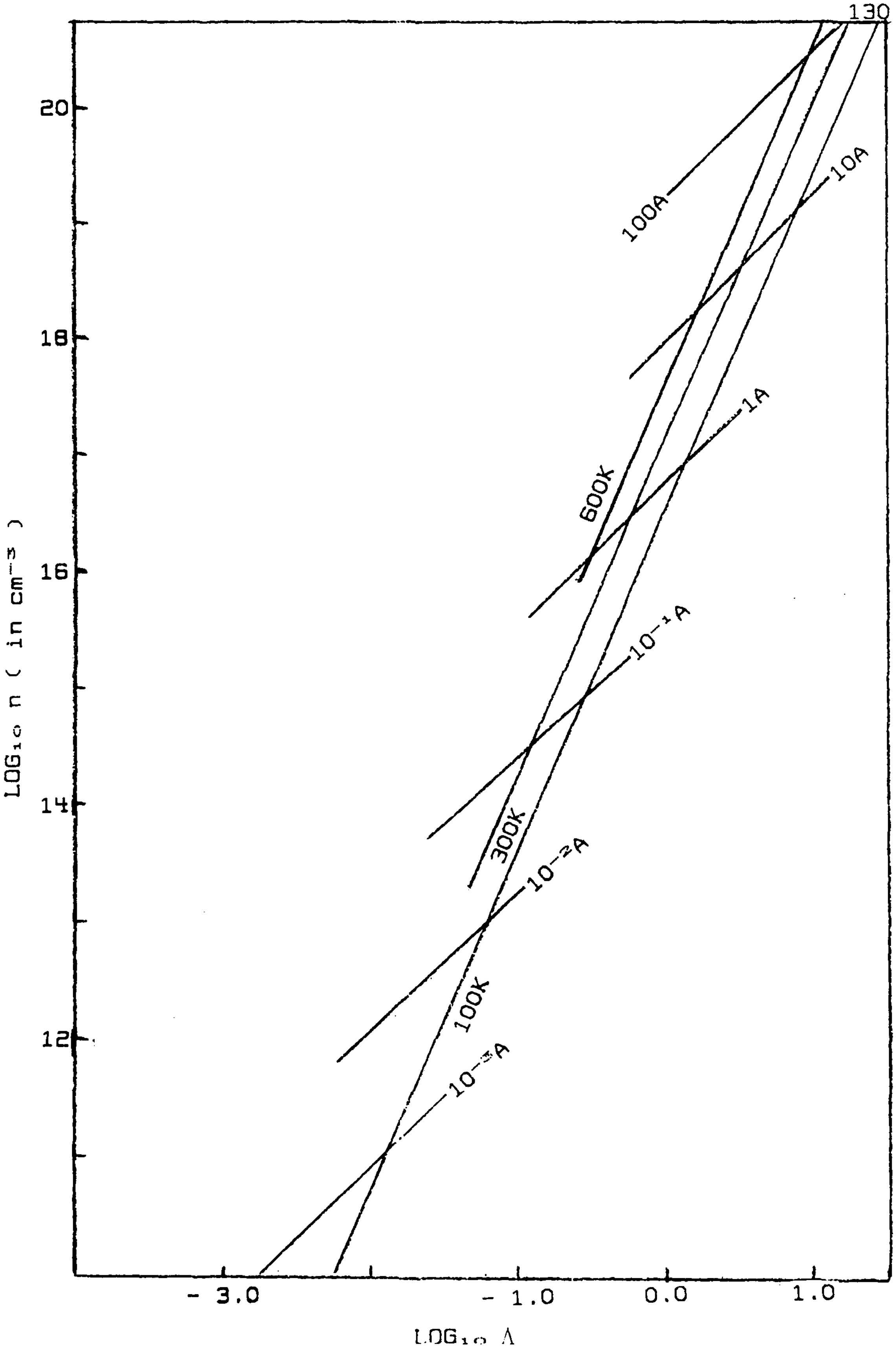
100A
10A
1A
600K
10^{-1}A
300K
10^{-2}A
100K
10^{-3}A
20
18
16
14
12
- 3.0
- 1.0
0.0
1.0
LOG_{10} n (in cm^{-3})
LOG_{10} Λ

Figure 22. Graph of the concentration versus the quantum degeneracy parameter for pinch conditions in silicon. Pinch radius is 10^{-2} centimeters.

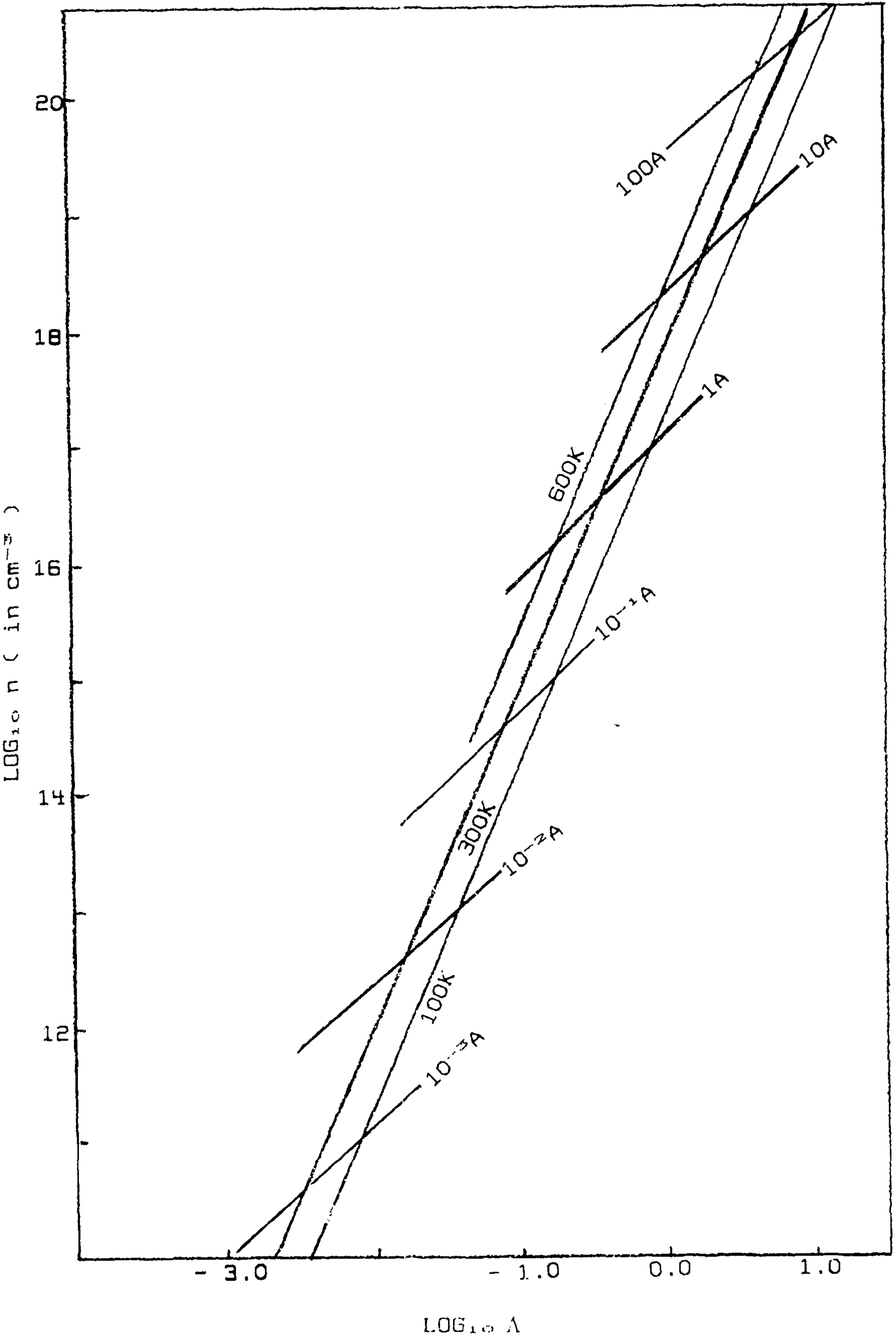
20
18
16
14
12
LOG_{10} n (in cm^{-3})
- 3.0
- 1.0
0.0
1.0
LOG_{10} Λ
100A
10A
1A
10^{-1}A
10^{-2}A
10^{-3}A
600K
300K
100K

Figure 23. Graph of the concentration versus the quantum degeneracy parameter for pinch conditions in gallium arsenide. Pinch radius is 10^{-2} centimeters.

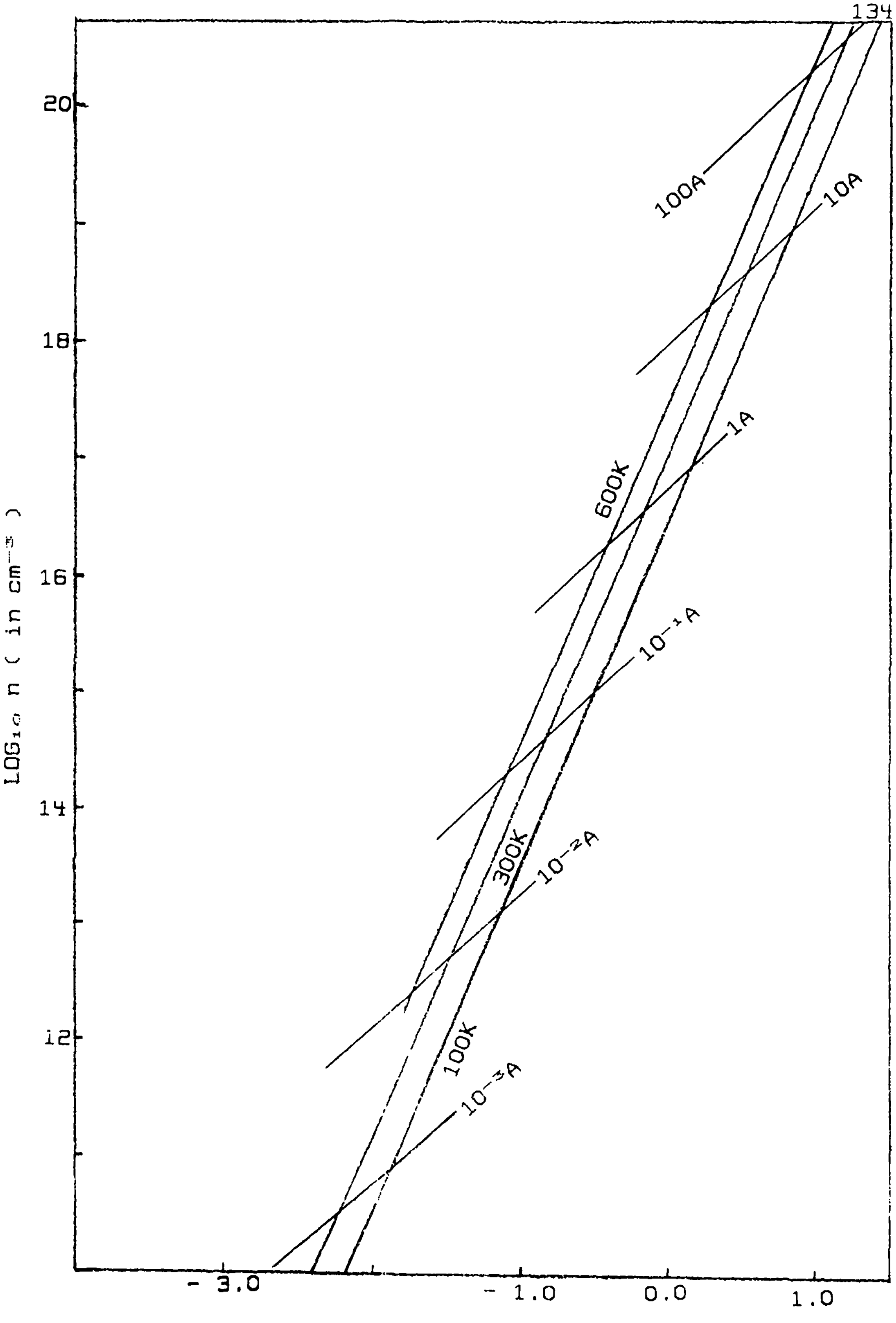
20
18
16
14
12
LOG₁₀ n (in cm⁻³)
- 3.0
- 1.0
0.0
1.0
LOG₁₀ Λ
100A
10A
1A
10⁻¹A
10⁻²A
10⁻³A
600K
300K
100K

below the maximum allowable values for the Bennett pinch criterion, and could be treated as a set of current carrying wires with appropriate repulsive forces. As the current in the material increases, filaments would coalesce back into a single filament which would become unstable once it achieves the maximum allowable current from the Bennett pinch criterion.

Further results are indicated on figures 22 and 23 for silicon and gallium arsenide respectively.

CHAPTER V

APPLICATION OF THE PLASMA PARAMETERS TO SEMICONDUCTOR JUNCTIONS

In this chapter, the Bennett pinch criterion, derived for a solid state plasma in a CCNR regime, will be applied to a transistor that is placed into second breakdown and recovered safely before damage can occur. These results for the transistor are the only known experimentally repeatable results of second breakdown and provide a means to determine if second breakdown in this device coincides with the conditions for unstable solid state plasma pinch.

As an introduction to these results, a short discussion on the current transport mechanisms in solid state devices (e.g., diodes and bipolar transistors) will be presented. The results of this discussion will be used to determine whether or not the transistor to be examined in a CCNR regime. Measurements of the collector current at second breakdown will be used to determine the carrier concentration available for a plasma whose initial radius is equal to the device's radius.

Description of Semiconductor Junctions

When two dissimilar semiconductors are brought into contact, a built-in potential is set up due to the difference in Fermi energies. This built-in potential sweeps free carriers from the general area of contact, in both materials, until enough charge has been displaced to counteract the built-in potential. The remaining charge free zone is called a depletion region.

Application of an external potential changes the electrical character of the depletion region depending on whether the potential aids (called reverse-bias) or counteracts (called forward-bias) the depletion region's built-in potential.

A single junction between two semiconductors is usually called a diode. In reverse-bias a diode passes very little current until the external potential is large enough to initiate impact ionization in the depletion region. As reverse-bias increases, the electrical character of the depletion region changes, from an insulator, to a semiconductor, when impact ionization occurs (see chapter II). In forward-bias the built-in potential is decreased by the external potential allowing a large number of carriers to be injected and a large current to flow. Under forward-bias conditions the depletion region is small enough that current flow resembles semiconductor injection (see chapter II).

If three dissimilar semiconductors are brought into contact, with the middle semiconductor relatively thin, two depletion regions occur separated by a very small distance. Injection activity at either junction can influence injection conditions at the other junction, creating what is called, the transistor effect.

Under different polarities and degrees of bias, these junctions can be used as an electronic switch, also known as a transistor (see figure 24). When the transistor is on, both junctions are forward-biased (the transistor is in quasi-saturation) or the base-emitter is forward-biased and the collector-base is slightly reverse-biased (the transistor is active). By reverse-biasing both junctions, neither junction will pass current and the transistor is off (in the cut-off state). Both situations are portrayed in figures 24 and 25.

These effects are attributed to the control of charge in the base region by the emitter's bias, and the degree of base drive used to drain or replenish stored charge in the base.

Under active, quasi-saturated or cut-off conditions, the quantity of stored charge varies. As shown in figure 26, the ability of a transistor to switch (from an on to an off state) is controlled by how quickly charge is drained out of the base (or the collector) to achieve cut-off conditions. This is complicated if the external bias on the collector or emitter continues to pour charge into the base region.

Figure 24. Schematic depiction of a (NPN) transistor. The upper figure shows the extent (not to scale) of the depletion regions with the built-in potential only. The bottom figure shows the transistor (not to scale) in a quasi-saturated state. Both depletion regions are reduced by forward-bias.

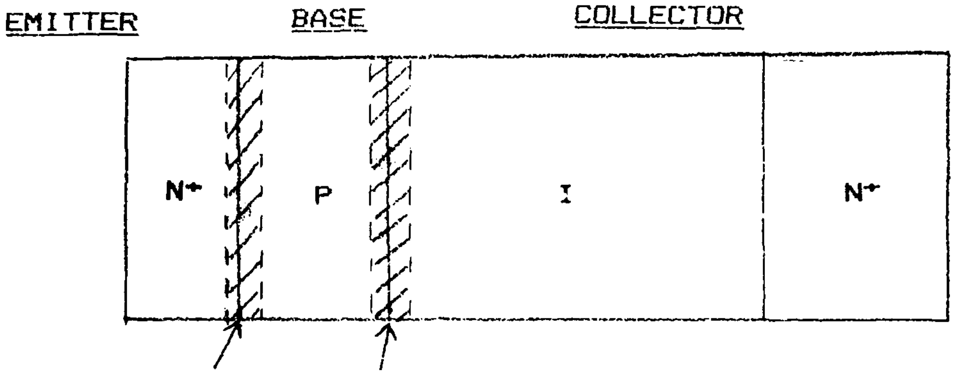
EMITTER
BASE
COLLECTOR
N+
P
I
N+

DEPLETION REGIONS (un--biased state)

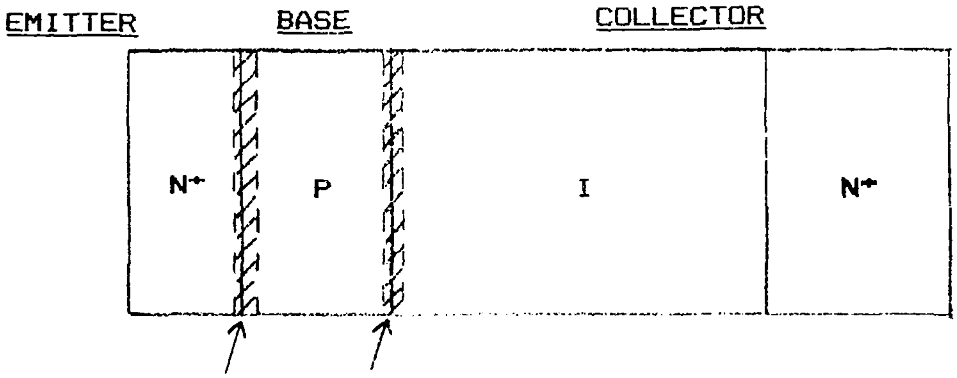
EMITTER
BASE
COLLECTOR
N+
P
I
N+

DEPLETION REGIONS (quasi--saturated state)

Figure 25. Schematic depiction of a (NPN) transistor in cut-off. Both depletion regions have expanded (not to scale) into the base region under reverse-bias.

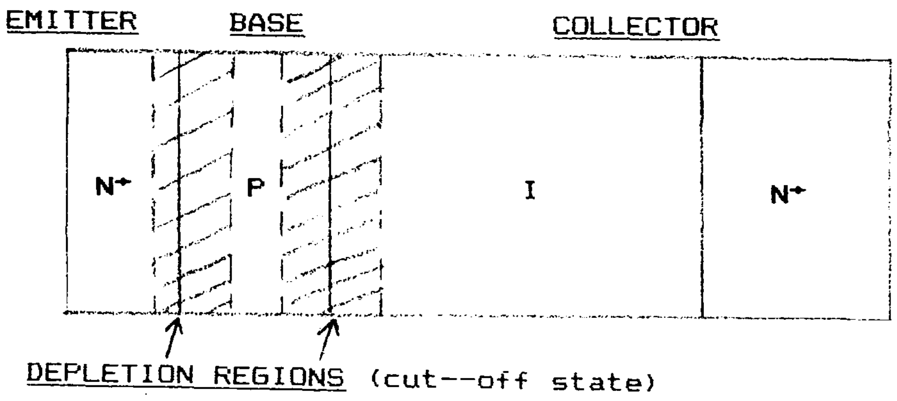
EMITTER
BASE
COLLECTOR
N+
P
I
N+
DEPLETION REGIONS (cut--off state)

Figure 26. Minority carrier density stored in the various regions of a NPN transistor in various conduction states. Here, n_p is the electron density injected into the p type base. The hole density being injected into the n type collector is p_n. Very little charge is stored in the emitter.

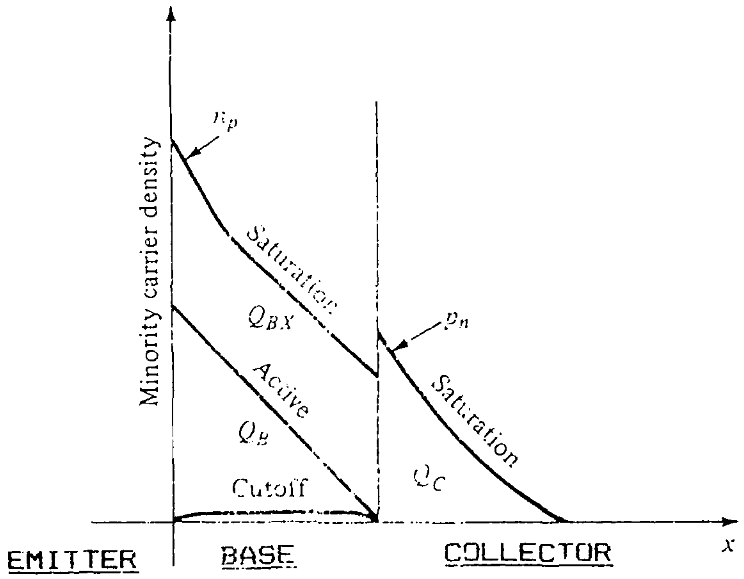
Minority carrier density
n_p
Saturation
Q_{BX}
p_n
Active
Saturation
Q_B
Cutoff
Q_C
x
EMITTER
BASE
COLLECTOR

For example, from the results of chapter II, a transistor could be modeled as a diode and PIN diode connected in series. Special consideration must be taken into account in modeling the intervening base region, but current flows outside the base will still meet the same primary obstacle of space charge limited current flow.

Conditions can be created where the collector and emitter potentials force their respective depletion regions to extend deep into the base until they coalesce (known as a punch-through condition). Once this occurs a transition from space charge limited, single carrier to double carrier current flow occurs and continued current flow cannot be restricted.

If conditions are created during transistor turn off where carriers are depleted from the base at the expense of carriers in the collector, space charge limited current flow in the collector can eventually increase the electric field at the I-N+ interface (see figure 25) to avalanche conditions. Avalanche creates a large number of electron-hole pairs which neutralize the space charge and leads to double carrier current flow and CCNR [71].

These situations provide a useful test of the conclusions reached in chapter IV. Knowing the current levels available at the collector prior to second breakdown, the collector area, the charge carrier concentration, and the maximum thermal velocity of carriers in the collector region we can see if the minimum predicted conditions for solid state plasma pinch coincide with experimental evidence of second breakdown initiation.

The only repeatable experiments driving transistors in to second breakdown, without damage, have been performed by Portnoy [72,73]. In the next section we will discuss these results and apply our pinch criterion to the tested devices.

Application of Plasma Pinch Criterion to Transistors

Portnoy's experimental set-up examines transistors in the common emitter configuration as they are switching under a large inductive load [72]. When second breakdown occurs, the inductive load is quickly switched, from the device, to an energy dump, preventing device failure. We will use the results of testing, listed in reference 73, for a transistor manufactured by Unitrode, with general characteristics described in figure 27.

Results of this study demonstrate that three types of second breakdown occurred dependent on the device's initial condition and the degree of reverse base drive. These types of second breakdown have been called types A, B, and C [72] by Portnoy.

Utilizing information derived in chapter IV, a graph of the necessary pinch conditions for the device were calculated for a column radius of 0.28 centimeters (see figure 28).

Figure 27. Doping profile for the Unitrode power transistor. The area of the device is a square 0.56 centimeters on each side. From [72].

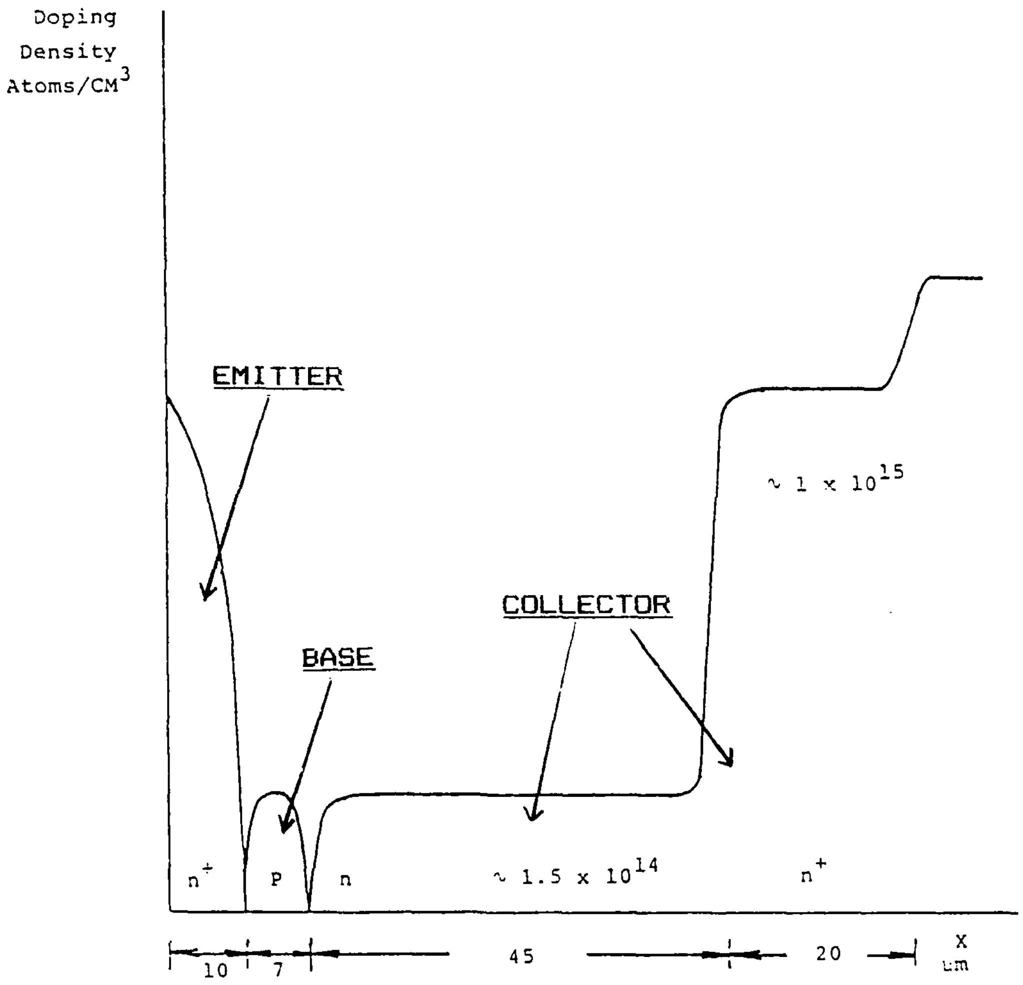
Doping
Density
Atoms/CM^3
EMITTER
BASE
COLLECTOR
~ 1 x 10^{15}
n$^+$
p
n
~ 1.5 x 10^{14}
n$^+$
10
7
45
20
X
um

Figure 28. Graph of the carrier concentration versus quantum degeneracy parameter for pinch conditions in the Unitrode device. The pinch radius is 0.28 centimeters for all curves.

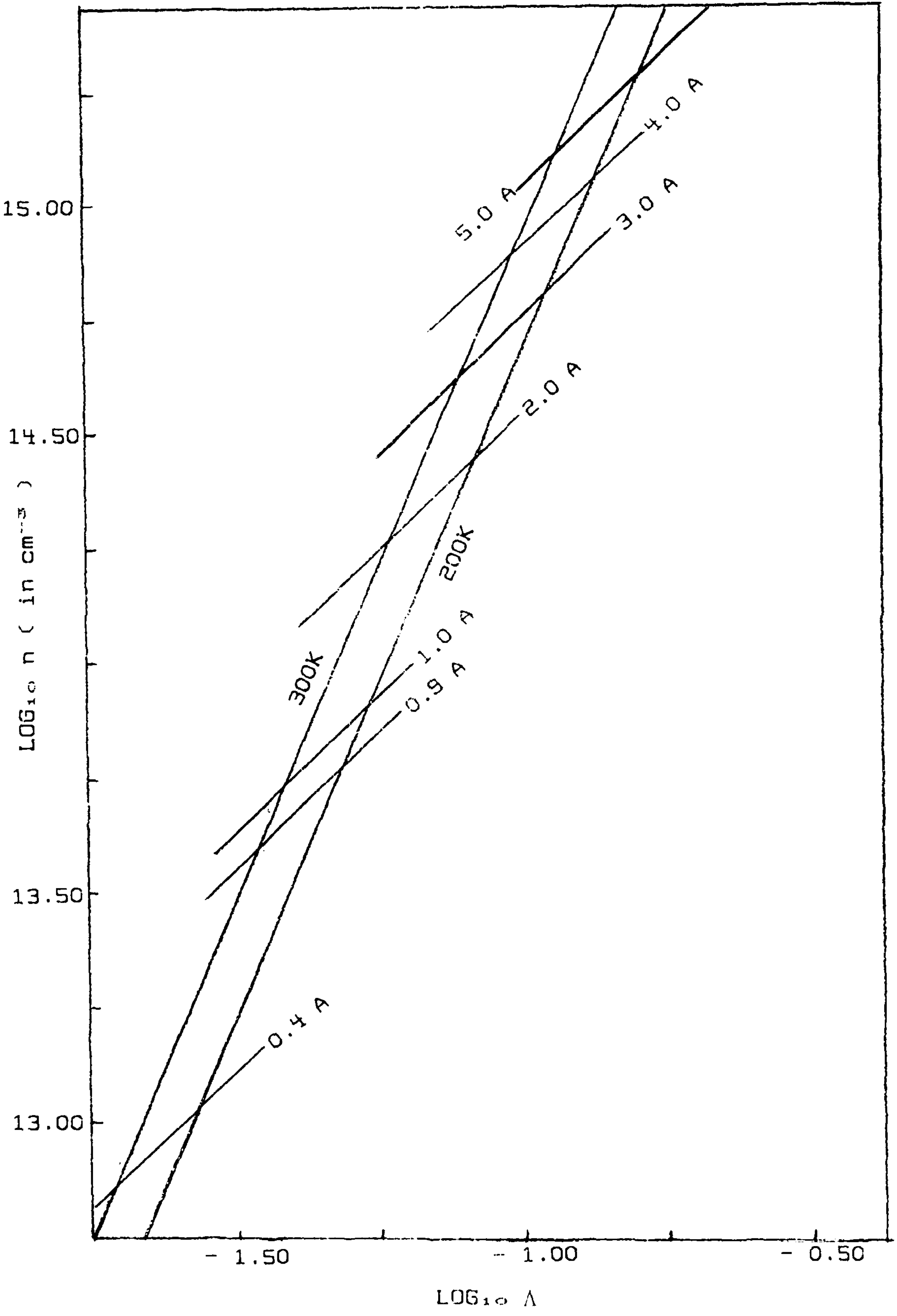
15.00
14.50
13.50
13.00
LOG₁₀ n (in cm⁻³)
- 1.50
- 1.00
- 0.50
LOG₁₀ Λ
5.0 A
4.0 A
3.0 A
2.0 A
1.0 A
0.9 A
0.4 A
300K
200K

The constant current lines on the graph of figure 28 represent maximum allowable values of current at specific values of the temperature and carrier concentration.

We can study each type of second breakdown individually to determine if CCNR characteristics are being initiated and compare the current and charge carrier concentration to those predicted for pinch.

We cannot necessarily specify whether a particular breakdown was initiated by punch-through or avalanche breakdown at the collector. Both events occur under very similar conditions and represent the only mechanisms possible in a transistor at these levels of voltage and current. Since information after breakdown is not available (without damaging the devices) deductive evidence for either situation is not available. In either case, the carriers transiting the collector will be at their maximum thermal velocity, which, with the collector current and area, allows us to specify a minimum carrier concentration in the collector.

Type A Second Breakdown

The general current and voltage trends with time for type A second breakdown at room temperature are shown in figure 29.

The initial state of the transistor in type A breakdown is active or quasi-saturation. This implies the emitter is forward-biased and the collector is forward-biased or

Figure 29. Typical waveforms of current and voltage for type A second breakdown. The top curve is the voltage across the collector-emitter (100 volts per square), the middle curve is the collector current (2 amperes per square), and the lower curve is the base-emitter voltage (0.5 volts per square). The time base is 5 microseconds per square. The waveform cut-off at the far right is where second breakdown occurs. From [72].

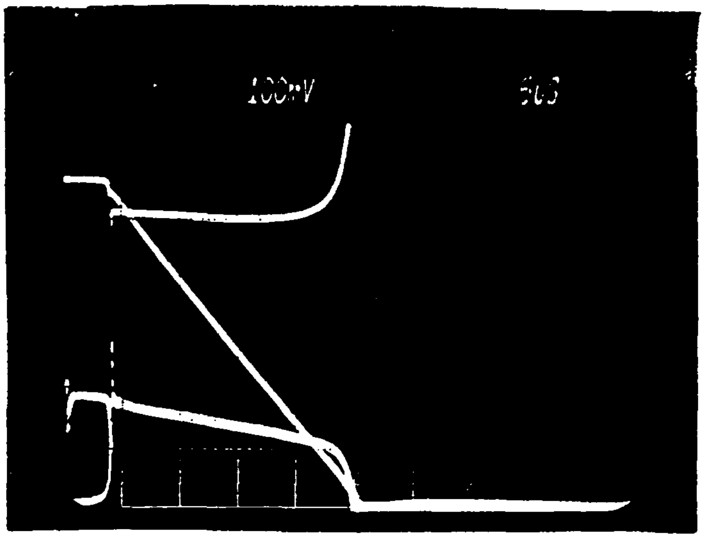
100mV
5uS

slightly in reverse-biased. In either case, the depletion regions are not very large and do not extend across the entire base region initially. The bias of the junctions creates an excess of carriers in the base from the forward-biased emitter (and collector). If the collector is slightly reverse-biased, a small number of these excess carriers will be drained off by the collector.

As the base drive is reversed to turn the transistor off, the inductor senses the bias change on the transistor and begins to de-energizes across the transistor forcing the collector into reverse-bias and trying to keep the emitter forward-biased.

General trends indicate that for type A breakdown the collector-emitter voltage remains constant and rises just before second breakdown. The collector current decreases linearly to zero and presumably becomes negative, and the base-emitter voltage decreases more or less linearly, then drops rapidly near second breakdown (see figure 29).

In terms of the device's switching dynamics, the emitter cannot become reverse-biased until all the excess charge in the base region is removed by the base drive and the collector. If this is correct, then second breakdown would not occur until all the base charge is removed. Once emptied, punch-through or avalanche at the I-N+ interface can occur.

Calculations of the minimum carrier concentration in the collector are based on a maximum thermal velocity of Results are listed in table 1.

The table lists the initial device conditions, in terms of the forward base drive, and the conditions as the transistor is being turned off by the reverse base drive. The time to second breakdown is the time after initiation of the reverse base drive until a rapidly increasing current flow is detected, and current is shunted away from the transistor. This is the transition from a high voltage, low current state, to a low voltage, high current state, or second breakdown.

The tabulated results show the collector current exceeds the maximum pinch criterion for the minimum concentration of carriers in the collector.

Type B Second Breakdown

The state of the transistor for this type of second breakdown is quasi-saturation. Typical current and voltage curves with time are shown in figure 30.

Figure 30 shows collector current is constant after applying reverse base drive with an initially positive emitter-base voltage and a small collector-emitter voltage. Near second breakdown the emitter base voltage tends to zero and the collector-emitter voltage rises rapidly to a sustaining voltage.

Table 1

Type A second breakdown.

Forward Base Drive (in amps)	Reverse Base Drive (in amps)	Time to Second Breakdown	Collector Current at Second Breakdown (in amps)	Minimum Charge Concentration in the Collector	Maximum Allowable Pinch Current (in amps)
0.05	0.05	7.0 µs	1.0	1.95×10^{12} cm^{-3}	.19
	0.10	3.5 µs	2.2	4.3×10^{12} cm^{-3}	.29
	0.20	0.8 µs	2.0	3.9×10^{12} cm^{-3}	.28
0.10	0.05	11.7 µs	1.0	1.95×10^{12} cm^{-3}	.19
	0.10	4.8 µs	4.1	8×10^{12} cm^{-3}	40
	0.20	0.56 µs	5.8	1.13×10^{13} cm^{-3}	.48
0.20	0.05	15.1 µs	1.2	2.34×10^{12} cm^{-3}	.22
	0.10	7.8 µs	4.4	8.6×10^{12} cm^{-3}	.41
0.50	0.05	21.3 µs	0.49	9.57×10^{11} cm^{-3}	.14

All currents and times are from [80]. Maximum allowable pinch currents are found using the concentration in the collector as a minimum value.

Figure 30. Typical waveforms of current and voltage for type B second breakdown. The top curve is the collector current (2 amperes per square), the middle curve is the base-emitter voltage (0.5 volts per square), and the bottom curve is the collector-emitter voltage (100 volts per square). The time base is 500 nanoseconds per square. Waveform cut-off at the far right is where second breakdown occurs. From [72].

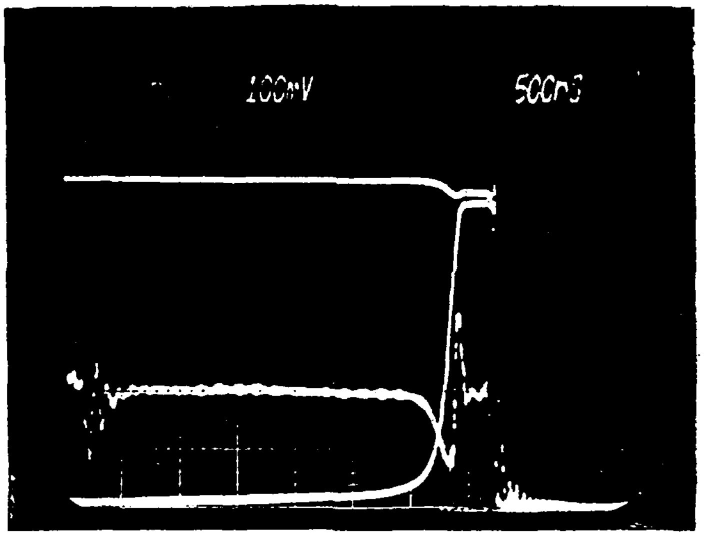
100mV
500nS

The initial conditions for type B second breakdown are quite different from type A. With both junctions well into forward-bias the base and collector regions are saturated with accumulated charge. As the inductor tries to drive the collector to reverse-bias, charge drains out of the collector. The emitter-base's forward bias pours additional charge into the base. This minority charge injected into the base may have enough energy upon entering the base to transit the narrow depletion region and aid in diminishing the collector's stored charge.

As the collector's stored charge diminishes, the collector moves to reverse-bias. Since, the base drive also removes charge, once the collector becomes reverse-biased the emitter also becomes reverse-biased and the conditions quickly move to punch-through or avalanche as described in type A breakdown.

Table 2 indicates that conditions are above the maximum levels dictated for pinching.

Type C Second Breakdown

The initial state of the device is the same as type B second breakdown. Typical current and voltage curves with time are shown in figure 31. The major difference between type B and C second breakdown is the occurrence of a negative voltage for the base-emitter before the collector became reverse-biased.

Table 2

Type B second breakdown.

Forward Base Drive (in amps)	Reverse Base Drive (in amps)	Time to Second Breakdown	Collector Current at Second Breakdown (in amps)	Minimum Charge Concentration in the Collector	Maximum Allowable Pinch Current (in amps)
0.5	0.1	2.2 µs	9.4	1.8×10^{13} cm^{-3}	.6
1.0	0.05	4.1 µs	11.3	2.2×10^{13} cm^{-3}	.67
	0.10	1.0 µs	12.9	2.52×10^{13} cm^{-3}	.72
	0.20	0.76 µs	12.0	2.34×10^{13} cm^{-3}	.69
2.0	0.05	1.5 µs	14.5	2.83×10^{13} cm^{-3}	.76

All currents and times are from [80]. Maximum allowable pinch currents are found using the concentration in the collector as a minimum value.

Figure 31. Typical waveform of current and voltage for type C second breakdown. The top curve is the collector current (2 amperes per square), the middle curve is the base-emitter voltage (0.5 volts per square), and the lowest curve is the collector-emitter voltage (100 volts per square). the time base is 500 nanoseconds per square. Waveform cut-off at the far right is where second breakdown occurs. From [72].

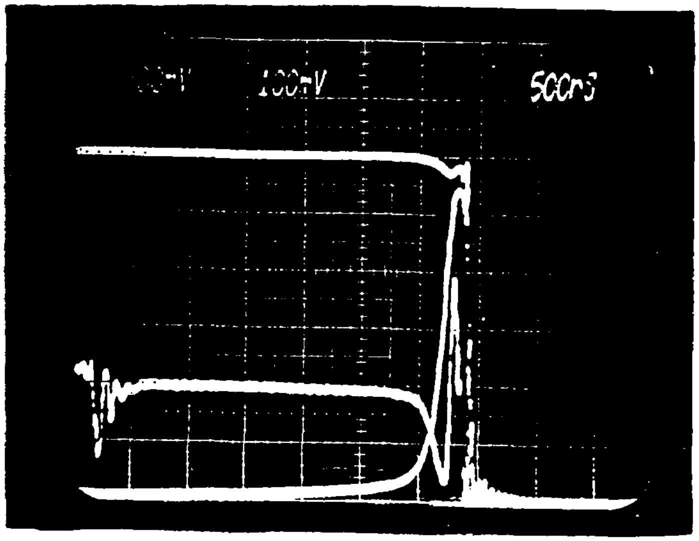
100mV
500ns

If the emitter-base becomes reverse-biased due to a high reverse base drive then the collector's stored charge (which is much smaller than the base's stored charge) will quickly be dissipated allowing the collector to move into reverse-bias and punch-through or avalanche conditions more quickly than in type B breakdown.

Table 3 shows once again, the collector current far exceeds the maximum allowable pinching current.

From the quantitative point of view taken for these results, the criterion for solid state plasma pinch appear to be satisfied in all cases, and the devices present characteristics that indicate the presence of a CCNR regime.

Table 3

Type C second breakdown.

Forward Base Drive (in amps)	Reverse Base Drive (in amps)	Time to Second Breakdown	Collector Current at Second Breakdown (in amps)	Minimum Charge Concentration in the Collector	Maximum Allowable Pinch Current (in amps)
0.05	1.0	0.2 µs	2.1	4.0×10^{12} cm^{-3}	.28
	2.0	0.1 µs	2.6	5.1×10^{12} cm^{-3}	.32
	5.0	0.09 µs	4.0	7.82×10^{12} cm^{-3}	.40
	11.0	0.06 µs	2.8	5.5×10^{12} cm^{-3}	.33
0.10	0.5	0.21 µs	4.4	8.6×10^{12} cm^{-3}	.42
	1.0	0.11 µs	4.6	9.0×10^{12} cm^{-3}	.43
	2.0	0.09 µs	4.4	8.6×10^{12} cm^{-3}	.42
	5.0	0.06 µs	3.3	6.4×10^{12} cm^{-3}	.36
	11.0	0.05 µs	4.5	8.8×10^{12} cm^{-3}	.42
0.20	0.2	0.46 µs	7.7	1.5×10^{13} cm^{-3}	.55
	0.5	0.17 µs	7.5	1.46×10^{13} cm^{-3}	.54
	1.0	0.16 µs	6.8	1.32×10^{13} cm^{-3}	.52
	2.0	0.07 µs	6.3	1.23×10^{13} cm^{-3}	.50
	5.0	0.04 µs	2.9	5.66×10^{12} cm^{-3}	.34
	11.0	0.03 µs	2.1	4.1×10^{12} cm^{-3}	.29

All currents and times are from [80]. Maximum allowable pinch currents are found using the concentration in the collector as a minimum value.

Table 3, continued

Forward Base Drive (in amps)	Reverse Base Drive (in amps)	Time to Second Breakdown	Collector Current at Second Breakdown (in amps)	Minbimum Charge Concentration in the Collector	Maximum Allowable Pinch Current (in amps)
0.50	0.20	0.55 µs	10.2	2.0×10^{13} cm^{-3}	.63
	0.50	0.23 µs	10.3	2.01×10^{13} cm^{-3}	.64
	1.0	0.15 µs	10.0	1.95×10^{13} cm^{-3}	.63
	2.0	0.08 µs	9.1	1.72×10^{13} cm^{-3}	.60
	5.0	0.05 µs	7.4	1.44×10^{13} cm^{-3}	.54
	11.0	0.03 µs	6.0	1.2×10^{13} cm^{-3}	.49
1.0	0.5	0.26 µs	13.0	2.53×10^{13} cm^{-3}	.72
	1.0	0.19 µs	13.4	2.62×10^{13} cm^{-3}	.73
	2.0	0.12 µs	12.7	2.48×10^{13} cm^{-3}	.71
	5.0	0.06 µs	11.3	2.2×10^{13} cm^{-3}	.67
	11.0	0.05 µs	10.0	1.95×10^{13} cm^{-3}	.63

All currents and times are from [80]. Maximum allowable pinch currents are found using the concentration in the collector as a minimum value.

Table 3, continued

Forward Base Drive (in amps)	Reverse Base Drive (in amps)	Time to Second Breakdown	Collector Current at Second Breakdown (in amps)	Minimum Charge Concentration in the Collector	Maximum Allowable Pinch Current (in amps)
2.0	0.10	1.0 µs	15.8	3.1×10^{13} cm^{-3}	.79
	.20	.63 µs	16.4	3.2×10^{13} cm^{-3}	.80
	.50	.36 µs	16.5	3.22×10^{13} cm^{-3}	.81
	1.0	.30 µs	16.0	3.12×10^{13} cm^{-3}	.79
	2.0	.22 µs	16.9	3.3×10^{13} cm^{-3}	.82
	5.0	.08 µs	14.1	2.75×10^{13} cm^{-3}	.75
	11.0	.05 µs	14.2	2.77×10^{13} cm^{-3}	.75
5.0	.05	.96 µs	18.4	3.6×10^{13} cm^{-3}	.85
	.10	.95 µs	19.7	3.84×10^{13} cm^{-3}	.88
	.20	.71 µs	19.9	3.88×10^{13} cm^{-3}	.89
	.50	.61 µs	17.0	3.32×10^{13} cm^{-3}	.82
	1.0	.47 µs	19.0	3.71×10^{13} cm^{-3}	.87
	2.0	.29 µs	20.0	3.9×10^{13} cm^{-3}	.89
	5.0	.12 µs	18.5	$3{,}61 \times 10^{13}$ cm^{-3}	.86
	11.0	.06 µs	15.7	3.06×10^{13} cm^{-3}	.79

All currents and times are from [80]. Maximum allowable pinch currents are found using the concentration in the collector as a minimum value.

CHAPTER VI

GENERAL CONCLUSIONS AND FUTURE WORK

This work has established the phenomena seen during second breakdown (in particular, current filamentation) in a semiconductor device is a consequence of the solid state plasma pinching under CCNR conditions.

To accomplish pinch, certain requirements in the semiconductor must be met. These requirements can be generally determined through the use of the carrier concentration, quantum degeneracy parameter, current, and temperature as dictated by the Bennett pinch criterion.

The solid state plasma pinch was calculated to be an unstable event, under first order approximation, which leads to growing oscillations and non-linear behavior.

Future Work

The calculations for stability of the static pinch could be solved to higher order modes with different distributions of carrier temperatures. This is not a simple task, and at some point, approximation, or advanced numerical techniques, will have to be utilized.

Yet, it seems inevitable that this task could be greatly simplified if repeatable experimental information on the solid state plasma pinch were available.

This may be accomplished by utilizing microwave interferometry on a semiconductor sample undergoing plasma pinch.

This technique would utilize comparison of the phase shifted microwave signal passing through the solid state plasma, to an unchanged reference signal, to find the plasma's index of refraction. This information will detail the concentration of the plasma in real time as the plasma grows.

Applications to Device Failure

The information developed in this effort was initially prompted by the desire to predict or explain device failure.

Certainly, the information detailed here-in has shown testing devices to thermal failure cannot accurately predict individual device failure. A semiconductor device is electrically unstable before thermal failure and going beyond this initial instability is extremely difficult to model.

Application of the plasma parameters developed in this effort could possibly determine the minimum requirements for plasma pinch in some devices, but, some device designs would initiate a kink instability before a sausage instability. Thus, further work is needed to determine a Bennett-like criterion for the kink instability in a semiconductor.

Further application to test cases would then determine unstable operating areas for semiconductor devices based on the base material parameters, temperature, and current levels. If successful, large scale testing of devices would not be necessary.

Also, some researchers have found that some plasma pinches in semiconductors can be stabilized by exciting higher order perturbations ($m=3,4,\ldots$) in the pinch. This concept will have to be explored for semiconductor devices. If found to be feasible, semiconductor devices could be designed to operate at much higher current levels then is presently possible.

LIST OF REFERENCES

1. Tauc, S. and Abraham, A., Phys. Rev. 108, pp. 936-937 (1957).

2. Thornton, C. G. and Simmons, C. D., IRE Trans. Elect. Dev. ED-5, pp. 6-10 (1958).

3. Snyder, M. E., AFWL-TR-83-22, Air Force Weapons Laboratory, Kirtland Air Force Base, New Mexico. pp. 2-3 (1983).

4. Bergman, F. and Geistner, D., IEEE Trans. Elect. Dev. ED-13 pp. 630-634 (1965).

5. Kalab, B. M., HDL-TR-1999, Harry Diamond Laboratories, U. S. Army Electronics Research and Development Comand, Adelphi, Maryland. p. 8 (1982).

6. Schafft, H. A. and French, J. C. , IEEE Trans. Elect. Dev. ED-13, 613 (1966).

7. English, A. C., Solid State Elect. 6, 511 (1963).

8. Wunsch, D. C. and Bell, R. R., IEEE Trans. Nuc. Sci. NS-15, pp. 244-259 (1966).

9. Tasca, D. M., IEEE Trans. Nuc. Sci. NS-17, pp. 364-372 (1968).

10. Kalab, B. M., HDL-TR-1915, Harry Diamond Laboratories, U. S. Army Electronics Research and Development Command, Adelphi, Maryland. (1980).

11. Ward, A. L., IEEE Trans. Nuc. Sci. NS-23, pp. 1697-1684 (1976).

12. Ward, A. L., HDL-TR-1978, Harry Diamond Labortories, U. S. Army Electronics Research and Development Command, Adelphi, Maryland. (1982).

13. Alexander, D. R., Karaskiewicz, R. J. and Enlow, E. W., AFWL-TR-80-128 pt 1, Air Force Weapons Laboratory, Kirtland Air Force Base, New Mexico. (1981).

14. Horgan, E. L., Adams, O. E., Rowan, W. H. and Templar, L. C. Electrical Overstress/Electrostatic Discharge Symposium Proceedings, EOS-3, pp. 151-166 (1981).

15. Portnoy, W. M. and Gamble, F. R., IEEE Trans. Elect. Dev. ED-11, 470 (1964).

16. Sunshine, R. A. and Lampert, M. A., IEEE Trans Elect. Dev. ED-19, 872 (1972).

17. Snyder, M. E., AFWL-TR-85-115, Air Force Weapons Laboratory, Kirtland Air Force Base, New Mexico. (1987).

18. Schafft, H. A. and French, J. C., IEEE Tran. Elect. Dev. ED-13, pp. 613-618 (1966).

19. Lampert, M. A. and Mark, P., Current Injection in Solids (Acedemic Press, New York, New York, 1970).

20. Snyder, M. E., AFWL-TR-85-115, Air Force Weapons Laboratory, Kirtland Air Force Base, New Mexico. (1987).

21. Jonscher, A. K., Brit Jrnl. Appl. Phys. 12, 366 (1961).

22. Marsh, J. W., Mayer, J. W. and Baron, R., Appl. Phys. Lett. 5, 74 (1965).

23. Mayer, J. W., Baron, R. and Marsh, O. J., Phys. Rev. 137, a286 (1965).

24. Snyder, M. E., AFWL-TR-85-115, Air Force Weapons Laboratory, Kirtland Air Force Base, New Mexico. (1987) p. 44.

25. Snyder, M. E., IBID p. 52.

26. Ridley, B. K., Proc. Phys. Soc. 82, 954 (1963).

27. Alekseev, M. E., Sov. Phys. Semicond. 3, 604 (1970).

28. Osipov, V. V. and Kholodnov, V. A., Sov. Phys. Semicond. 7, 604 (1973).

29. Vladimirov, V. V., Golovinskii, P. M. and Gorshkov, V. N., Sov. Phys. Semicond. 3, 1514 (1981).

30. Ridley, B. K. and Pratt, R. G., Phys. Lett. 4, 300 (1964).

31. Langmuir, I., The Collected Works of Irving Langmuir, volume 4, Electrical Discharge, volume 5, Plasma Oscillations. (pergamon Press, New York, New York, (1961).

32. Bennett, W. H., Phys. Rev. 45, 890 (1934).

33. Tonks, L., Phys. Rev. 56, 360 (1958).

34. Eckersley, T., Nature 135, 104 (1935).

35. Barkhausen, H., Phys. Zs. 20, 401 (1919).

36. Alfven, H., Ark. Mat. Astro. and Phys. B29, 2 (1942).

37. Rutheman, G., Ann. Phys. 2, 113 (1948).

38. Lang, W., Optik 3, 333 (1948).

39. Pines, D. and Bohm, D., Phys. Rev. 82 625 (1951) and 85, 338 (1952).

40. Steele, M. C. and Glicksman, M., Jrnl. Phys. Chem. Sol. 8, 242 (1959).

41. Chynoweth, A. G. and Murray, A. A., Phys. Rev. 123, 515 (1961).

42. Ivanov, Y. L. and Ryvkin, S. M., Sov. Phys. Tech. Phys. 3, 722 (1958).

43. Galt, J. K. and Yager, W. A., Phys. Rev. 114, 1396 (1959).

44. Glicksman, M., Phys. rev. 124, 1655 (1961).

45. Buchsbaum, S. J. and Galt, J. K., Phys. Fluids 4, 1514 (1961).

46. Glicksman, M. and Steele, M. C., Phys. Rev. Lett. 2, 461 (1959).

47. Vladimirov, V. V., Sov. Phys. Usp. 18, pp. 690-711 (1975).

48. Ando, K. and Glicksman, M., Phys. Rev. 154 316 (1967).

49. Gunn, B., Solid State Comm. 1, 88 (1963).

50. Vladimirov, V. V., Sov. Phys. Usp. 18, 691.

51. Chen, F. F., Introduction to Plasma Physics and Controlled Fusion, volume 1. (Plenum Press New York, New York, 1985) p. 297.

52. Chen, F. F., IBID pp. 1-4.

53. Tanenbaum, B. S., Plasma Physics. (McGraw-Hill book Comp. New York, New York, 1967) pp. 3-5.

54. Ancker-Johnson, B., Semiconductors and Semimetals, volume 6, Injection Phenomena, chapter 11 (1970).

55. Liboff, R. L., Jrnl. Appl. Phys. 56, 2530 (1984).

56. Ichimaru, S., Rev. Mod. Phys. 54, 1017 (1982).

57. Liboff, R. L., Jrnl. Appl. Phys. 56, 2533 (1984).

58. Kubat, M. Power Semiconductors, chapter 2. (Springer-Verlag, New York, New York, 1984)

59. Volkov, A. F. and Kogan, Sh. M., Sov. Phys. JETP 25, 1095 (1967).

60. Takeyama, K. and Kitahara, K. Jrnl. Phys. Soc. of Jpn. 39 123 (1975).

61. DeGroot, S. R. Thermodynamics of Irreversible Processes (North-Holland Pub. New York, New York, 1951) p. 75.

62. Prigogine, I. Introduction to Thermodynamics of Irreversible Processes (John-Wiley and Sons, New York, New York, 1951) p. 94.

63. Prigogine, I. IBID, pp. 76-77.

64. Prigogine, I. IBID, p. 96.

65. Snyder, M. E. and Volkin, H. AFWL-TR-85-116. Air Force Weapons Laboratory, Kirtland Air Force Base, New Mexico, (1987).

66. Brodkey, R. S. The Phenomena of Fluid Motion (Addison-Wesley Pub. Comp., Reading, Mass. 1967) pp. 38-39.

67. Brodkey, R. S., IBID, p. 105.

68. Jackson, J. D., Classical Electrodynamics (John-Wesley and Sons, New York, New York, 1962) p. 259.

69. Boyd, T. J. and Sanderson, J. J., Plasma Dynamics (Barnes and Noble Inc., New York, New York, 1969) p. 86.

70. Snyder, M. E. and Volfin, H. AFWL-TR-85-116. Air Force Weapons Laboratory, Kirtland Air Force Base, New Mexico. (1987) pp. 31-37.

71. Snyder, M. E., AFWL-TR-85-115, Air Force Weapons Laboratory, Kirtland Air Force Base, New Mexico, (1987). pp. 77-85.

72. Portnoy, W. M., AFWL-TR-82-139, Air Force Weapons Labortory, Kirtland Air Force Base, New Mexico, (1983).

73. Portnoy, W. M. and McMullen, S. A., AFWL-TR-84-111, Air Force Weapons Laboratory, Kirtland Air Force Base, New Mexico, (1985).